COMPUTATIONAL ANALYSIS OF 3D GENOME ORGANIZATION AND ITS EFFECT ON NUCLEAR MORPHOLOGY AND MECHANICS

A THESIS SUBMITTED TO

THE GRADUATE SCHOOL OF ENGINEERING AND SCIENCE

OF BILKENT UNIVERSITY

IN PARTIAL FULFILLMENT OF THE REQUIREMENTS FOR

THE DEGREE OF

MASTER OF SCIENCE

MATERIALS SCIENCE AND NANOTECHNOLOGY

By

ALİ GÖKTUĞ ATTAR

OCTOBER 2023

COMPUTATIONAL ANALYSIS OF 3D GENOME ORGANIZATION AND ITS EFFECT ON NUCLEAR MORPHOLOGY AND MECHANICS

By Ali Göktuğ Attar

October 2023

We certify that we have read this thesis and that in our opinion it is fully adequate, in scope and in quality, as a thesis for the degree of Master of Science.

Aykut Erbaş (Advisor)

Tevfik Tamer Önder

Bahar Değirmenci Uzun

Approved for the Graduate School of Engineering and Science:

Orhan Arıkan

Director of the Graduate School

ABSTRACT

COMPUTATIONAL ANALYSIS OF 3D GENOME ORGANIZATION AND ITS EFFECT ON NUCLEAR MORPHOLOGY AND MECHANICS

Ali Göktuğ Attar

M.S. in Materials Science and Nanotechnology

Advisor: Dr. Aykut Erbaş

October 2023

Several disorders, including progeria, cancer, and Emery-Dreifuss muscular dystrophy, share abnormalities in eukaryotic cells' nuclear structure and mechanics. One of the contributors to nuclear morphology and mechanics is the chromatin filling the 10-micron elastic nucleus. The polymer physics principles behind the relationship between chromatin and nuclear morphology and its mechanics need to be clarified. To elucidate this relationship between chromatin and polymer and nuclear morphology and mechanics, we concentrate on chromatin phase separation utilizing a coarse-grained polymer model encapsulated in an elastic shell. Our approach can capture the conventional and inverted nucleus organization while allowing nuclear deformability. Heterochromatin can be one of the key determinants of the nuclear shape by revealed by examining heterochromatin-heterochromatin interactions, as well as the interaction between chromatin and lamina inspecting through the biologically relevant volume fractions. The simulations showed that the heterochromatin-nuclear shell interactions influence the variation in the nuclear shape

fluctuations, thus leading to nuclear deformations. The interplay between heterochromatin-heterochromatin interactions and its interaction with the nuclear shell plays a role in phase separation and nuclear shape fluctuations. Higher heterochromatin concentration resulted in abnormal morphology in lower volume fraction, in contrast to some experiments suggesting the opposite trend. The volume fraction exhibits a suppressing effect on the nuclear shape fluctuations in all examinations of heterochromatin interactions. Additionally, the tethering and crosslinking of the heterochromatin provide a chromatin-based stiffness to the nuclear shell revealed by force-strain relationships. Altogether, our results imply that chromatin, mainly heterochromatin, considerably contributes to nuclear morphology and mechanics.

Keywords: Polymer Modelling, 3D Genome Organization, Nuclear Morphology, Nuclear Mechanics

ÖZET

3D GENOM ORGANİZASYONUN VE HÜCRE ÇEKİRDEĞİNE VE MEKANİĞİNE OLAN ETKİSİNİN HESAPLAMALI ANALİZİ

Ali Göktuğ Attar

Malzeme Bilimi ve Nanoteknoloji Yüksek Lisans

Tez Danışmanı: Dr. Aykut Erbaş

Ekim 2023

Progeria, Emery-Dreifuss kas distrofisi ve kanser türleri dahil olmak üzere birçok hastalıkta, hücre çekirdeği yapısında ve mekaniğinde değişimler gözlenmektedir. Bu değişimlerin sebeplerinden bir tanesi de 10-mikron boyuta sahip olan elastik hücre çekirdeğini dolduran kromatindir. Kromatin ve hücre çekirdeğinin arasındaki ilişkinin polimer fizik prensipleri tam olarak bilinmemektedir. Kromatin polimeri ve hücre çekirdeğinin arasındaki ilişkiyi açıklayabilmek için elastik çekirdek için iri taneli polimer modelinden yararlanarak kromatin faz dağılımı üzerinde yoğulaştık. Yaklaşımımız normal ve ters kromatin organizasyonunu modelleyebildi ve aynı zamanda hücre çekirdeğinin deforme olmasını sağladı. Biyolojik kromatin hacim oranlarını elde ederek, heterokromatinin kendisiyle ve çekirdekle olan etkileşimi incelenmesi sonucunda heterokromatinin, hücre çekirdeği yapısını etkileyen önemli faktörlerden biri olabileceği görüldü. Simulasyonlar, heterokromatin-çekirdek kabuğunun arasındaki etkileşimlerindeki

değişikliğin, hücre çekirdeğinin dalgalanmasını etkileyebileceğini ve yapısının bozulabileceğini gösterdi. Ayrıca heterokromatin-heterokromatin ve heterokromatin-kabuk etkileşimleri arasındaki bağlantının faz dağılımda ve hücre çekirdeği dalgalanmalarında rol oynamadığı gözlemlenmiştir. Yüksek heterokromatin oranları düşük kromatin hacim oranlarında normal olmayan hücre çekirdeği yapısına sebep olmaktadır ve bu bazı deneysel sonuçlarla ters bir eğilim göstermektedir. Heterokromatin etkileşimlerini incelediğimiz her durumda, kromatin hacim oranının hücre çekirdeği dalganlamalarını baskılayıcı bir etki gösterdiği görülmüştür. Ek olarak, kuvvet-gerilim ilişkisi: heterokromatinin çekirdek kabuğuna bağlanması ve kendi içinde çapraz bağlanmasının, çekirdek kabuğuna kromatin temelli bir sertlik kazandırdığını gösterdi. Tüm bulgular incelendiğinde sonuçlarımız, kromatinin (özellikle heterokromatinin), önemli bir ölçüde hücre çekirdeğinin morfolojisine ve mekaniğine katkı sağladığını gösterdi.

Anahtar Kelimeler: Polimer Modellemesi, 3-Boyutlu Genom Organizasyonu, Hücre Çekirdeği Morfolojisi, Hücre Çekirdeği Mekaniği

Acknowledgments

I extend my deepest gratitude to Dr. Aykut Erbaş for the excellent mentorship he offered during my Master's Science and senior year studies in my Bachelor's. I learned a lot from him during our extensive discussion sessions about the project and from the courses he taught.

I would like to thank my trainer both in experimental and computational studies, Zafer Koşar, for his mentorship and guidance since we began doing research together.

I want also to thank my friends and colleagues Cem Özdemir, Doğuş Akboğa, Mehmet Emin Bakar, and Ömer Can Ergül for the strong bond of friendship and invaluable support.

I also thank to my friends especially Tevfik Berkay Gertel, Ata Orhan Sever, Suay Bilgin and Beyzanur Erdivan.

I want to thank UNAM for providing excellent research environment and financial support.

Many thanks to my family and especially to my mother who was always there for me. She was a mother and a father simultaneously, and made a great effort to raise me and my twin sister.

I thank my twin sister, Melis Attar, for being my half other part. I am glad you are my sister, and you should also be glad that you have a brother like me.

Last and most precious, I would like to thank my fiancée Eylül Çalıkyılmaz whom I dedicate this thesis, for the invaluable love and support she has been continuously showing me. I am fortunate to be with the person who is my best friend and greatest love at the same time (Çalıkyılmaz, 2023).

Contents

List of Tables

List of Figures

1 INTRODUCTION

1.1 The 3D Genome Organization

Micron-sized eukaryotic nuclei enclose the chromosomes, forming the eukaryotic genome. Heterogonous chromatin is packaged with structural proteins, forming the chromosomes. Structural proteins mediate the packaging of the chromosomes with heterogeneous chromatin. Meanwhile, a set of essential biological processes[1–3], such as transcription, replication, and differentiation, are regulated by the 3D organization of chromatin. The chromosomes inside the nucleus occupy distinct territories, and the specific localization of the chromosomes influence various biological processes such as gene regulation[4]. The chromosomes are further organized into compartments revealed by the Hi-C method, namely Compartments A and B[5,6]. Hi-C is a method utilized for capturing chromatin conformation and analyzing the captured DNA with sequencing[5]. This method allows for finding the interactions between chromatins and defining the compartments. These compartments correspond to distinct chromatin, often identified in two forms, differentiated by its transcriptional activities and packing density. The histone modifications on histone proteins on nucleosome determines the features of chromatin, in which heterochromatin becomes condensed, and euchromatin becomes less dense[7,8]. In addition, strong transcriptional activity is affiliated with the euchromatin, while heterochromatin is the domain where transcriptional activity is low[8]. While the heterochromatin domains are primarily found at the nuclear periphery, the euchromatin

portion is majorly located at the nuclear interior in conventional nuclei[9]. Additionally, the biophysical properties show variance which heterochromatin is stiffer than euchromatin, having a persistence length between 100-200 nm, whereas euchromatin is characterized by a persistence length between 10-50 nm[10], and this difference can affect chromatin organization via entropic effect[11,12]. In addition, nuclear elastography shows that heterochromatin is significantly stiffer than euchromatin[13]. Additionally, euchromatin portions exhibit weak self-affinity while heterochromatic domains, Compartment B, show stronger self-affinity[14].

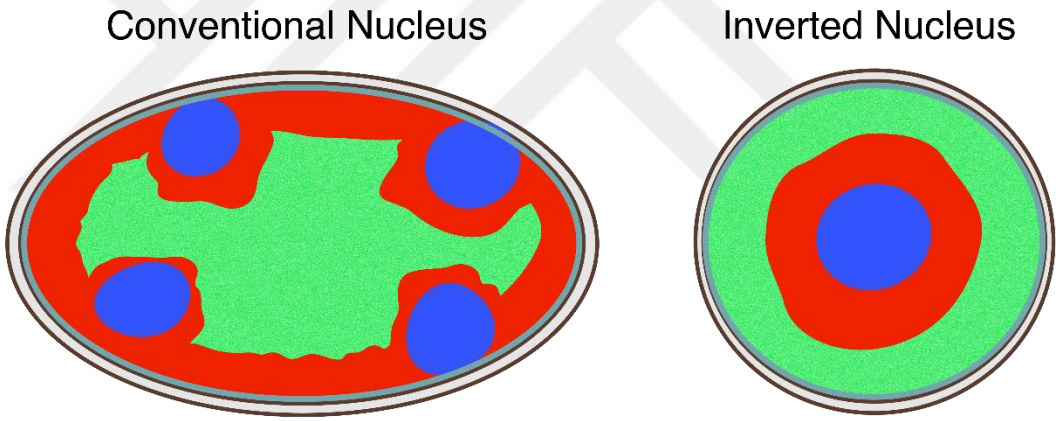

Figure 1 The illustrations of conventional and inverted nuclear architecture in mice rod cells.

1. 2 Nuclear Morphology and its Function in Health and Disease

The nuclear envelope (NE), and nuclear lamina provide the elasticity of the nucleus. Intermediate filament lamins form a complex meshwork attached to the inner nuclear

membrane (INM), creating a barrier between chromatin and the INM[15]. This meshwork, nuclear lamina, formed by lamins, consists of two types of lamins, A-type and B-type[16,17]. The organization of the network is specified by the localization of the lamins, forming the nuclear lamina with the lamin A/C network residing closer to the nucleoplasm, whereas lamin B1 is stacked between lamin A/C meshwork and INM[18]. The complex structural network of lamins influences the mechanobiology and morphology of the cell nucleus; in turn, the organization of this meshwork influences the nuclear morphology[19,20]. Such as stem cells have a spherical structure, and owing to their lamina organization, they have flexible cell nuclei due to the absence of lamins A/C expression[21]. However, the mutations in lamins can alter the nuclear morphology and be associated with diseases (Figure 2). The point mutation in the LMNA gene can alter the organization of the lamin meshwork, associated with laminopathies such as Hutchinson-Gilford Progeria Syndrome (HPGS), which leads to abnormal nuclear morphology[22,23]. A different laminopathy, Emery-Dreifuss muscular dystrophy, is associated with mutations in the LMNA gene exhibiting significant deformations in the nucleus[24,25]. Furthermore, the experiments revealed that nuclear remodeling is observed in other diseases and can alter the nuclear morphology. In different cancer types, the mutations and fluctuations in the level of lamins are associated with the cancer progression[26–28]. Hence, the structural alteration in lamin proteins that form the meshwork between the genome and the nuclear envelope is crucial for determining nuclear morphology and mechanics.

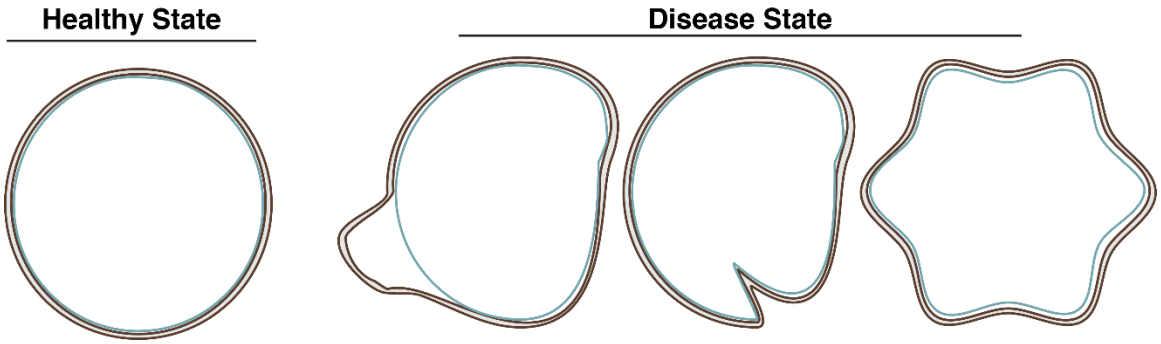

Figure 2 The sample drawing of the nuclear morphology in a healthy state and examples of nuclear abnormalities such as nuclear blebbing, invagination, and undulations in a disease state.

1. 3 The Role of Chromatin on Nuclear Morphology and Mechanics

The fluorescence in situ hybridization (FISH) and immunofluorescence staining experiments uncovered the connection between nuclear morphology and spatial organization of the chromatin [9,29]. Most relevantly, loss of LBR and lamin A/C drives heterochromatin localization from the nuclear periphery to the interior in mice rod cells during differentiation. Meanwhile, the initial oval shape of the nucleus is changed into a spherical one[30]. The chromatin contribution to nuclear mechanics was revealed by micropipette manipulation experiments in which chromatin was shown to influence the nuclear mechanics in short extensions where lamins were involved in long extensions[20]. Additionally, valproic acid (VPA) and 3-Deazaneplanocin-A (DZNep) treatment of the isolated nuclei exhibited the formation of the nuclear blebs as the euchromatin was increased or heterochromatin was decreased[31]. Furthermore, the same study demonstrated that the normal morphology was recovered by increasing heterochromatin levels.

Additionally, a strain-force response by micropipette manipulation experiments demonstrated the causation in which the packing density of chromatin impacts the nuclear rigidity where increasing the heterochromatin amount elevates nuclear rigidity, and euchromatin reduces. Moreover, increasing heterochromatin content through divalent cations was helpful in recovering the nuclear morphology in the disease, progeria where abnormal nuclear shape and display of a loss of heterochromatin are two hallmarks of the disease[32], the state in which abnormal morphology restored significantly similar to the wild-type cells[33]. During aging in *C. elegans*, peripheral heterochromatin is lost, and misshaped nuclei were observed[34]. The misshaped nuclei is also correlated with the loss of HP1α, which mediates the crosslinking of heterochromatin domains and drives the phase separation of heterochromatin *in vitro*[35–37]. The study exhibited that degrading HP1α resulted in decreased nuclear stiffness, suggesting that crosslinking heterochromatin plays a role in nuclear mechanics, hence the morphology[35]. Furthermore, the nuclear mechanics of the cells that encounter the deformation were shown to be regulated by heterochromatin marked with H3K9me3, whose loss is associated with a reduction in nuclear rigidity, helping cells adapt to the stress in the environment[38]. Also, a recent study revealed that heterochromatin formation was induced during and after migration of the cells through narrow channels, exhibiting a force on cells, which speculated that changing the levels of heterochromatin might govern nuclear mechanics[39].

The studies suggested that the morphology of the nucleus is regulated by the chromatin and its density. The regulation is achieved by chromatin generated entropic pressure inside the nucleus[40] or chromatin decompaction. Increasing euchromatin leads to higher chromatin decompaction, which changes the nucleoplasm's density by increasing the

nuclear size[41]. Additionally, overexpression of HMGN5 protein, which binds to nucleosome without modifying chromatin, induces decompaction and deformed morphology in adult cardiomyocytes[42]. Furthermore, the change in nuclear morphology is observed when the homogenously organized chromatin is redistributed due to the increased osmotic pressure[43]. Hence, evidence suggests that the 3D chromatin organization in nuclear confinement can be crucial for determining nuclear mechanics and morphology.

1.4 Nuclear Membrane Proteins and its Chromatin Association Regulate the Nuclear Morphology and Mechanics

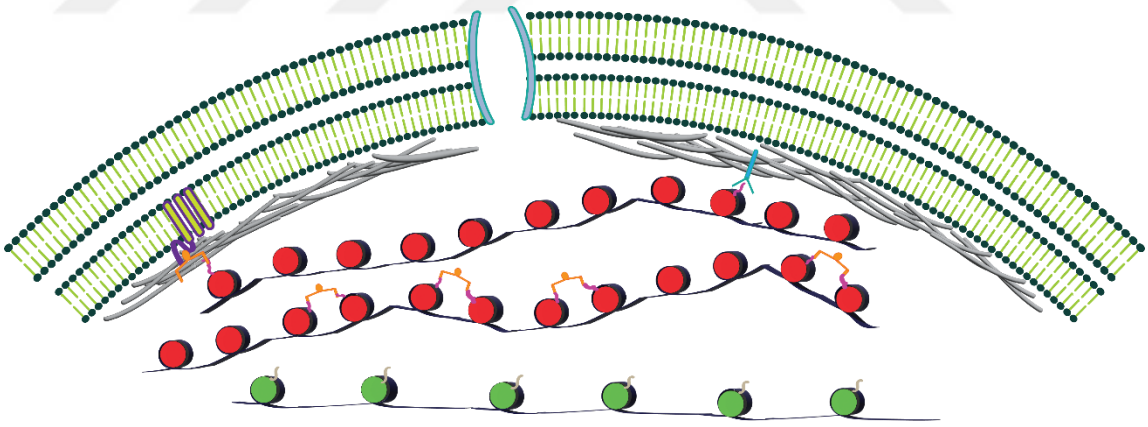

Figure 3 The representation of the nuclear periphery demonstrates euchromatin (green) and crosslinking of heterochromatin (red) along its association with the chromatin tethers which are bound to the nuclear lamina or soluble.

Chromatin self-interactions and interactions with the proteins at the nuclear borders lead to phase separation while regulating its organization in the nucleus (Figure 3). Tethering proteins which are embedded in the nuclear membrane or soluble tethering proteins anchor the chromatin at the nuclear boundaries[44]. The association of the chromatin with tethering proteins is crucial for nuclear morphology and the disruption in the tethering mechanism can alter the nuclear morphology and the 3D chromatin organization. Correspondingly, constitutive heterochromatin labeled with H3K9me3 is tethered to nuclear lamina by PRR14 in association with HP1, and knockdown of PRR14 leads to misshaped nucleus[45]. Moreover, the heterochromatin marked with H3K9me2 can bind to the nuclear lamina, forming a uniform layer at the periphery via CEC4 protein[46,47]. Furthermore, in the lamin-free nucleus of *S. pombe*, the deformation in the nuclear morphology was observed when heh1, heh2, and ima1 tethering proteins were knocked out. Meanwhile, the nuclear stiffness was reduced[48]. Deficiency in tethering protein emerin led to abnormal morphology while preserving the nuclear mechanical properties[49]. Moreover, nuclear blebs are associated with the organization and the strength of the chromatin tethers, mainly emerin, located on the nuclear lamina in an HPGS model[50].

1.5 Modeling the Eukaryotic Genome and the Nucleus

Previous studies utilizing polymer modeling proposed that the volume fraction of the chromatin, chromatin-lamina interactions, and phase separation influence the organization of the chromatin[51–53]. Conventional and inverted nuclear architecture were controlled by phase separation driven by heterochromatin revealed by the polymer simulations in a rigid

shell and experiments[14] (Figure 1). To model the regulation of nuclear morphology by chromatin, an elastic shell model that can encapsulate the chromatin polymers while allowing for deformation is necessary. Previously, the effect of chromatin in nuclear mechanics and how motor activity regulates the nuclear shape fluctuations were effectively demonstrated by an elastic shell model confining a chromatin's homopolymer model[52,53]. However, instead of a homopolymer chromatin model, modeling chromatin as a multi-block copolymer is more accurate since chromatin has a highly heterogeneous structure.

Here in this study, we use Molecular Dynamics (MD) simulations to investigate the role of chromatin in nuclear shape fluctuations. For that purpose, we utilize a coarse-grained heteropolymer model of mouse chromosomes, which was successful in recapitulating the conventional and inverted nuclear architecture[25]. A coarse-grained spherical model that strongly projects the force-strain relation of isolated nuclei[20,35,52] was employed to encapsulate the chromosome polymers. Our simulations reveal that the heterochromatin interaction with the nuclear shell impacts the nuclear morphology. Strong attraction affinity further increases nuclear shape fluctuations, which exhibits biologically abnormal morphologies. In addition, the phase separation's contribution to nuclear shape fluctuations is influenced by the volume fraction of the chromosome polymers. The increase in nuclear shape fluctuations and deformations in the nuclear shell is observed when the heterochromatin amount is increased.

Furthermore, we investigated the nuclear mechanics imitating the micropipette manipulation experiments[20,31,33,52]. Our simulations show that molecular tethering of heterochromatin increases the nuclear stiffness. As the concentration of tethered chromatins increases, our nuclear model becomes stiffer. Further, we crosslinked heterochromatin, and crosslinking provided additional nuclear stiffness. Increasing the heterochromatin fraction slightly increased the nuclear stiffness; however, combining crosslinking with tethering additively provided more rigidity. Hence, our findings suggest that heterochromatin and volume fraction are physical determinants of nuclear morphology that might be manipulated to govern nuclear architecture. In addition, molecular tethering and crosslinking of the chromatin regulates the nuclear mechanics.

2 METHODOLOGY

2.1 Designing Deformable Shell Representing Eukaryotic Cell Nucleus

The eukaryotic cell nucleus has a complex structure. While compartmentalized by two lipid membranes, lamin proteins form meshwork, the nuclear lamia, between chromatin and INM. The levels of different types of lamins, A-type, and B-type, can vary between different cell types, defining the characteristic and biophysical properties of nuclear morphology and cell. To avoid this complexity, we decided to use a simplistic shell model consisting of a single-layer meshwork of beads with the same biophysical properties to encapsulate the chromosome polymers.

We designed and optimized our shell model and determined the number of beads as N=15000 (Figure 4). The beads forming the nuclear lamina are randomly placed on distinct coordinates represented by the following equation.

$$r_{\text{bead}} = \sqrt{(x^2 + y^2 + z^2) \pm 5}$$

The x, y, and z coordinates are randomly generated, and coordinates meeting the above equation are selected.

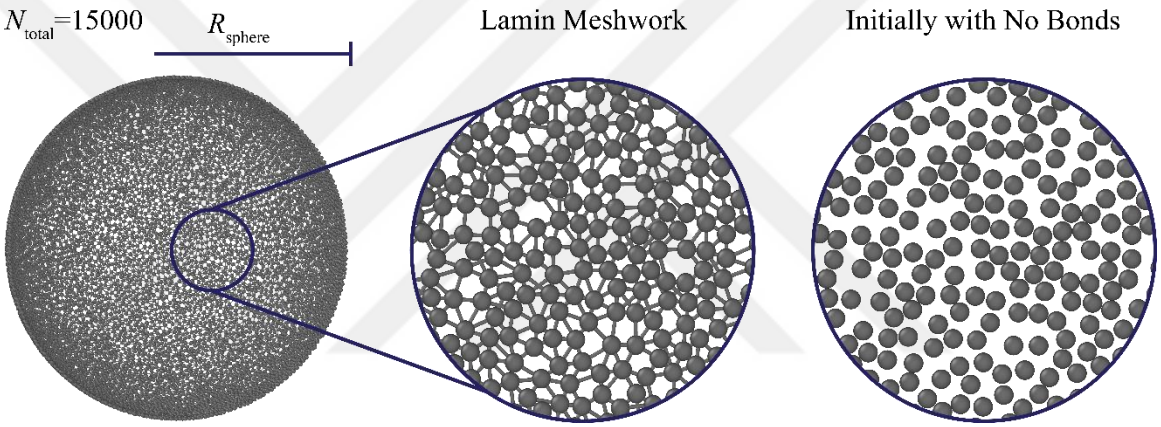

Figure 4 The snapshots of the shell model. The lamin meshwork replicated in our shell model was demonstrated with bonding and without bonding configuration.

We defined a distance parameter between previously placed beads and beads to be placed in the next step. The beads that satisfy the above equation must also meet the below equation to prevent overlapping of beads, and putting the beads prevents holes absent from beads.

$$0.66 \times factor < d < 1.0 \times factor$$

Selecting the bead positions was a random process. Therefore, in some trials, such bead positioning might decrease the probability of assigning the beads satisfying the distance

condition. Hence, we implemented the same algorithm but set different distance parameters to fill the tight spaces.

$$0.60 \times factor < d < 0.80 \times factor$$

Optimization is done by designing the shell having a smaller initial radius, r_{sphere}= 28σ. *N*=15000 is the sufficient number of beads that can occupy the sphere having r_{sphere}= 28σ, filling the surface to prevent tight holes. We extended our shell size, imitating the collapse of the nucleus after mitosis. We determined the factor as 1.5, having r_{sphere}= 42σ.

The beads are connected via FENE (Finitely Extensible Nonlinear Elastic) bonding (Figure 4). Each bead was assigned to have a minimum of five bonds and a maximum of 8 bonds. The distance criteria were set according to the following conditions.

$$0.66 \times factor < r < 0.90 \times factor$$

If the minimum number of bonds could not be achieved, the beads were allowed to bond with distant beads following the below condition.

$$0.90 \times factor + r_{inc} < r < 1.00 \times factor + r_{inc}$$

$$r_{inc} \leq 0.30 \times factor$$

Additionally, the recurrence of bondings was inhibited. Ultimately, the average bond number that each bead connected was $< n_{bond} > \approx 5.5$. For each new replicate, a shell was generated, leading each replicate to obtain a randomized shell structure.

2.2 Modeling Eukaryotic Genome

The genome is a combination of multiple polymer chains that occupy spatial locations inside the cell nucleus. The polymer chains are compacted at the start of the mitosis to secure proper segregation to daughter cells[54]. Therefore, we employed the same approach that initiated simulation with the condensed triblock copolymers polymers. Our genome model is represented by eight self-avoiding Kremer-Grest (KG)[55] bead-spring triblock copolymers in implicit solvent. The sequence of the polymer block was obtained from Hi-C data that each bead represented either Compartment A, euchromatic regions, or Compartment B, heterochromatic regions mainly facultative heterochromatin. Hence, each bead represents 40kb, which this resolution is consistent with Hi-C contact map scaling, sufficient for generating contact maps resembling Hi-C experiments[56,57].

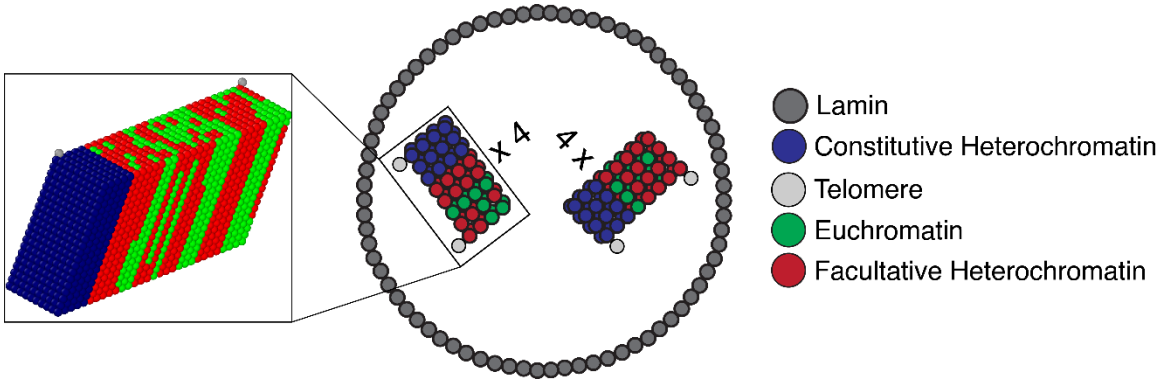

Figure 5 The representative schematics of the modeling eukaryotic genome and the snapshot of a triblock copolymer from our model

Each polymer block consists of 6002 beads. The first and the last beads were assigned as telomere beads. The telomeres are found at each chromosome, protecting the chromosome against DNA damage, providing stability, and positioned around clustered centromeres at

the nuclear periphery and the chromocenters[9,58]. The following 1000 beads were specified as constitutive heterochromatin, and the remaining 5000 beads were determined using compartment sequence[14] (Figure 5). In total, there were eight triblock copolymers polymers. The first 4 represent the mature rod cells of mice Chromosome 1, and others represent Chromosome 2. It was shown that utilizing Chromosome 1 and Chromosome 2 was sufficient to recapitulate the contact map and internal chromatin organization by molecular dynamics simlations[14]. In addition, the first and last five beads of the polymer were assigned differently, which preserved their compartment profile however, their interaction with the shell was enhanced to let the polymer gain permanent territories.

2.2.1 Crosslinking the Chromosome Copolymers

The constitutive heterochromatin is crosslinked via heterochromatin protein 1 (HP1) α proteins. These proteins are involved in the phase separation of the heterochromatin and ensure biological activities[35–37,59]. The crosslinking was utilized for constitutive and facultative heterochromatin. We assigned bonds to beads within the same types of chromatin for crosslinking. Each crosslinking bond that was assigned had the same physical properties. The beads were crosslinked randomly by defining a probability of selecting the beads that would assign bonds between their neighbors. If the bead was chosen, it could assign a specified number of bonds, which, in our default cases, the maximum was set to n_{bond}=2 and the minimum was n_{bond}=1. Then, the neighbors were selected from a distance parameter following the condition below.

$$1.0\sigma < r_{difference} < 2.5\sigma$$

The neighbor could have, at most, the number of bonds it initially assigned. Even though the bead was not selected to assign bonds between its possible neighbors, it could be specified as a neighbor by one of the other chosen beads, satisfying the distance parameters and containing an available bond slot. Additional algorithms were implemented to prevent bonding between the adjacent beads and the recurrence of bondings.

In the scenario where crosslinking was applied to constitutive heterochromatin to study nuclear shape fluctuations, we split the polymer relaxation simulations. At first, we ran the simulations for a 2×10^4 time step, allowing constitutive heterochromatin to lose the initial polymer structure, and after, these domains were crosslinked (Figure 6). Then, we continued the simulations for 8×10^4 to complete the relaxation of polymers with crosslinked constitutive heterochromatin.

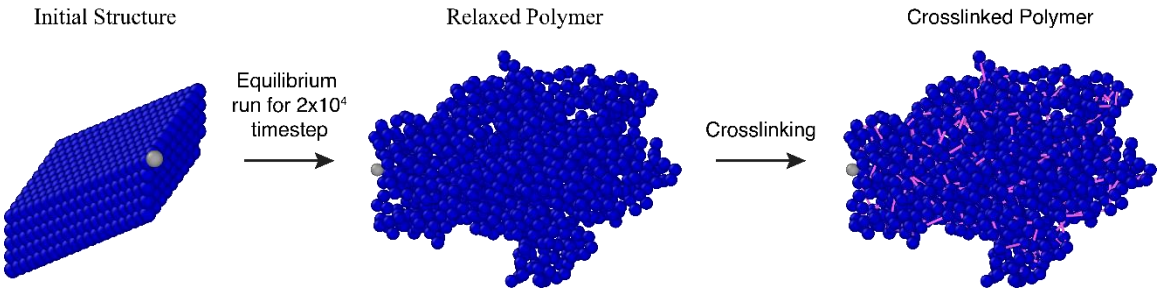

Figure 6 The images of a single constitutive heterochromatin domain show the structural changes and the assigned crosslinks (pink).

For pulling simulations, we crosslinked both constitutive and facultative heterochromatin using the end product of conventional nuclei simulations, then we performed pulling simulations (Figure 7).

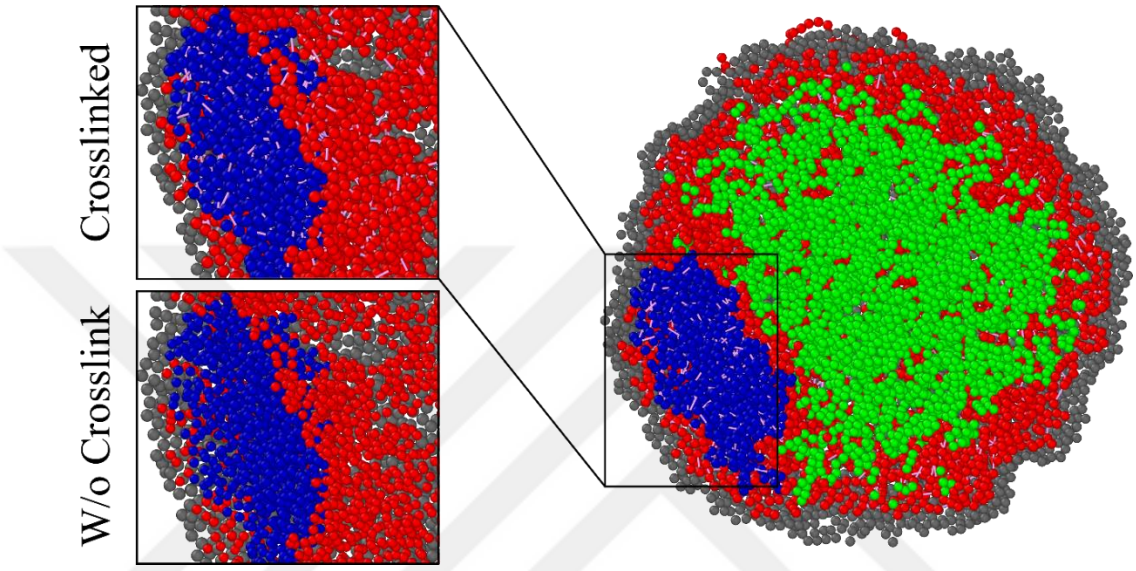

Figure 7 The retrieved snapshots from our model show the crosslinks (pink) assigned in pulling simulations for constitutive and facultative heterochromatin.

2.2.2 Modifying the Chromosome Copolymers

To better understand the role of heterochromatin on nuclear morphology and mechanics, the polymer sequence was randomly altered, imitating the experiments of chromatin pertubrations[31,33,42]. The type of beads, either initially designated for facultative heterochromatin or euchromatin, were converted (Figure 8). To increase the facultative fraction of heterochromatin, random euchromatin beads were selected and converted to the facultative heterochromatin, and the same method was approached to increase the

fraction of euchromatin. The desired fraction, *f*, of facultative heterochromatin, was initially specified, and the beads were converted until the fraction was obtained. We obtained various fractions of heterochromatin in range between *f*=0.10 to *f*=0.75 with increments of *f*=0.10 (i.e *f*=0.10, *f*=0.20, *f*=0.30, *f*=0.45 (Default), *f*=0.55, *f*=0.65, *f*=0.75)

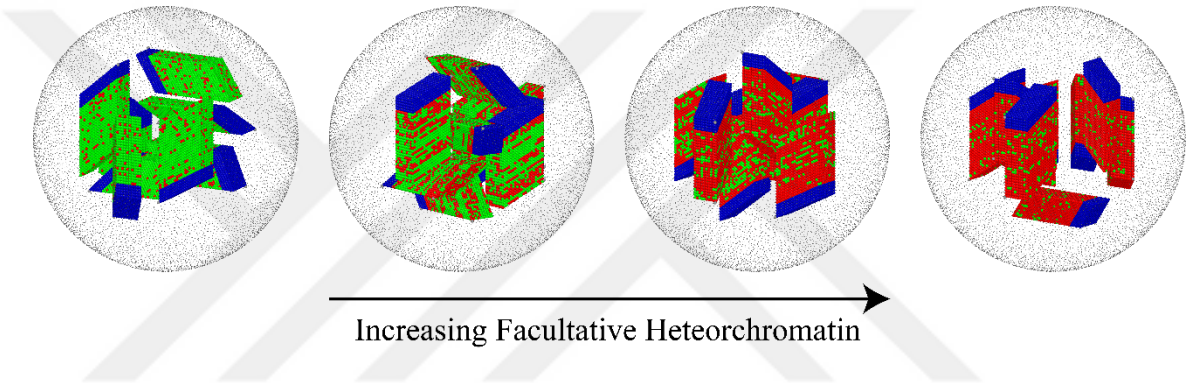

Figure 8 The fraction of the intended chromatin type is achieved at the initial structure.

A different approach for pulling simulations was employed. The beads were still randomly converted to the beads of the intended type, however, we defined a distance parameter, *d*, that only converts the bead within this distance from the shell periphery (Figure 9). Hence, we aimed to investigate thoroughly the role of peripheral heterochromatin on nuclear mechanics.

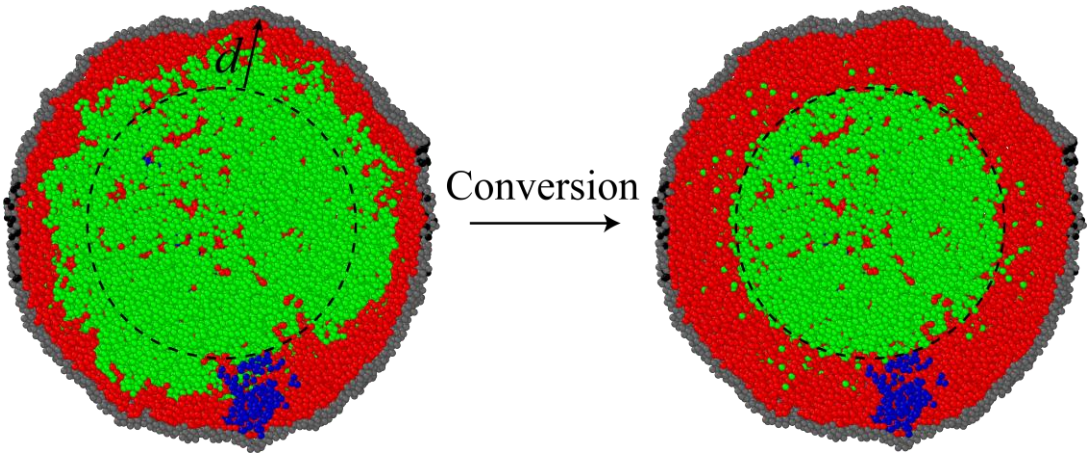

Figure 9 The chromatin beads among the specified distance, *d*, are converted in the conventional nucleus for pulling simulations.

2.2.3 Molecular Tethering of Chromosome Copolymers

The heterochromatin domains were tethered -bonded- to the shell, imitating the function of the membrane-associated proteins or the lamina-associated proteins[60]. The probability for tethering was defined to vary the number of tethers, and randomly selected heterochromatin beads that satisfied the following distance criteria were tethered.

$$1.0\sigma < r < 1.5\sigma$$

The distance was set only to tether the heterochromatin domains closest to the shell, forming a layer of tethers on the surface (Figure 10B). The probability of assigning bonds was set p(B) = 1.0, unless noted. Hence, all the beads within the specific distance could be tethered to the shell. Additionally, each bead, which was randomly selected and satisfied the distance condition, could have only one bond connected to a shell bead (Figure 10A)

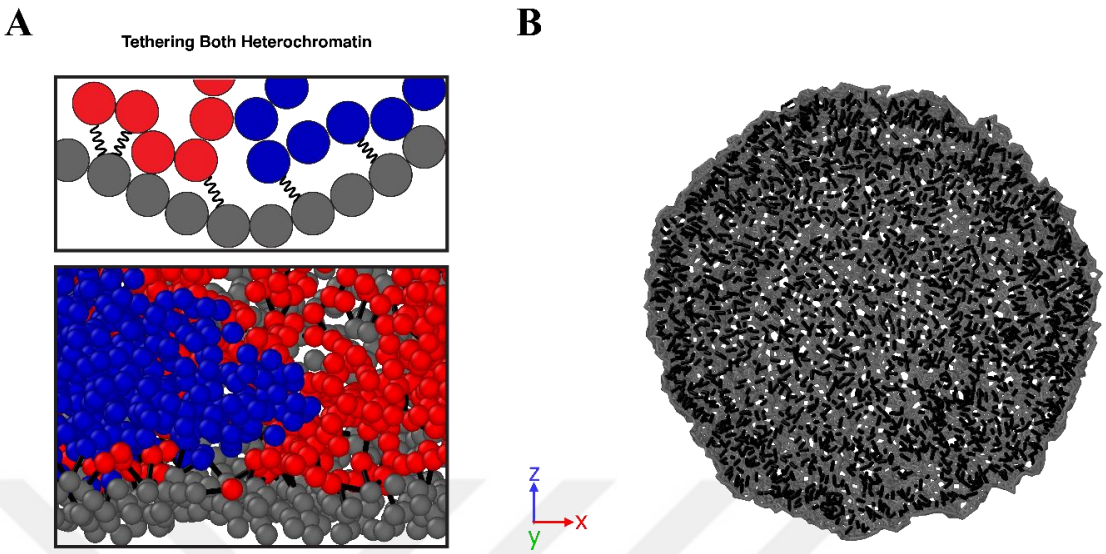

Figure 10 Tethering of heterochromatin to the shell **A)** Schematics and snapshots from the model show the molecular tethering (black). **B)** The image shows that the layer of tethering is formed on the inner surface of the shell.

2.3 Confining Eukaryotic Genome Inside the Deformable Shell

The beads were placed in order to generate the triblock copolymer. Initially, a random coordinate inside the shell was assigned from the coordinates of the shell having a radius of r_{sphere}= 28σ. These coordinates defined the starting positions for the first bead of each triblock copolymer. Selecting coordinates from the shell having a size of r_{sphere}= 28σ, prevented the escape of the polymers during shrinking of the larger shell, r_{sphere}= 42σ. Moreover, each triblock copolymer assigned with a different direction provided by a randomly defined angle according to the following equation.

$$\sqrt{(x_{polymer} - x_{shell})^2 + (y_{polymer} - y_{shell})^2 + (z_{polymer} - z_{shell})^2} \geq 30\sigma$$

This equation provided possible angles that each block could have, and the angle was randomly selected in the next step. The defined angle determined the direction of the triblock copolymer, hence, the positioning of the beads belonged to that. At first, the beads were positioned to create a 20-bead long linear chain with determined increments for each coordinate. Then, the next linear chain was generated again by consecutively placing 20 beads in the reverse direction. Using this approach, an initial rectangle block was generated, which consisted of 200 beads that were composed of 10 linear chains (Figure 11). When the first block was formed, the next block was generated on top or the bottom according to the randomly selected direction that block would have had, and the distance between each block was set as $d = 0.90\sigma$, not as $d = 1\ \sigma$, to provide more available space in the shell for other blocks to be generated. The next block was again created following the same approach in which beads were ordered to develop linear chains recursively.

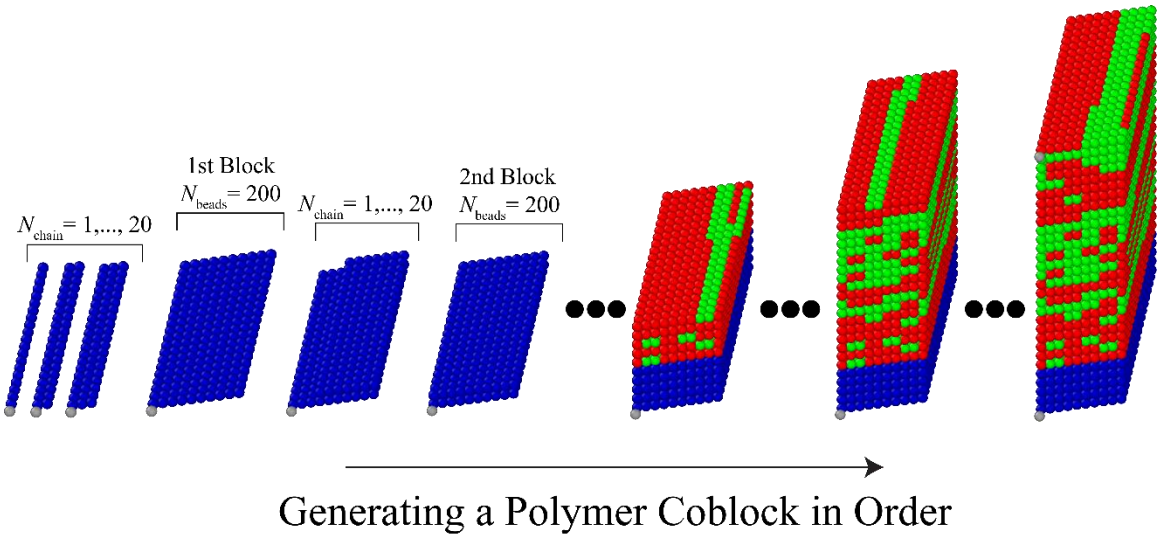

Figure 11 The representative images from a triblock copolymer explaining how each is designed.

The same approach was employed for the next polymer blocks to be placed. To ensure that blocks were not collapsing with each other, the distance parameter was set to prevent collapsing. If the radial distance between any beads of the placed polymer and the beads of triblock copolymers polymer that will be placed exceeds 1.5σ, a new triblock copolymer was generated until there was no overlapping. Additionally, random directions assigned for polymers could lead polymers to exceed the shell boundaries. Hence, an additional distance requirement was employed that if any beads of triblock copolymer exceeded the r_{sphere}= 28σ, it was not placed, and a new one was generated.

2.3.1 The polymer simulation and non-bonded interactions

The interactions between beads were modeled by Lennard-Jones (LJ) Potential, and the simulations were run using LAMMPS[61]. The simulation box dimensions were set to $60 \times 60 \times 60\sigma^{3,}$ and periodic boundaries were applied. Each bead in our simulation shared the same mass in units of LJ, m = 1. Moreover, the size of the beads is identical across all different types of beads, which is r = 1σ. The non-bonded short-range interactions were governed by shifted and truncated Lennard-Jones potential, which is,

$$V(r) = \begin{cases} u\left[\left(\frac{\sigma}{r}\right)^9 - \left(\frac{\sigma}{r}\right)^6 + v_s\right] & r \le r_c \\ 0 & r > r_c \end{cases}$$

For attractive interactions, the cutoff distance was set to $r_c = 2.5\sigma$, and the shift factor was set to $v_s = 0$. For these interactions, various attraction affinities were set between different types of beads and demonstrated in Table 1. Besides the interactions shown in the table, all other interactions were repulsive. On the other hand, for repulsive interactions, the cutoff distance and shift factor was $r_c = 2^{\frac{1}{6}}\sigma$ and $v_s = \frac{1}{4}$, respectively. The repulsive interaction strength was set to $u = 1kT$ where *k* denotes for the Boltzmann constant, and *T* for the temperature. Timestep was defined as $\Delta t = 0.005\tau$ unless otherwise noted.

The Langevin thermostat was used in our simulations with the microcanonical ensemble (*NVE)* to perform Brownian dynamics. The temperature was kept constant, and the damping factor was set to 1000τ unless otherwise noted.

Type	Interaction Energy
Euchromatin - Euchromatin	0.05 kT
Euchromatin - Facultative Heterochromatin	0.25 kT
Euchromatin – Cons. Heterochromatin	0.50 kT
Fac. Heterochromatin – Fac. Heterochromatin	0.65 kT
Heterochromatin-Shell	0.75 kT
Fac. Heterochromatin – Cons. Heterochromatin	0.85 kT
Cons. Heterochromatin – Cons. Heterochromatin	1.10 kT
Telomere-Shell	2.20 kT

Table 1 The interaction energies set for various beads in the simulations

2.3.2 The Bonded Interactions

We utilized two approaches for bonded interactions. Except for the crosslinking, the assigned bonds for other purposes followed the FENE potential[55].

$$V(r) = -0.5kR_0{}^2\ln[1-\left(\frac{r}{R_0}\right)^2]$$

The bond distance was set to r=1 and R_0=1.5, which is the maximum distance that a FENE bond can extend. For the FENE interactions between the beads composing the shell, the bond energy was set to $K = 5\frac{kT}{\sigma^2}$ to achieve a more flexible shell for extensively observing the polymer's effect on the shell. The bond energy for the chromatin and tethering was taken $K = 30\frac{kT}{\sigma^2}$. While crosslinking the chromatin beads, we preferred the harmonic bonds following the below potential,

$$V(r) = K(r-r_0)^2$$

where r_0 = 1.5σ and the bond energy was set to $K = 10\frac{kT}{\sigma^2}$.

2.3.3 Angles

While modeling the polymer flexibility provided by the harmonic angle potential. Heterochromatin fiber have a longer persistence length (i.e., the distance below which a polymer behaves like a rod), which is between 100-200 nm, whereas euchromatin is characterized by a persistence length between 10-50 nm[10]. Therefore, harmonic potentials

were only defined for facultative heterochromatin beads in our model regulated by the following equation.

$$V(\theta) = K(\theta - \theta_0)^2$$

Following this potential, the angle energy was set to $K = 1\frac{kT}{rad^2}$ while the angle was set to $\theta = 180°$.

2.3.2 Shrunking the Initial Shell Model

The initial shell had r_{sphere}= 42σ, shrunk by 10% with energy minimization simulations. The process closed the tight gaps in the surface and aimed to prevent the polymer from escaping (Figure 12). Moreover, the energy was minimized, and the beads in polymer blocks were prevented from high repulsive forces that could have resulted in breaking the FENE bond. The simulations ran for 3×10^4 simulation time, and the timestep was defined as $\Delta t = 0.001\tau$. The damping factor was 0.1τ.

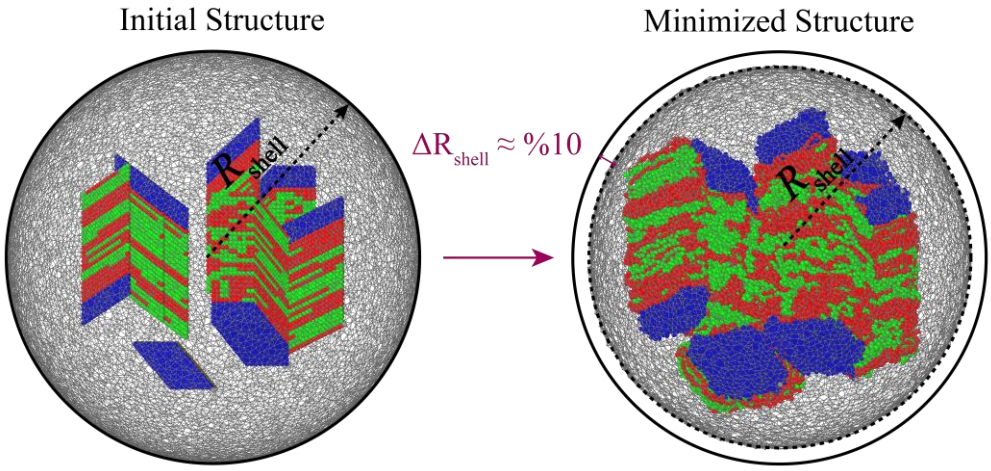

Figure 12 The initial model is minimized to prevent the tight holes and allow the chromatin beads to achieve minimized local energy.

Upon minimization, the bond network of the shell was recreated. It was aimed to decrease the width of the shell layer, which in this process, the bonds were assigned to the closer beads following the same distance criteria used for initial optimization.

$$0.60 \times factor < d < 0.80 \times factor$$

The initial number of bonds to be assigned was set to 5 for all the beads however, they could store up to 8 bonds if the minimum number of bonds could not be obtained for the neighbor. The exact distance requirement was utilized following the below condition.

$$0.80 \times factor + r_{inc} < r < 0.90 \times factor + r_{inc}$$

$$r_{inc} \leq 0.30 \times factor$$

2.3.3 Relaxing the Chromosome Copolymers

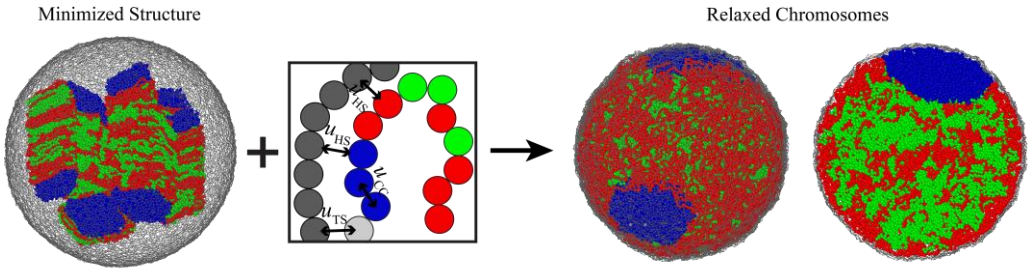

Figure 13 The minimized structures are run with attractive interactions with the shell and allow for polymer relaxation.

After the minimization simulations, the system was relaxed for $1 \times 10^{5,}$ timestep allowing for the polymer and shell relaxation (Figure 13). Relaxation simulations helped the polymer to lose the initial structure. Attractive interactions were set for the

heterochromatin and telomere beads between the shell to initiate phase separation and between each constitutive heterochromatin domain to prevent their dispersing.

2.3.4 Conventional and Inverted Nuclei Simulations

During relaxation, we allowed polymers to relax and heterochromatin domains to be located at the periphery initially. We assigned additional interaction parameters for conventional simulations, which we optimized for our model following the previous work[14] (Figure 14). All the simulations were completed in 3 replicates. The conventional simulations ran for 5×10^6 timestep. The phase separation was mainly achieved at 2.5×10^6, however, we ran the simulation until $5 \times 10^{6,}$ and during the last half period, we did our analysis since the model was in equilibrium.

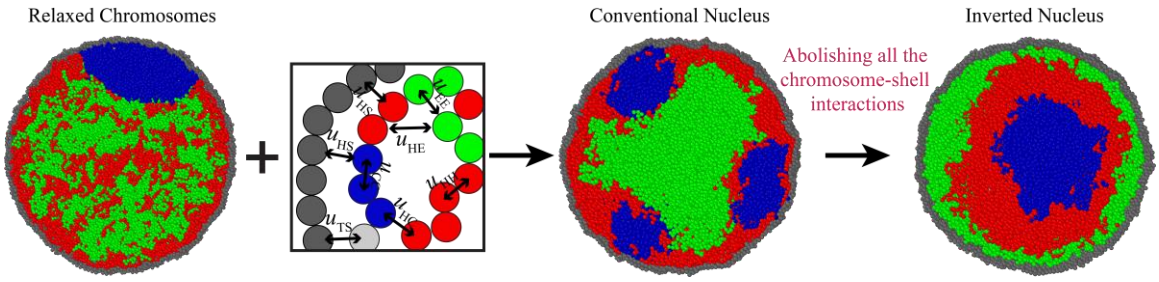

Figure 14 The conventional nucleus pattern is obtained with intra-chromatin interactions. The inverted nucleus pattern is observed by preserving the intra-chromatin interactions while removing all the shell-chromatin interactions.

After establishing the conventional nuclei and continuing with the end product, we turned off all the attractive interactions we defined between chromatin domains and the shell (Figure 14). Abolishing the interactions provided the inverted nuclei pattern consistently with the previous studies[14,30]. The inverted nuclei simulations ran for 1×10^7 timestep, and again, inversion was completed at halfway; hence, the last half period was used for analysis.

2.3.5 Pulling Simulations

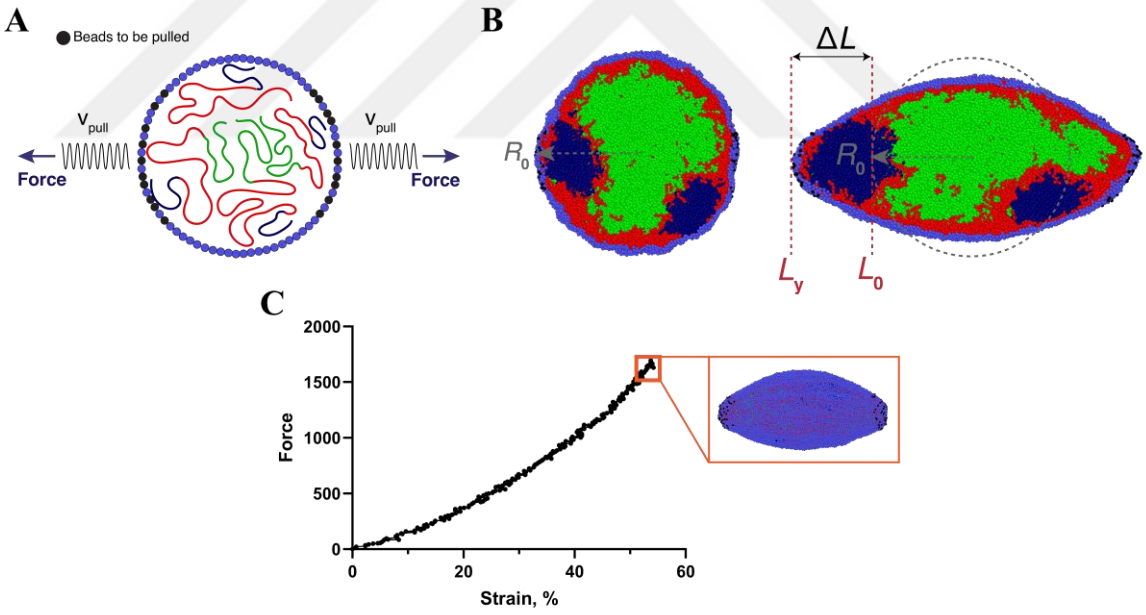

Figure 15 The pulling simulations for investigating nuclear mechanics **A)** The representative illustration defines how pulling simulations are performed. **B)** The snapshots demonstrate the deformation after pulling. **C)** A sample force-strain curve and snapshots from the deformed model.

We followed the previous studies that investigated the nuclear mechanics[31,33,35,52]. Hence, we imitated the micropipette manipulation experiments by applying pulling force on our model. We utilized the end-product of the conventional nuclei simulations to perform pulling simulations and ran the simulation using ten replicates. For each trial we conducted, the same ten replicates were used. At first, we determined random shell beads in opposite poles for pulling the shell in opposite directions (Figure 15A). We selected 80 random beads from each pole on the y-axis that satisfied, $r \geq 28\sigma$, corresponding to only a tiny fraction of the shell beads.

For this purpose, we utilized the "fix smd" command from LAMMPS packages. The force was principally applied by two springs tethered at the boundaries, $y_{spring} = 60\sigma$ and $y_{spring} = -60\sigma$. The spring constant of those springs was set to $K = 20\frac{kT}{\sigma^{2,}}$ and the constant velocity defined for pulling was $v = 0.10\frac{\sigma}{\tau}$. The simulations ran for 2×10^5 time step. The strain was increased to $\varepsilon_y \cong 80\%$ in maximum extensions.

2.4 Extracting and Analyzing the Simulation Data File

The generated trajectory file after each simulation by LAMMPS was used for each analysis mentioned in the following sections. The trajectory file contained all the coordinates of the beads in each simulation step, providing necessary information for our analysis.

2.4.1 Calculating the Volume Fraction of the Chromosome Copolymers

In our simulations, we varied three different volume fractions. To do that, the default number of triblock copolymers, $N_{\text{polymer}} = 8$, was decreased to $N_{\text{polymer}} = 6$ and $N_{\text{polymer}} = 4$. Therefore, while keeping all the shell designs and parameters the same, the initial number of triblock copolymers was altered to obtain three different volume fractions. We only calculated the final volume fraction from the default conventional nuclei simulations since altering the chromatin interactions or polymer content can change the size. The volume fraction was calculated with the equation below.

$$V_{\text{shell}} = \frac{4}{3} \times \pi \times < R_{\text{sphere}} >^3$$

$$V_{\text{chromatin}} = N_{\text{chromatin}} \times (\frac{4}{3} \times \pi \times {R_{\text{chromatin}}}^3)$$

$$V_{\text{fraction}} = \frac{V_{\text{shell}}}{V_{\text{chromatin}}}$$

where,

$$N_{\text{chromatin}} = N_{\text{polymer}} \times 6002$$

$$R_{\text{chromatin}} = 0.5\sigma$$

2.4.2 Radial Distance and Density Profiles of the Chromosome Copolymers

The chromatin distributed inside the cell nucleus varies for different cell types. We calculated the average radial distances separately for each chromatin type in our simulations at each timestep to quantitatively analyze the chromatin distribution with the following equation.

$$r_{\text{bead}} = \sqrt{x^2 + y^2 + z^2}$$

$$< r > = \frac{\sum r_{\text{bead}}}{N_{\text{bead}}}$$

The density profile was also obtained from the end configuration in our simulations to compare quantitatively with the experimentally observed chromatin density profile (Figure 16)[9,14].

$$r_{\text{bead}} = \sqrt{x^2 + y^2 + z^2}$$

The volume inside the shell is measured step-by-step following a constant increment rate, which was $k_{\text{step}} = 0.5$.

$$k = 0, k = 0.5, k = 1.0, k = 1.5, \dots, k = \max(r_{\text{shell}})$$

$$V = \frac{4}{3} \times \pi \times k^3$$

The beads in determined volume were considered accordingly by the following equation.

$$k - k_{\text{step}} < r_{\text{bead}} < k$$

Hence, the density in the determined volume was determined by the number of same-type beads positioned in the bound volume and the total number of same-type beads.

$$\rho = \frac{N_{\text{bead}}}{N_{\text{total}}}$$

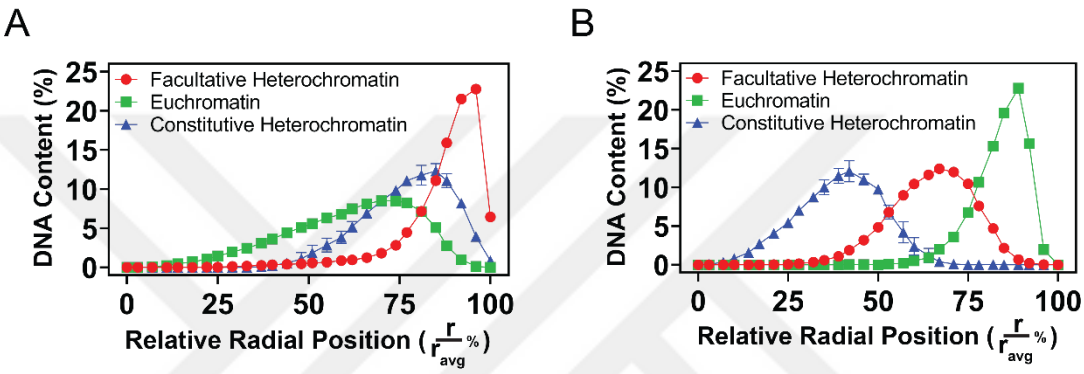

Figure 16 The density profiles of conventional and inverted nuclear architecture.

2.4.2 Investigating the Chromocenter Compaction, Separation and Radius of Gyration

Chromocenter compaction was measured by calculating the radius of gyration for each chromocenter, followed by the equation below.

$$R_g(N) = \frac{1}{N}\sum_{i=1}^{N}(r_i - r_{cm})^2$$

$$r_{cm} = \frac{1}{N}\sum_{i=1}^{N}\sqrt{x^2 + y^2 + z^2}$$

Since the calculations were done for each chromocenter, which was formed by 1000 beads of constitutive heterochromatin, the N=1000. The number of separated chromocenters was manually measured and counted from the retrieved snapshots.

2.4.3 The Nuclear Shape Fluctuation Analysis on the Shell Model

We utilize the Fast Fourier Transform algorithm (FFT)[52,53] at each timestep to calculate nuclear shape fluctuations. FFT computation was directly used from the NumPy[62] library.

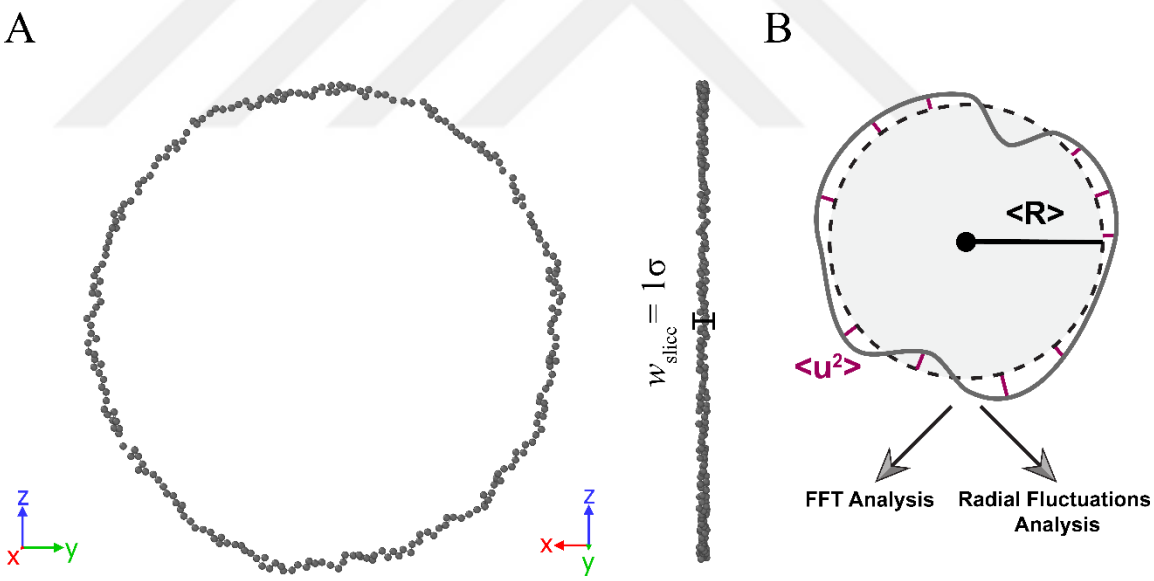

Figure 17 The nuclear shape fluctuation analysis **A)** A sample thin slice image **B)** The schematics define the method of shape fluctuation analysis.

The fluctuations were calculated from a single slice obtained from our model. Therefore, we first got a thin slice, w=1σ, on the x-axis from our model (Figure 17A). Since the shell was rotating, our thin slice contained different beads of the shell at each time step. Then,

we measured the angle from the center for each beads on the slice and ordered the beads accordingly with their angle. Lastly, we calculated the radial distance of each bead on the obtained slice with the average radial distance of the same beads. For FFT calculation, we randomly selected 230 beads since the rotation of the shell provided a different number of beads that were a member of the taken slice (Figure 17B). We ran the FFT algorithm on the obtained radial distances and corresponding angles, on 230 modes, q. We took an average of the calculations done on each timestep of the last half period of the simulations, where phase separation was finalized. As a complementary metric of bead fluctuations, we measure root-mean-squared distance, which we calculated by taking the average standard deviation of the radial distance difference with the average radial distance at each timestep at the last half period of the simulations (Figure 17B).

2.4.4 Profiling the Contact Map of Chromosome Copolymers

The genomic contact maps, Hi-C, are derived for understanding the interactions of the elements in the genome, providing an insightful understanding of 3D genome organization of different cell types or in pathological conditions such as cancer. We utilized contact maps to investigate the change in interactions of compartments after pulling simulations and for initial optimization of the genome organization.

The contact between the chromatin beads was determined by a distance parameter. For each bead, at each time step, we calculated the beads that were in contact with the selected beads one by one, following the contact condition below.

$$r_{\text{selected bead}} = \sqrt{x^2 + y^2 + z^2}$$

$$r_{\text{bead}} = \sqrt{x^2 + y^2 + z^2}$$

If,

$$r_{\text{selected bead}} - r_{\text{bead}} < 2.5\sigma$$

Then, it counted as contact, including the self-contacts as well. The contacts were deposited into the array with a size of 6002×6002 and a unit box corresponding to an interaction of the beads. Again, the recurrence was inhibited if selected; bead contact with another bead was already counted. In addition, to increase statistics, we summed up the *cis* interactions of the polymer blocks of the same chromosome type.

2.4.5 Calculating the Contact Probability

Contact probability measurements assess the chromatin interaction as a function of genomic distance within the same chromosome. We benefited from this approach to understand the conformational changes in our polymer genome after pulling experiments, and for the methodology, we were inspired by the previous study[63].

At first, we defined genomic distance intervals starting from $k = 4\sigma$, initial 4 beads contact were excluded. The initial distance was increased geometrically with the increment rate of 1.11 (i.e., 4, 5, 6, 7, 8, …, 540, 599, 665, …, 5952). The recurrent

distances were eliminated, and float numbers were rounded up. Each bead on the same polymer chain was considered, and each contact satisfying the below criteria was counted as a contact, as precisely in contact map generation.

$$r_{\text{selected bead}} - r_{\text{bead}} < 2.5\sigma$$

Within this genomic distance interval, the number of contacted beads was counted and divided by the genomic distance interval. Additionally, we also measured the contact probability separately for the euchromatin and the facultative heterochromatin domains, in which we only calculated the contact probability within these segments. For instance, to calculate the contact probability of heterochromatin, the contacts are counted only within a polymer segment of facultative heterochromatin belonging to the selected bead, excluding the distant contacts with the next segments if a different type of chromatin separates the same segments.

2.4.6 Force, Strain, and Nuclear Spring Constant Calculations

We investigated how the mechanical properties of our model were changed by measuring the deformation strain. The force values were obtained from the LAMMPS at each time step. The strain was measured by calculating the average change in the y-axis, which was the pulling direction, of the shell beads. Then, the average y-axis positions were calculated and divided by the initial average y-coordinates to measure the strain rate.

$$\varepsilon = \frac{< y_{\text{sphere}} > - < y_{\text{initial sphere}} >}{< y_{\text{initial sphere}} >} \times 100$$

Then, the graphs were generated with the strain and corresponding applied force extracted from the LAMMPS. Additionally, we calculated the spring constant of the shell through the following equation.

$$k_{\text{spring}} = \frac{F}{\varepsilon}$$

3. RESULTS AND DISCUSSION

3.1 Crosslinking Constitutive Heterochromatin Helps Separating the Chromocenters

Previous studies exhibited the role of crosslinking mediated by HP1, which involved phase separation, providing mechanical rigidity and reorganization of genome[35–37,59,64]. We seek to understand the spatial organization of the chromocenters, compacted and merged constitutive heterochromatin structures, relation with crosslinking. In our default case, conventional nucleus simulations, we assigned attractive interaction between constitutive heterochromatin domains; hence, the chromocenters became compacted. However, due to the attractive interaction, they could be merged. Therefore, we developed two crosslinking trials where the attractive interaction was depleted or present. These simulations ran for a 2.5×10^6 time step, which was sufficient to complete phase separation.

At first, the attractive interaction was kept, which was $u_{\text{H-H}}$=1.10 kT. The number of crosslinks that constitutive heterochromatin beads could assign was varied to investigate

the amount of crosslinking contribution to the chromocenter structure. Initially, the employed approach was changing the initial number of bonds each bead could assign and the probability factor that alters the number of selected beads that could assign bonds. Eventually, these two parameters changed the average number of bonds assigned in the model. Four probability parameters were selected which are $P(B)=0.2$, $P(B)=0.4$, $P(B)=0.6$ and $P(B)=0.8$. In addition, the initially assigned bonds varied for each trial per bead where $n_{bonds}=[1,2]$, $n_{bonds}=[2,3]$, and $n_{bonds}=[3,4]$. The compaction and separation of the chromocenters were visually (Figure 18) and quantitively investigated. Since combining probability with multiple bonding capacity resulted in many cases, the figures only contain the selected cases of distinct numbers of average crosslinks. In the figures, each constitutive heterochromatin domain belonging to the different chromosome polymer was assigned a color for increased visualization.

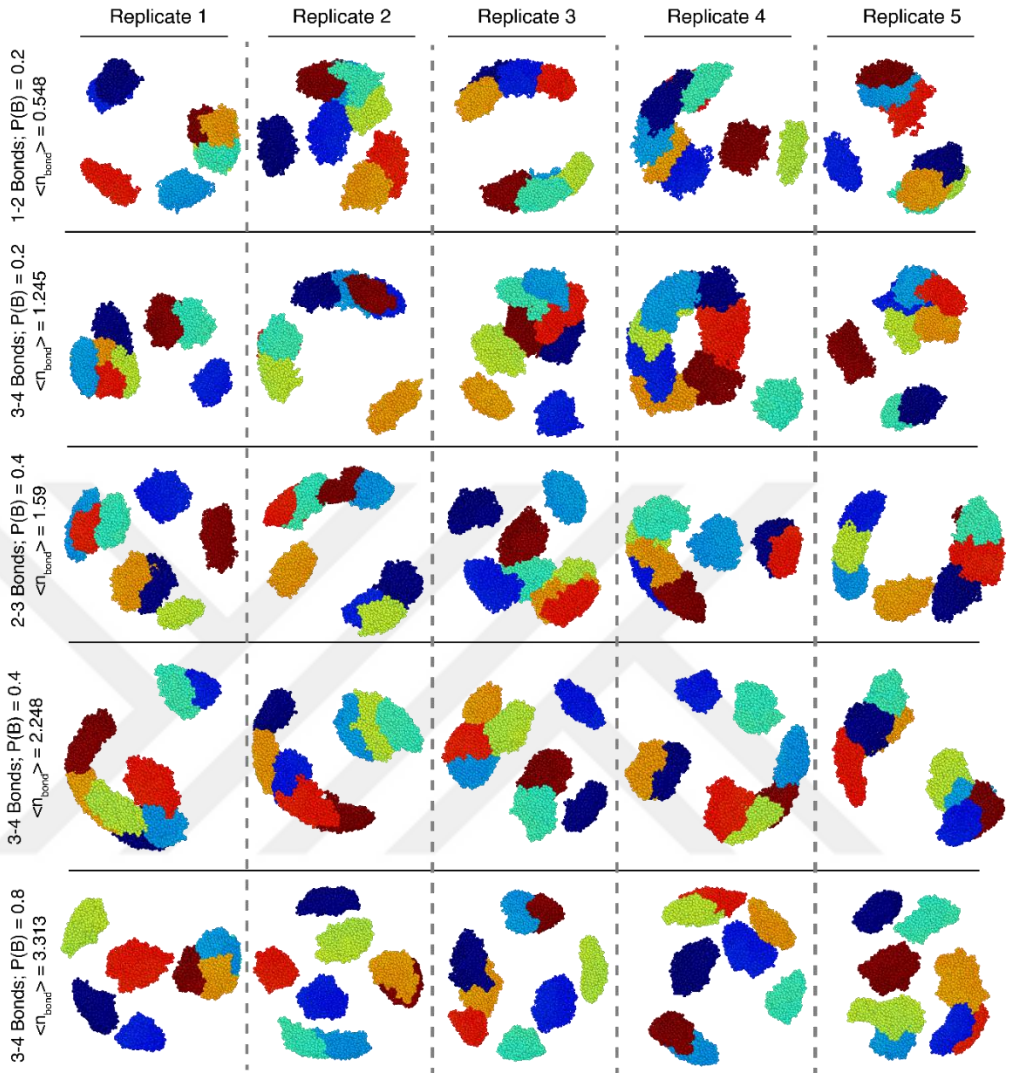

Figure 18 The compaction of the chromocenters is influenced by the amount of crosslinking.

The chromocenters became compacted as the average assigned crosslinks were increased and resulted in separation. The simulations were also analyzed to gain better insight into the compaction and separation of the chromocenters.

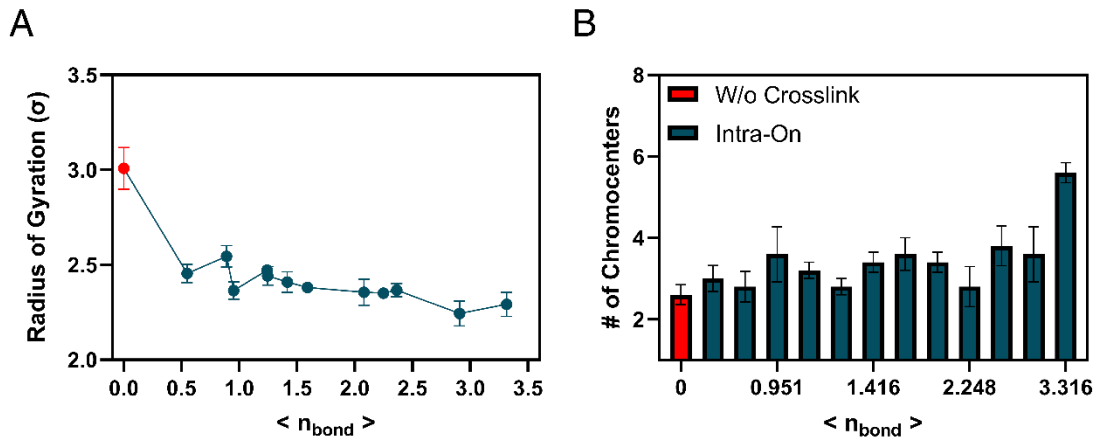

Figure 19 The compaction and separation of the chromocenters. **A)** The impact of the amount of crosslinking on the chromocenter size exhibited by the radius of gyration analysis and **B)** the number of the chromocenters formed in the simulations.

Our analysis showed that increasing the crosslinking effectively reduced the size of the chromocenters (Figure 19A). Furthermore, the crosslinking affected the size of the chromocenters and decreased the number of merged chromocenters (Figure 19B). Most segregated chromocenters were observed when average crosslinking was maximum in our cases. The number of chromocenters was dependent on initial localization as well. Since the chromosome polymers were randomly located, the probability of merging the closely located chromocenters was high. Hence, this also impacted the overall number of separated chromocenters. However, increasing the crosslinking still resulted in separated chromocenters, possibly decreasing the volume occupied by each chromocenter and their mobility, reducing the possibility of contact with other chromocenters. In addition, the crosslinking impaired the mobility and led the structure to gain a solid-like state.

3.1.1 Depleting Constitutive Heterochromatin Attractive Interactions Regulate the Chromocenter Separation Mediated By Crosslinking

The attractive interactions between constitutive heterochromatin domains were abolished in our next case. Hence, there was no attraction between any of the constitutive heterochromatin beads in this case. If there were no crosslinking when the attractive interactions were depleted, it would have resulted in the dispersion of chromocenters in which constitutive heterochromatin would have mixed with the rest of the polymer chain. Therefore, even though interactions were abolished, the crosslinking maintained the compacted structure of the chromocenters (Figure 20). In this trial, increasing the average crosslinking resulted in compaction of the chromocenters. In the cases where $<n_{\mathrm{bond}}> = 0.543$,, the structure was loose because there were no attractive interactions, only the crosslinks were keeping the structure away from dispersing (Figure 20). Therefore, increasing the crosslinks provided more compaction to each chromocenter. We also assessed the size and separation of chromocenters quantitatively.

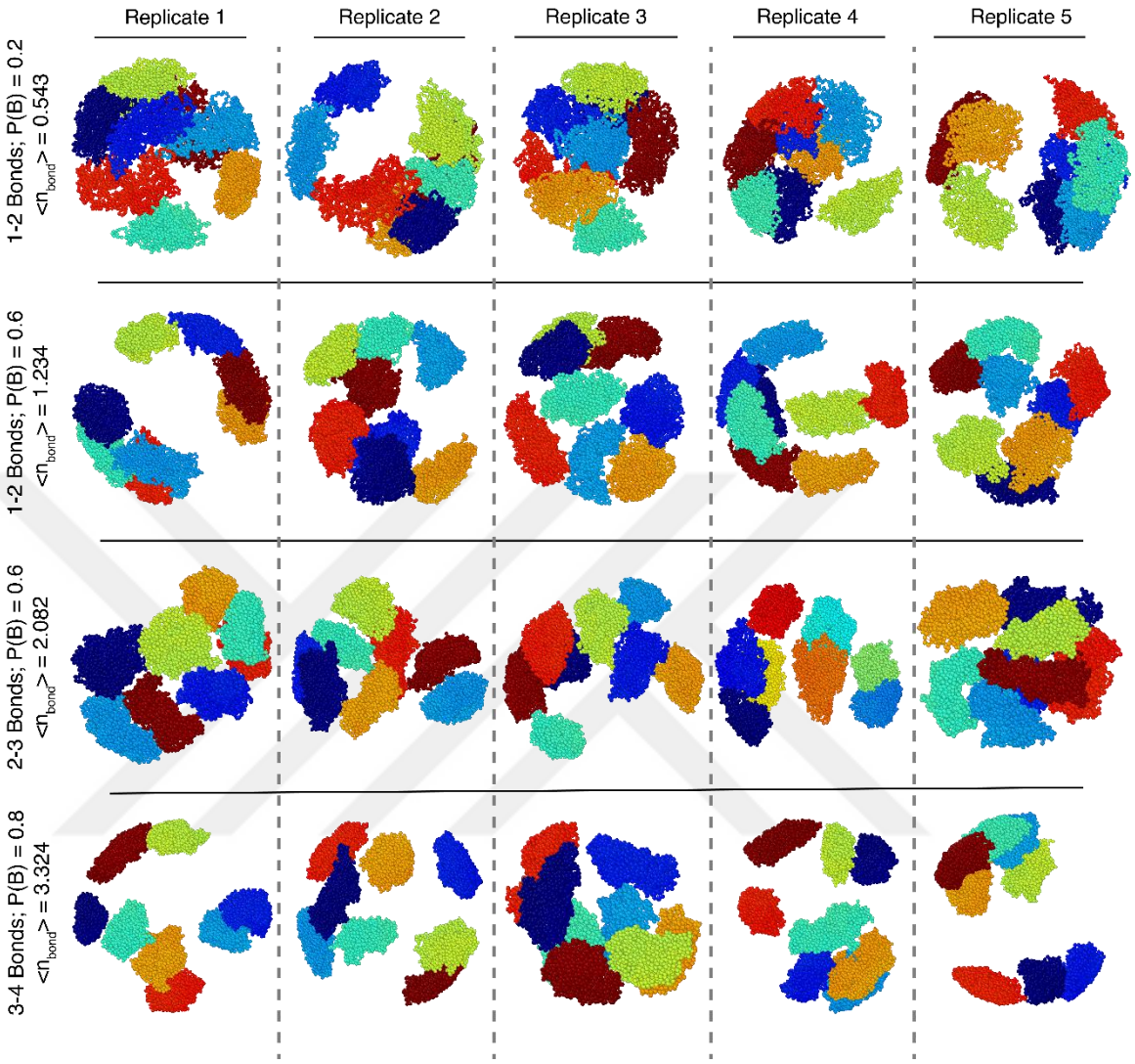

Figure 20 The simulations' snapshots show that crosslinking preserves the globular chromocenter structure and regulates the compaction.

As noted by a visual inspection, the radius of gyration calculation also revealed that chromocenters became compacted while the crosslinks were increased (Figure 21). In addition, since the attractive interactions were turned off, all the chromocenters were segregated across the elastic sphere shell.

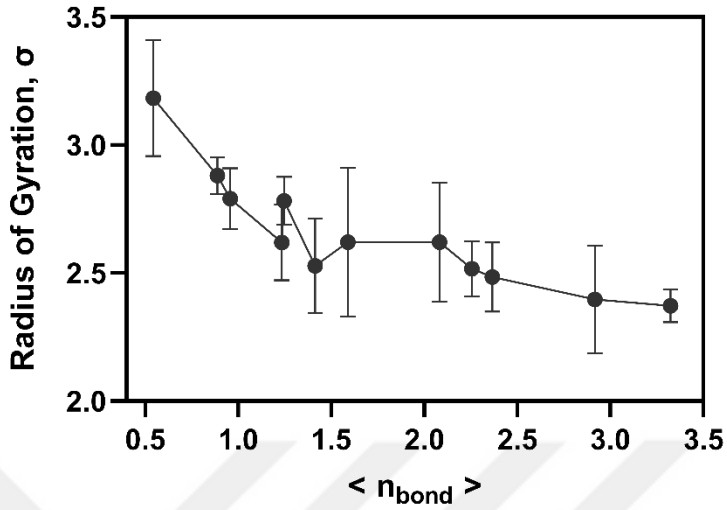

Figure 21 The radius of gyration values for the corresponding average number of bonds

3.1.2 The Kinetics of The Chromocenters Is Affected By Crosslinking

The crosslinking impacted the diffusivity of those structures. The radial positioning of each constitutive heterochromatin bead was calculated to understand how the kinetics altered. For this analysis, we only compared the n_{bonds}=[2,3] and P(B)=0.2 cases, which provided sufficient structural preservation, $<n_{\text{bond}}> \approx 0.89.$, which did not lead to extreme compaction. In addition, these conditions made default for our simulations described in the next section.

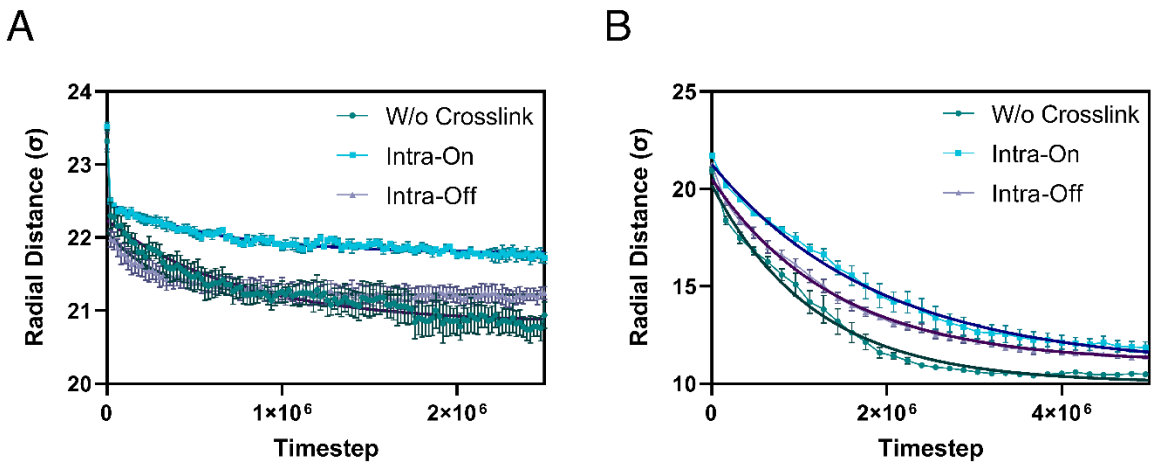

Figure 22 The crosslinking impairs the mobility A) in conventional and B) inverted nucleus simulations.

The average radial distance of constitutive heterochromatin revealed that the diffusivity of chromocenters decreased in conventional nucleus simulations. When there were no attractive interactions between constitutive heterochromatin, intra-off case, the chromocenters diffused closer distances from their initial position. At the same time, phase separation occurred and maintained their average radial position (Figure 22A). When the attractive interactions were present for constitutive heterochromatin, the mobility of chromocenters also reduced however, the chromocenters, in this situation, remained closer to the nuclear periphery and merged to form multiple chromocenters.

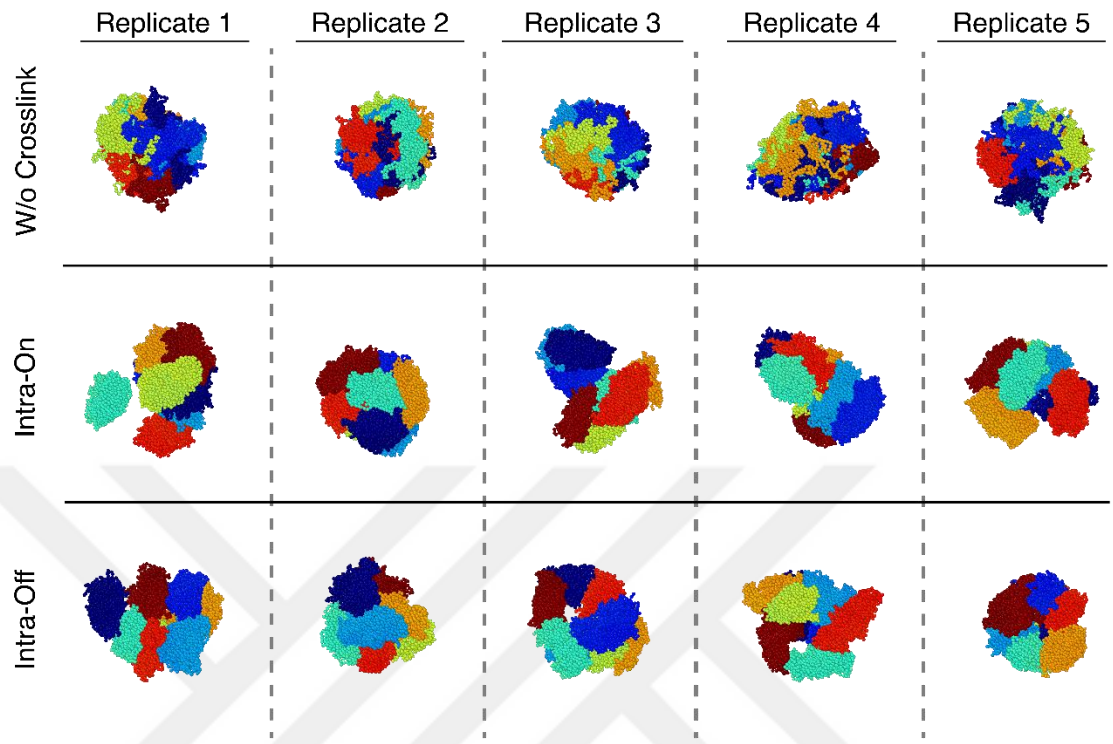

Figure 23 The chromocenters are dispersed and mixed without crosslinking during inversion, demonstrated by snapshots from the default parameters, n_{bonds}=[2,3] and P(B)=0.2.

In inverted nucleus simulations, the attractive interactions between constitutive heterochromatin were present since eliminating the attractions could not form an inversion pattern. Hence, the legend is written according to the conventional nucleus simulations since the end-product of the conventional nucleus was run in inverted nucleus simulations. The extracted radial positions revealed that crosslinking limits the diffusivity compared to without crosslink simulations (Figure 22B). In the intra-off case, the chromocenters individually moved toward the center and merged with other chromocenters, whereas in the intra-on case, some were already merged. This could explain the deviancy in each case. In addition, the chromocenters mixed without crosslinking, whereas crosslinking

maintained the structure and led to the merging of the chromocenters (Figure 23). Overall, our results indicate that crosslinking contributes to the compaction and separation of the chromocenters.

3.2 **The Polymer Volume Fraction Impacts the Nuclear Shape Fluctuations**

The nuclear morphology was shown to be influenced by the chromatin itself and the volume it occupies[41–43]. Moreover, it was revealed that chromatin's phase separation was influenced by the volume it occupies[65]. We varied the chromatin volume fraction within the simulated nucleus to understand the interplay between chromatin organization and nuclear shape (See 2.4.1). In the simulations, the 3 volume fractions were set, φ=23%, φ=19%, and φ=14%. The conventional nucleus simulations were run with those volume fractions, and inverted nucleus simulations were run with the conventional nucleus.

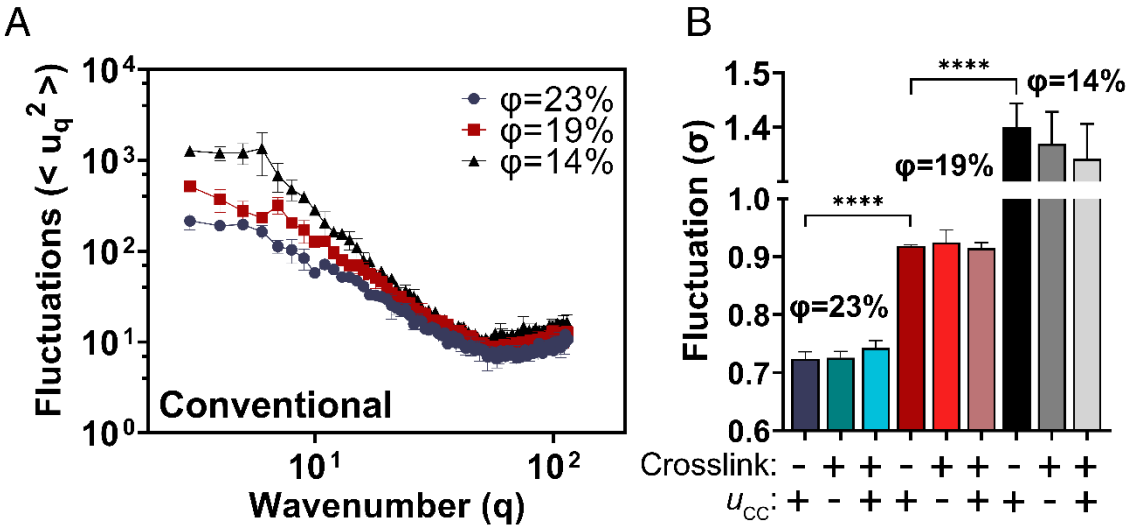

Figure 24 The nuclear shape fluctuations influenced by volume fraction **A)** The nuclear shape spectra of various volume fractions **B)** RMS radial deviations of various volume

fractions and crosslinking in conventional nucleus simulations. An unpaired two-tailed Student's t-test was conducted for statistical analysis.

In conventional nucleus simulations, decreasing the volume fraction and chromatin density, increased the amplitudes of nuclear shape fluctuations, especially at long wavelengths, corresponding to small wavenumbers, q (Figure 24A). Moreover, we next investigated the RMS radial deviations across three volume fractions and included the crosslinking as well. The results revealed that decreasing volume fraction leads to increased fluctuations in all cases independent of crosslinking. Moreover, we studied simulations to investigate the role of crosslinking on nuclear shape fluctuations with and without crosslinking, employing the same approach described in the previous section. Our result exhibited that; the mean fluctuation amplitude was unresponsive to crosslinking. Even though the spatial organization of the heterochromatin was affected by crosslinking, the fluctuations were insensitive to crosslinking of constitutive heterochromatin.

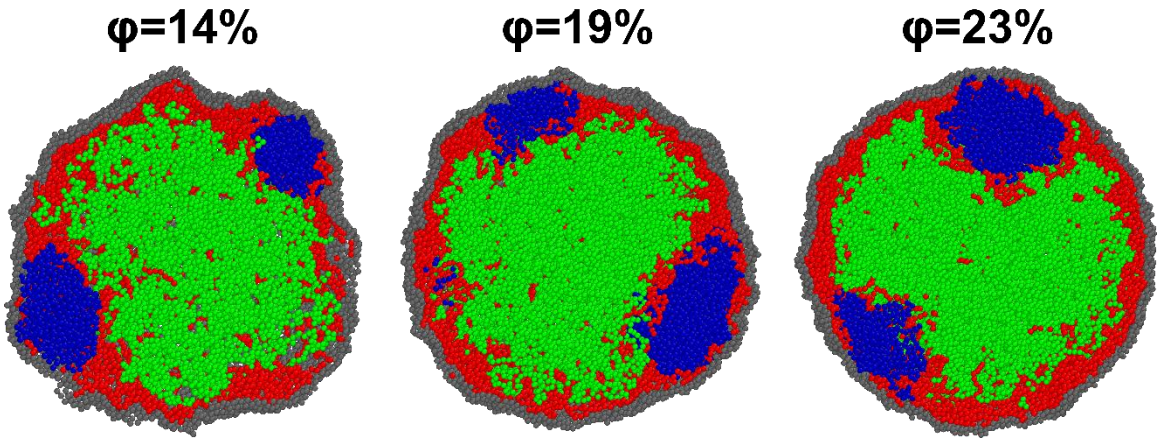

Figure 25 The snapshots of our conventional nucleus model under different chromatin densities.

Next, we investigated the effect of volume fraction by running inverted nucleus simulations where heterochromatin-shell interactions were depleted. This depletion results in heterochromatin relocating in the nuclear interior (Figure 25).

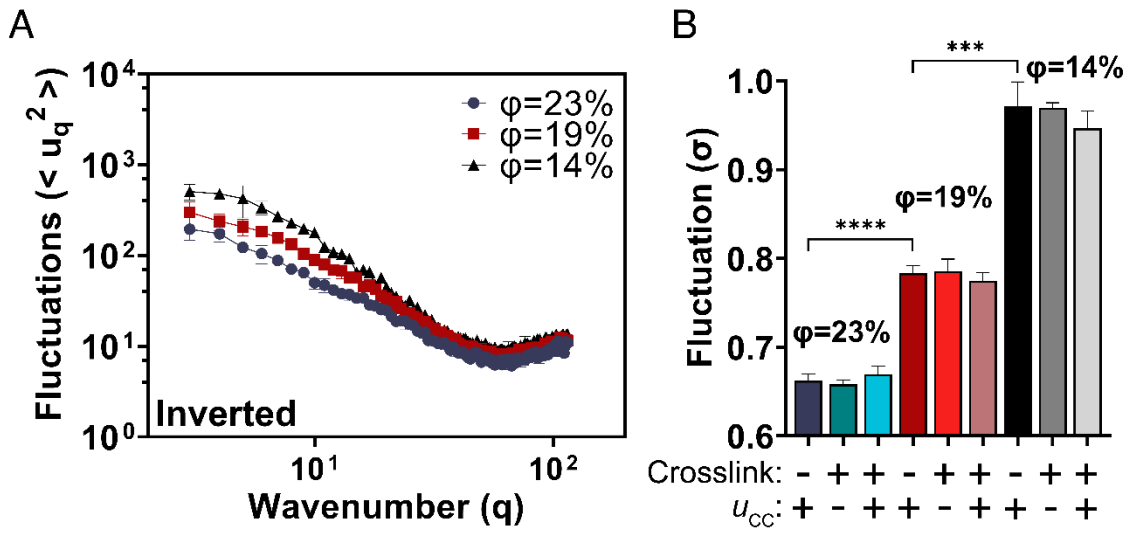

Figure 26 A) The nuclear shape fluctuations and **B)** RMS radial deviations of various volume fractions and crosslinking in inverted nucleus simulations. An unpaired two-tailed Student's t-test was conducted for statistical analysis.

In inverted nucleus simulations, the fluctuations were significantly decreased compared to those in conventional nucleus simulations (Figures 26A & 27). In addition, RMS radial deviations exhibited reduced fluctuations, and crosslinked chromocenters did not contribute to fluctuations. For inversion to occur, all heterochromatin-shell interactions are depleted, hence, the absence of heterochromatin-shell interactions can explain the reduced nuclear shape fluctuations. Altogether, our simulations propose that the volume fraction, chromatin density, is crucial for restraining the shell fluctuations. In addition,

heterochromatin-shell interactions influence the nuclear shape fluctuations via the peripherally located heterochromatin.

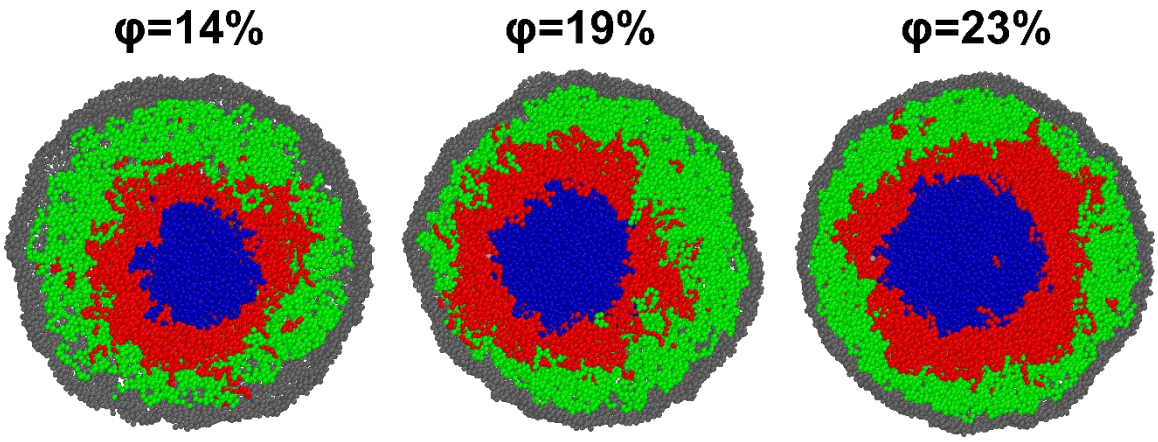

Figure 27 The inverted nucleus images from our model under different volume fractions

3.3 Chromatin-Lamina Interactions Governs Nuclear Morphology

There is evidence that heterochromatin-lamina interactions are crucial for regulating nuclear morphology[45,48,50,66]. The epigenetic patterning on chromatin determines the localization. H3K9me3 labeled constitutive heterochromatin localizes to the nuclear lamina with HP1 as a mediator binding to PRR14[67] and LBR[46]. The facultative heterochromatin marked with H3K9me2 can also attach to the nuclear lamina, forming a uniform layer at the periphery via CEC[46,47]. Disruption in lamin interactions of different chromatin was shown to influence chromatin organization[14,30,46,47] and morphology[35,45]. We investigated how the heterochromatin-lamina interactions regulate

the nuclear shape's fluctuations by altering the interaction energies under different chromatin densities, influencing the fluctuations.

3.3.1 Facultative Heterochromatin-Shell Interactions Regulate The Nuclear Shape Fluctuations

To study the role of facultative heterochromatin attraction in nuclear shape fluctuation, we varied the attraction affinities while maintaining the default attraction affinity of constitutive heterochromatin to the shell. The nuclear shape fluctuation analysis revealed that increasing the strength of facultative heterochromatin-shell interactions led to nuclear deformations (Figure 26). In addition, the fluctuations were also contributed by volume fraction. In the defined chromatin densities except φ=23%, decreasing the attraction affinity by half from the typical value, from u_{HS}=0.75 kT to u_{HS}=0.375 kT, reduced the nuclear shape fluctuations in conventional nucleus simulations. Moreover, the organization inside was also changed, so the facultative heterochromatin could not form the peripheral layer. Instead, these domains surrounded the constitutive heterochromatin, forming local phases inside (Figure 27A). The reduction in the fluctuations was more significant when the volume fraction was set to φ=14%. After that, the attraction affinities were elevated via doubling, u_{HS}=1.50 kT, or quadrupling, u_{HS}=3 kT, and the typical attraction affinity, u_{HS}=0.75 kT. We observed that increasing the strength of the attraction increased the nuclear shape fluctuations across all modes demonstrated by the shape fluctuation spectrum (Figure 28A, B, C & Figure 29B, C). Moreover, higher attraction strength's impact became more prominent when the volume fraction was decreased, in

which the nuclear deformations were significantly apparent (Figure 29B, C). When volume fractions were set to φ=19% and φ=14%, we saw increased shell shape fluctuations additionally in higher modes, corresponding to short wavelengths.

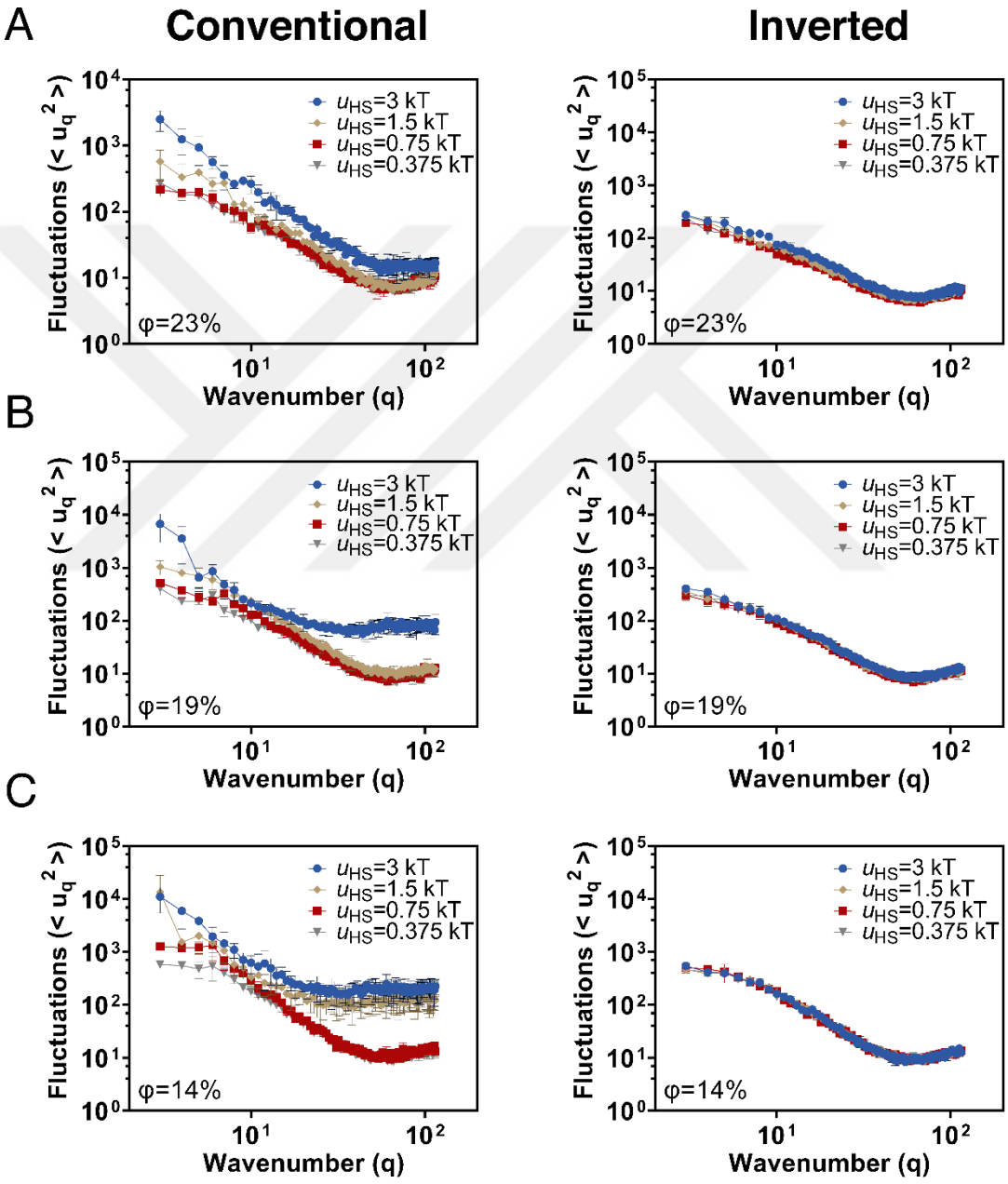

Figure 28 Facultative heterochromatin-shell attraction strength regulates the nuclear shape fluctuations together with volume fraction, **A)** φ=23%, **B)** φ=19%, and **C)** φ=14%.

These observations were consistent with the alteration in the shape morphology, in which we observed multiple localized folding on the shell (Figure 29B). In addition, when φ=14%, the difference between u_{HS}=1.50 kT and u_{HS}=3 kT was smaller compared to the other chromatin density trials, φ=19% and φ=23%, when u_{HS}=1.50 kT and u_{HS}=3 kT. Since φ=14% was a considerably low volume fraction, the impact of those attraction energies was not far from each other (Figure 28C). Therefore, the heterochromatin-shell interactions together with volume fraction govern the nuclear shape fluctuations.

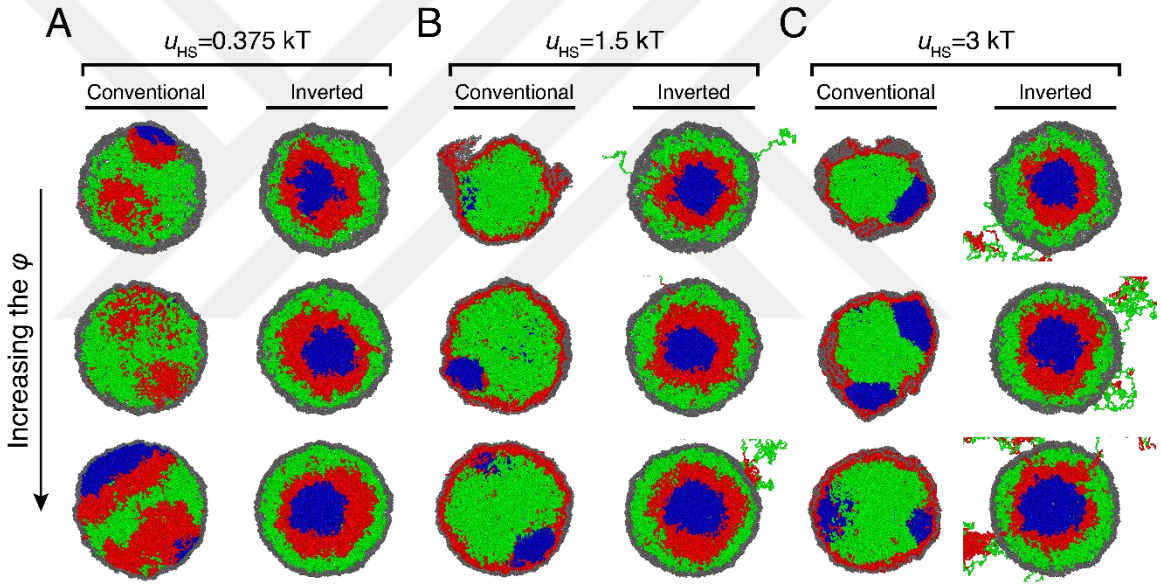

Figure 29 The conventional and inverted nucleus simulations snapshot from the model under different chromatin densities and various facultative heterochromatin-shell attraction strengths **A)** u_{HS}=0.375 kT **B)** u_{HS}=1.50 kT and **C)** u_{HS}=3 kT.

In inverted nucleus simulations, the nuclear shape fluctuations were dramatically decreased consistently with our previous results (Figure 28A, B, C & Figure 29A, B, C). In addition, the difference between shape fluctuations among the different volume

fractions was solely due to the chromatin density. Therefore, our results demonstrated the effect of volume fraction, although the heterochromatin-shell interactions were abolished. Furthermore, the depletion of attraction affinity between heterochromatin and shell recovers the normal morphology where the deformations were eliminated (Figure 29 A, B, C). In some cases, some polymer chains escaped (Figure 29B, C). In conventional nucleus simulation, few beads escaped during minimization or relaxation; however, due to the heterochromatin-shell interactions, those beads bound to the shell at the outside. When the heterochromatin-shell interactions were depleted, the escaped beads left from the surface, and the rest of the following chain partially escaped as well. Thus, these results further demonstrated that the global chromatin organization mediated by heterochromatin-shell interactions was critical for the nuclear shape fluctuations.

3.3.2 Constitutive heterochromatin-shell interactions alter the genome organization and shape's fluctuations

Next, we investigated the role of constitutive heterochromatin on the shell's shape fluctuations. We employed the same approach for this study, where the attraction strength was identical for the facultative heterochromatin while this affinity varied for the constitutive heterochromatin. Conventional nucleus simulations depicted the influence of constitutive heterochromatin in nuclear shape fluctuations (Figure 30A, B, C & Figure 31A, B, C). Decreasing the typical attraction affinity, u_{HS}=0.75 kT, by half did not influence the nuclear shape fluctuations in every trial of various volume fractions (Figure 30A, B, C).

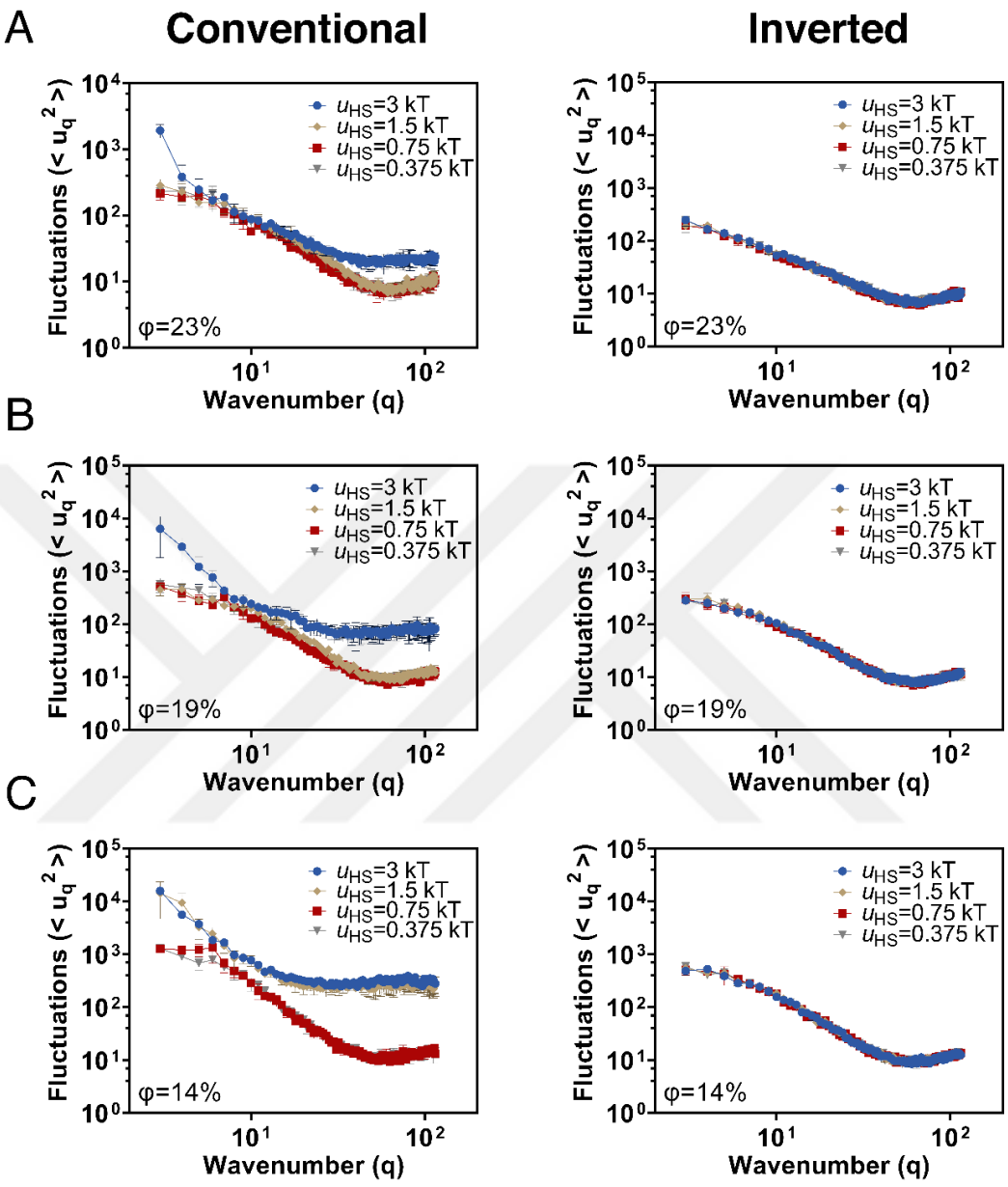

Figure 30 The constitutive heterochromatin-shell attraction strength regulates the nuclear shape fluctuations together with chromatin density, **A)** φ=23%, **B)** φ=19%, and **C)** φ=14%.

However, the contacts between constitutive heterochromatin and the shell were increased, which the facultative heterochromatin formed a uniform layer on the periphery while

excluding the constitutive heterochromatin (Figure 31A). In addition, doubling the default strength of the attraction to u_{HS}=1.50 kT slightly affected the fluctuations except when the volume fraction was set to φ=14% (Figure 28C). When φ=14%, setting u_{HS}=1.50 kT resulted in increased fluctuations in all wavenumbers, showing a similar impact as u_{HS}=3 kT. Again, at this low volume fraction, defining the affinity to u_{HS}=1.50 kT was sufficient to deform the morphology identical to when the attraction was set to u_{HS}=3 kT. In addition, the compacted constitutive heterochromatin chromocenters were dispersed in various chromatin density cases and located at the periphery as a uniform layer (Figure 31B). Hence, disrupting the compacted state of chromocenters altered the organization and the morphology. Further increasing the strength of attraction to u_{HS}=3 kT modified the amplitude and spectrum of shape fluctuations.

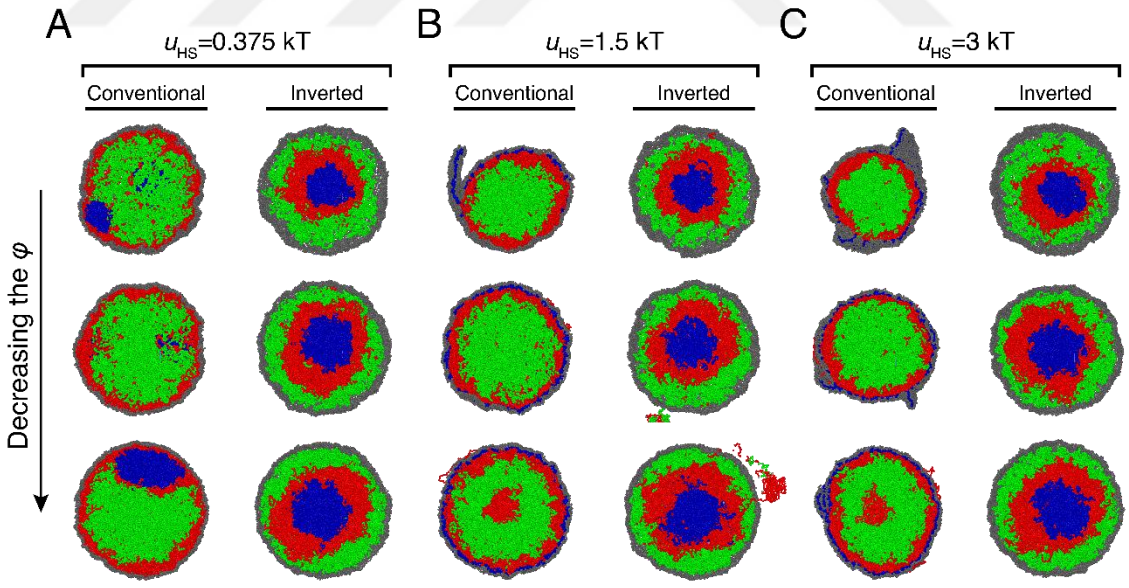

Figure 31 The conventional and inverted nucleus simulations snapshots from the model under different volume fractions and various constitutive heterochromatin-shell attraction strengths **A)** u_{HS}=0.375 kT **B)** u_{HS}=1.50 kT and **C)** u_{HS}=3 kT

Moreover, for all the attraction affinities, we observed an increase in the fluctuations as the chromatin density decreased (Figure 30A, B, C & Figure 31A, B, C). In addition, the same organization of the polymers was observed as in the u_{HS}=1.5 kT trial (Figure 31C). Thus, this explains the role of volume fraction and its additive effect on nuclear shape fluctuations as heterochromatin attraction with the shell strengthens. The volume fraction suppresses the fluctuations where increased heterochromatin attraction strength with the shell exhibited the opposite effect in our simulations. Also, inversion was accompanied by the critical reduction in the nuclear shape fluctuations, recovering the normal nuclear morphology (Figure 30A, B, C & Figure 31A, B, C). Still, the chromatin beads escaped from the interior due to the initially located beads at the outside surface of the shell, leaving as the heterochromatin-shell interactions were abolished (Figure 31B). Again, the fluctuations in inversion were only influenced by the chromatin density. This supports our previous conclusions that the heterochromatin-shell interactions regulate the shell's shape fluctuations. Overall, our simulations showed that the interaction of the constitutive heterochromatin with the shell can also regulate the nuclear morphology.

3.3.3 The Additive Regulation of Shape's Fluctuations by Both Heterochromatin Types

Subsequently, we simulated the contribution of both heterochromatin types in our model. The findings were consistent with our previous trials in which the strength of heterochromatin attraction to the shell influenced the nuclear shape fluctuations; however, the fluctuations spectrum differed (Figure 32A, B, C & Figure 33A, B, C). When the

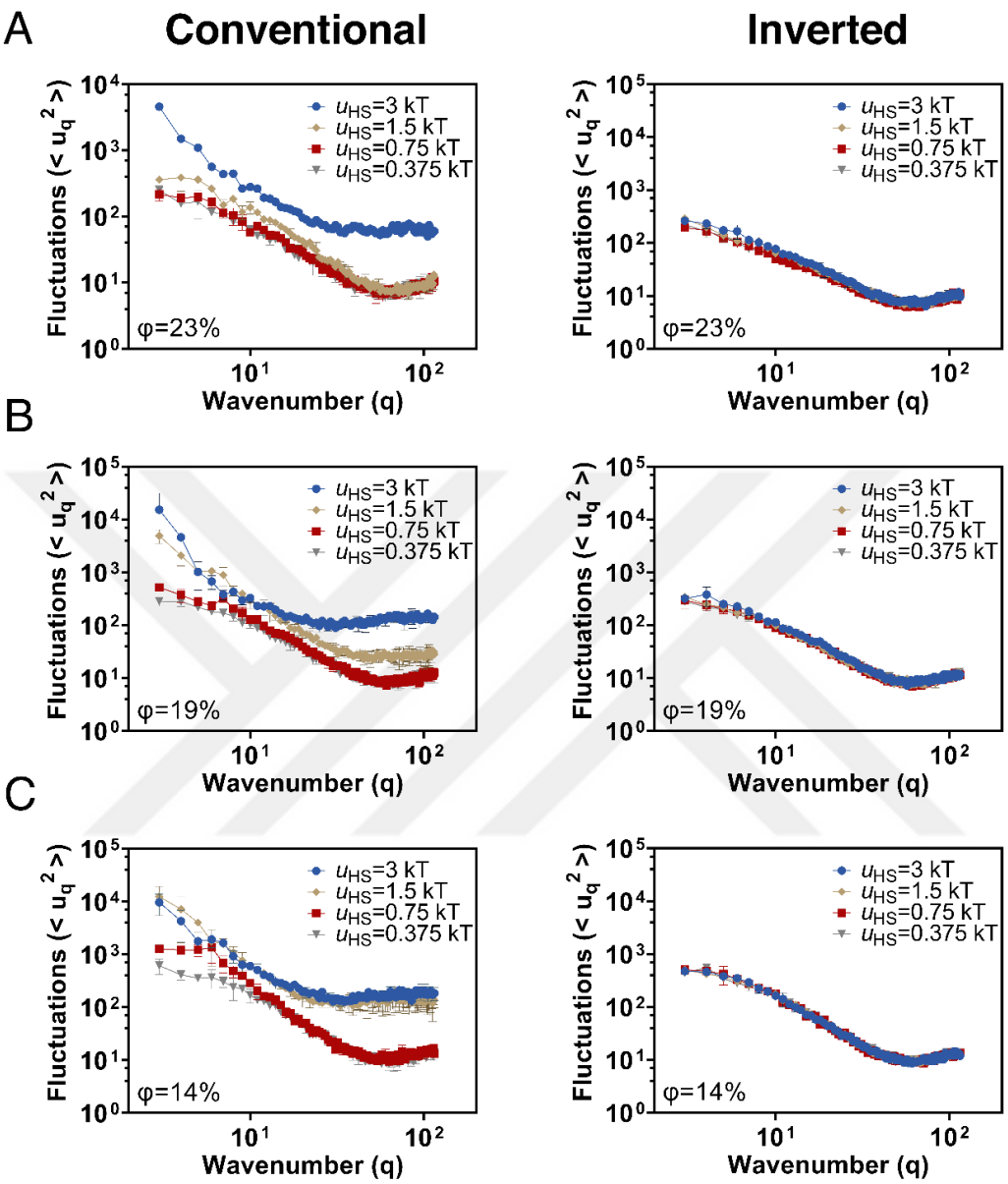

Figure 32 The heterochromatin-shell attraction strengths collectively regulate the nuclear shape fluctuations while the volume fraction **A)** φ=23%, **B)** φ=19%, and **C)** φ=14% suppresses the fluctuations.

attraction strength was set to u_{HS}=0.375 kT, the amplitude of the fluctuations was similar to simulations ran with u_{HS}=0.75 kT, however, with altered chromatin organization (Figure 31A). However, the difference in fluctuations between each was relatively the same as the volume fraction decreased (Figure 31A). Moreover, setting the affinity

u_{HS}=1.5 kT increased the amplitudes in higher and lower wavenumbers, except when φ=23% (Figure 31B). In the previous trials, setting u_{HS}=1.5 kT did not alter the amplitudes in high wavenumbers when φ=19% (Figure 30B & 28B), thus, this can describe the collective impact of both heterochromatin (Figure 33B). Increasing the attraction strength to u_{HS}=3 kT drastically increased the nuclear shape fluctuations in every corresponding wavenumber (Figure 32A, B, C & 33A, B, C).

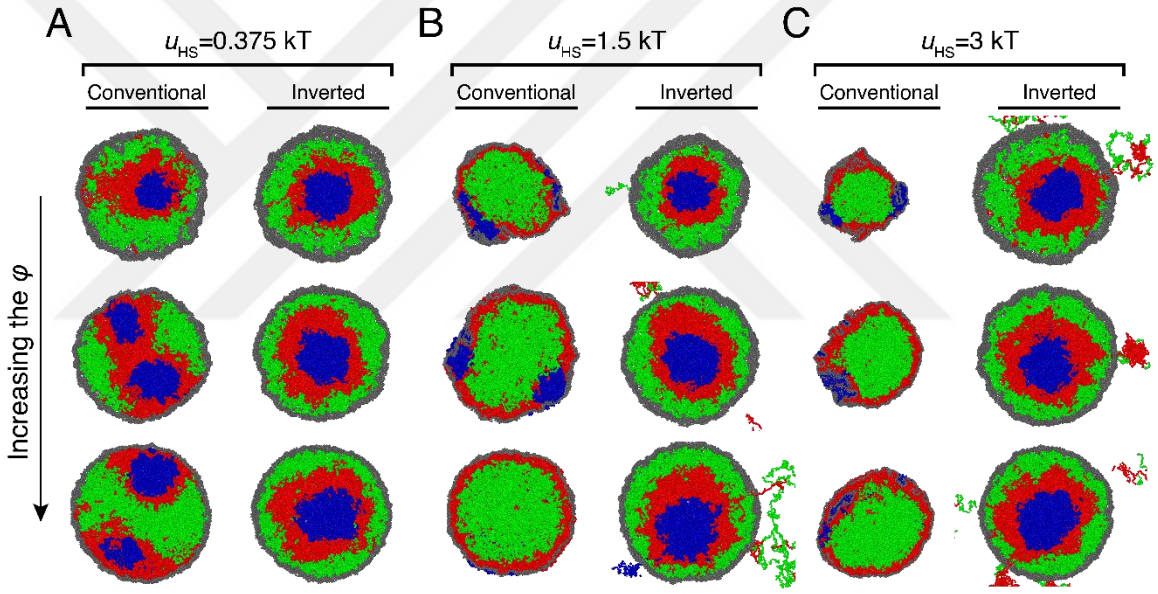

Figure 33 The images obtained from our model with conventional and inverted nucleus patterns under different chromatin densities varied both heterochromatin-shell interactions **A)** u_{HS}=0.375 kT **B)** u_{HS}=1.50 kT and **C)** u_{HS}=3 kT.

Even when the volume fraction was highest, u_{HS}=3 kT was efficacious enough to deform the nuclear morphology majorly as in our previous trials, exhibiting the additive effect that emerged from both heterochromatin. As the chromatin density decreased, the volume of the shell also reduced due to the stronger heterochromatin-shell interactions leading to

a collapse of the shell (Figure 33B, C). Furthermore, the reduction in nuclear shape fluctuations due to the inversion did not contradict our previous observations (Figure 32A, B, C & Figure 33A, B, C). Still, the abnormal morphology was rescued, and increased nuclear shape fluctuations were observed while the volume fraction decreased.

3.3.4 The impact of different chromatin types is not dominant on each other

We also evaluated the fluctuations by RMS radial deviations and compared each simulation trial's mean fluctuation. In conventional nucleus simulations, when the chromatin density was φ=23%, as shown by shape fluctuations, increasing the attractions with the shell did not drastically alter the fluctuations for each case until u_{HS}=3 kT. When heterochromatin interactions, either facultative or constitutive or both, between shell were set to u_{HS}=3 kT, we observed a critical increase in the fluctuations (Figure 34A). The effect was more substantial when the attraction of both heterochromatin with shell was increased compared to the other two trials. In inverted nucleus simulations, even though the heterochromatin-shell interactions were turned off, there was a slight increase in the fluctuations (Figure 34B). This outcome can be attributed to the various deformed morphologies in conventional nucleus simulations, which alter from different states through inversion and random shell network that varies for each replicate. When the chromatin density was φ=19%, the fluctuations were significantly increased through increased heterochromatin-shell attraction starting with u_{HS}=1.5 kT (Figure 34B). Again, the fluctuations were drastically higher than in the other trials when only one of the heterochromatin-type interactions varied. If the pattern was inversed, the fluctuations were

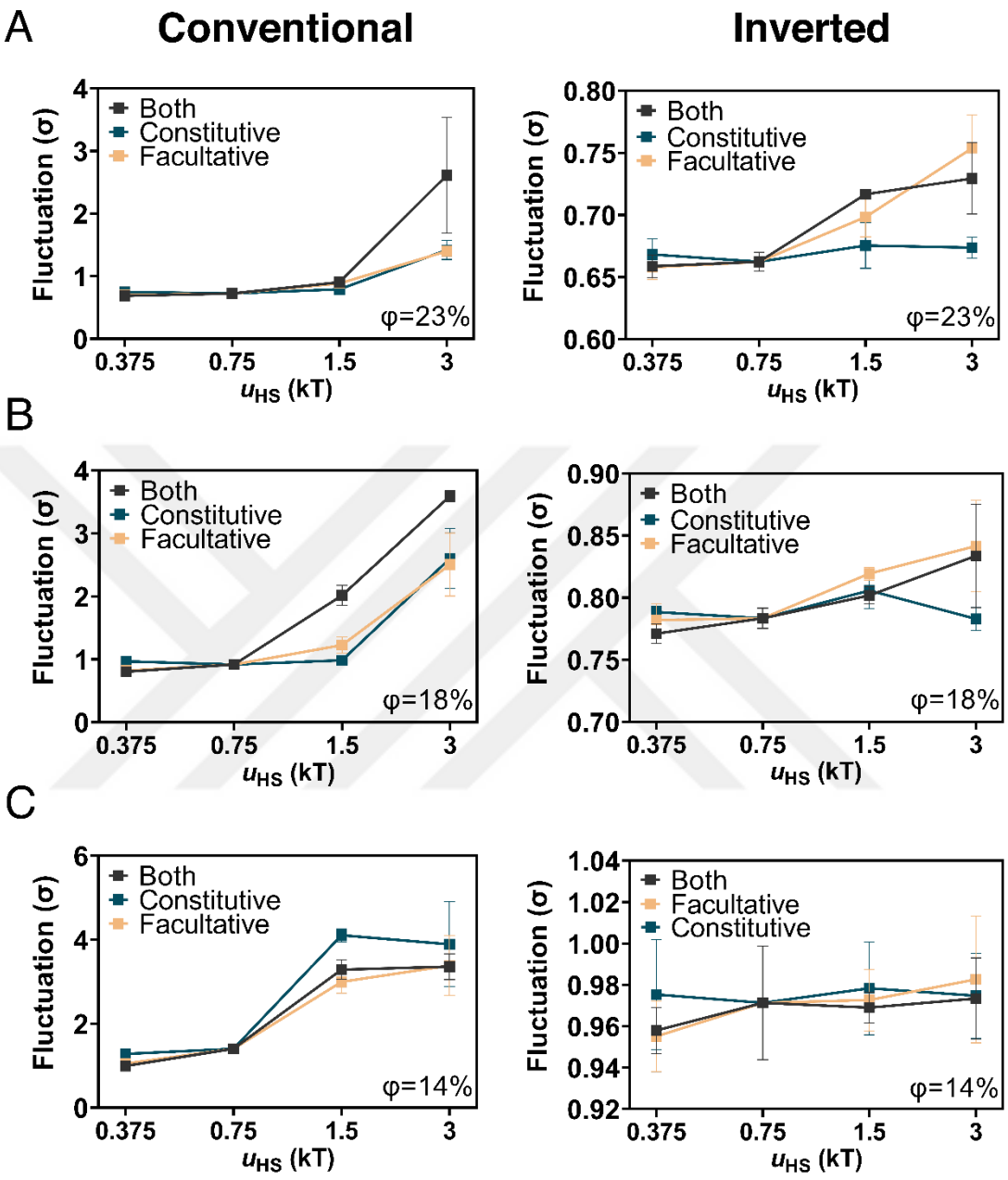

Figure 34 The images obtained from our model with conventional and inverted nucleus patterns under different chromatin densities varied both heterochromatin-shell interactions **A)** u_{HS}=0.375 kT **B)** u_{HS}=1.50 kT and **C)** u_{HS}=3 kT.

critically reduced (Figure 32B), and the variations in the fluctuations still can be attributed to the reasons that were explained for φ=23%. In the last volume fraction trial, the

fluctuations between all cases were close except u_{HS}=1.5 kT (Figure 34C). Setting the interaction to u_{HS}=1.5 kT between constitutive heterochromatin and the shell resulted in higher fluctuations than in other trials. In inverted nucleus simulations, all fluctuations were drastically reduced (Figure 34C). Our simulation results demonstrated that the heterochromatin-shell interactions were critical for regulating nuclear shape fluctuations while were not dominated by one or other chromatin types and the volume fraction suppressing the fluctuations.

3.4 Interplay between heterochromatin-heterochromatin and heterochromatin-shell interactions govern phase separation and influence nuclear shape fluctuations.

The chromatin's spatial organization is affected by the competition between heterochromatin's self-interaction and its interaction with nuclear lamina[65,68]. Impact of this competition on nuclear shape fluctuation is uncertain. Thus, we studied the facultative heterochromatin's self-interaction as well as its interaction with the nuclear shell to reveal the role of this competition in between. For that purpose, we investigated heterochromatin-shell and heterochromatin's self-interaction energies at various strengths and under different volume fractions.

Our investigation started by selecting the chromatin density as φ=23% with conventional nucleus simulations. Firstly, the strength of the heterochromatin with shell was reduced to half, u_{HS}=0.375 kT. When the facultative heterochromatin self-affinity was abolished, the

phase separation could not occur properly, which the facultative heterochromatin diffused across the shell (Figure 35A). Increasing the self-affinity to the default value, u_{HH}=0.65 kT, led to the compaction of the facultative heterochromatin, but due to the low heterochromatin-shell interactions, the facultative heterochromatin was not located at the periphery meanwhile, the nuclear shape fluctuations were slightly increased.

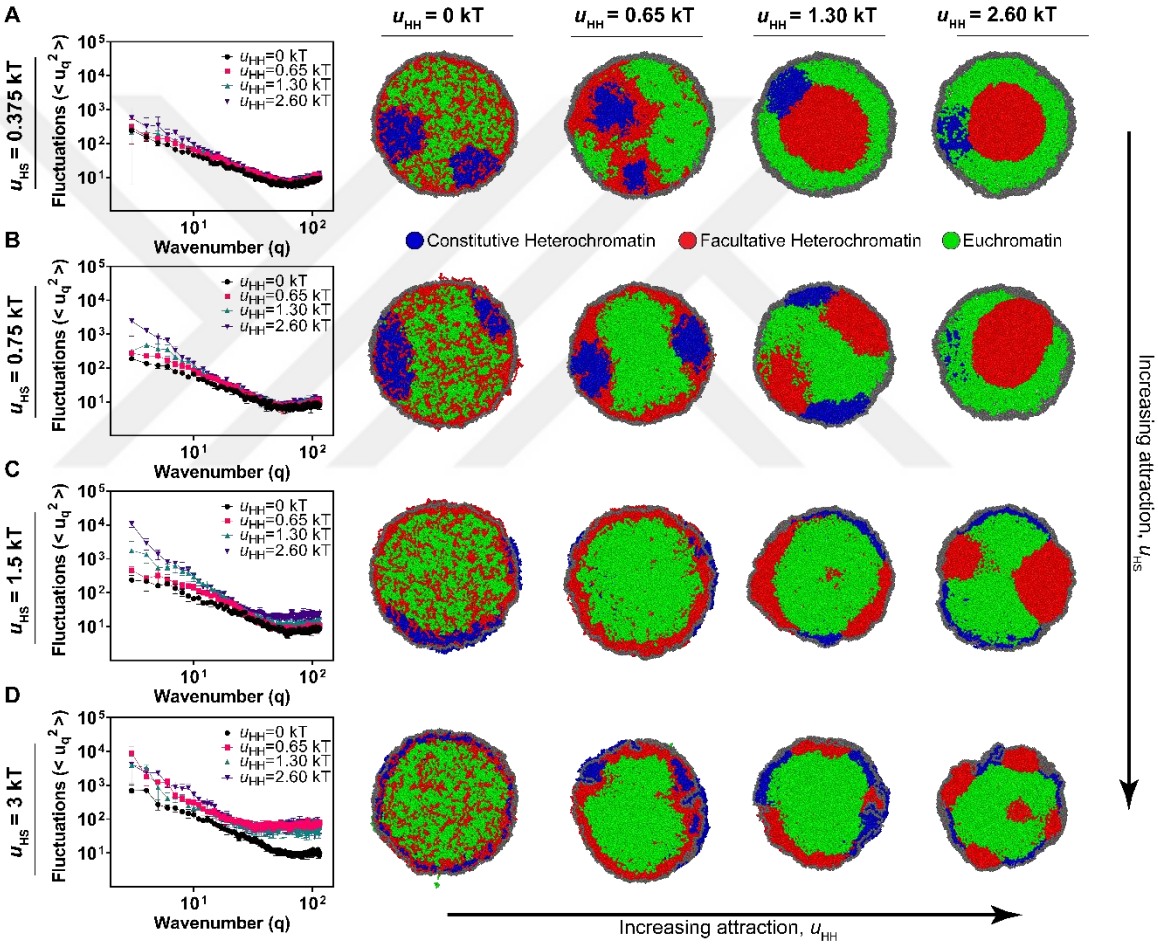

Figure 35 The images and fluctuation analysis extracted from our model with conventional nucleus organization with various facultative heterochromatin self-affinity strengths and heterochromatin-shell interactions **A)** u_{HS}=0.375 kT **B)** u_{HS}=1.50 kT and **C)** u_{HS}=3 kT. The volume fraction was set to φ=23%.

Further increasing the self-affinity of the facultative heterochromatin by doubling and quadrupling the typical value, u_{HH}=1.30 kT, and u_{HH}=2.60 kT, resulted in the compaction at the center, demonstrating inverted phase separation behavior while the chromocenters could not be surrounded by facultative heterochromatin. In addition, a slight increase in the nuclear shape fluctuations was observed. Next, various facultative heterochromatin self-affinities were studied using the default heterochromatin-shell interactions. In this case, when the self-affinity of the facultative heterochromatin was absent, u_{HH}=0 kT, the phase separation could not be completed (Figure 35B). As the facultative heterochromatin's self-affinity strengthened, the nuclear shape fluctuations were increased only in the smaller wavenumbers, which correspond to long wavelengths.

In this trial, distinct phases were observed when u_{HH}=1.30 kT and u_{HH}=2.60 kT. For example, when self-affinity was set to u_{HH}=1.30 kT, two distinct facultative heterochromatin phases were found inside however, setting the strength of the attraction to u_{HH}=2.60 kT completed a single phase at the center. Setting the heterochromatin-shell interactions to double the default value, u_{HS}=1.5 kT, increased the shape's fluctuations further as the self-affinity became stronger (Figure 35C). Not only in the small wavenumbers but also in the high wavenumbers, which correspond to short wavelengths, the fluctuations were increased for the two highest self-affinity strengths, u_{HH}=1.30 kT and u_{HH}=2.60 kT. Still, there were distinct phases of facultative heterochromatin. Additionally, the chromocenters were dispersed entirely due to the increased heterochromatin-shell interactions. Moreover, facultative heterochromatin did not form a single phase at the center when self-affinity was u_{HH}=2.60 kT, as observed in the previous cases since the heterochromatin-shell interactions competed with the self-affinity

mediated the preserving those domains at the periphery. Lastly, the simulations ran with the highest heterochromatin-shell interactions defined. Still, the loss of self-affinity could not achieve the phase separation (Figure 35D). Increasing the strength of the self-affinity of the facultative heterochromatin increased the shape's fluctuations in every wavenumber. Significantly, the high wavenumbers were affected, which can be characterized by the folding of the shell and pointed protrusions. Furthermore, the facultative heterochromatin formed multiple phases that were distinctly localized. For all the various heterochromatin-shell interactions, the nuclear shape fluctuations were similar when the self-affinity of the facultative heterochromatin was depleted. Hence, the interplay between heterochromatin-shell interactions and the facultative heterochromatin's self-affinity plays a role in nuclear morphology. Thus, our simulation results demonstrate that the facultative heterochromatin's self-affinity is crucial for regulating the nuclear morphology, and the interplay exists between the facultative heterochromatin's self-affinity and its interaction with the shell.

Using the same approach and the defined parameters, we ran the conventional nucleus simulations under the chromatin density set to φ=19%. Changing the volume fraction did not alter the genome organization (Figure 36A, B, C, D), and we observed highly similar organizations as in the previous trial where the volume fraction was φ=23% (Figure 35). Hence, the nuclear shape fluctuations were highly close to each other for each case of various self-affinity strengths when u_{HS}=0.375 kT and u_{HS}=0.75 kT. However, the volume fraction contributed to the shape's fluctuations in high heterochromatin-shell interactions

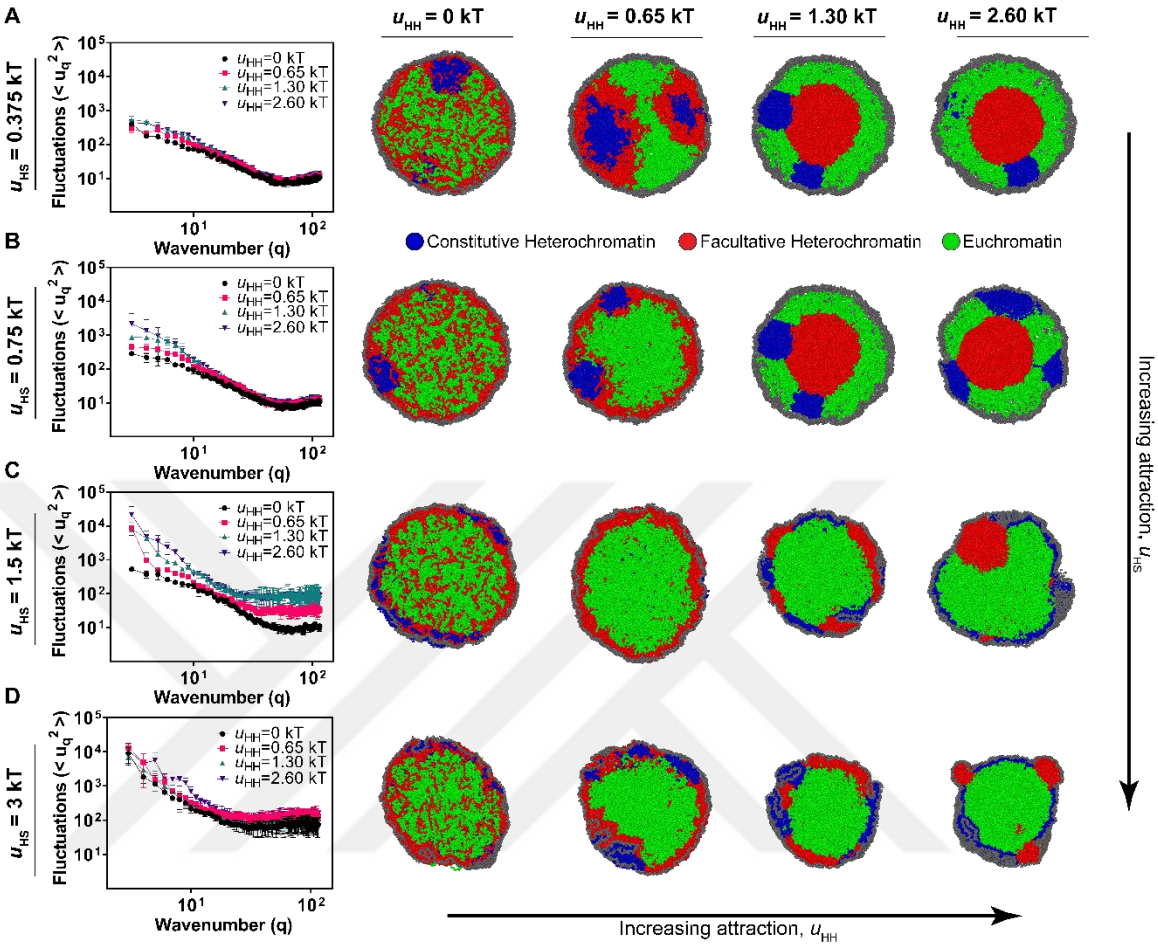

Figure 36 The images and fluctuation analysis extracted from our model with conventional nucleus organization with various facultative heterochromatin self-affinity strengths and heterochromatin-shell interactions **A)** u_{HS}=0.375 kT **B)** u_{HS}=1.50 kT and **C)** u_{HS}=3 kT. The volume fraction was set to φ=19%.

(Figure 36C, D & Figure 35C, D). For instance, setting the heterochromatin-shell interactions as u_{HS}=1.50 kT significantly influenced the fluctuations across all wavenumbers, especially when we observed a drastic increase in the high wavenumbers except where self-affinity was depleted u_{HH}=0 kT (Figure 36C). Further, assigning the heterochromatin-shell interactions as the maximum strength we defined for our simulations, u_{HS}=3 kT, the shape fluctuations were significantly elevated for all the

various strengths of facultative heterochromatin even when the facultative heterochromatin self-attraction was depleted (Figure 34D). All models had deformed morphologies, and the shape's fluctuations were highly similar.

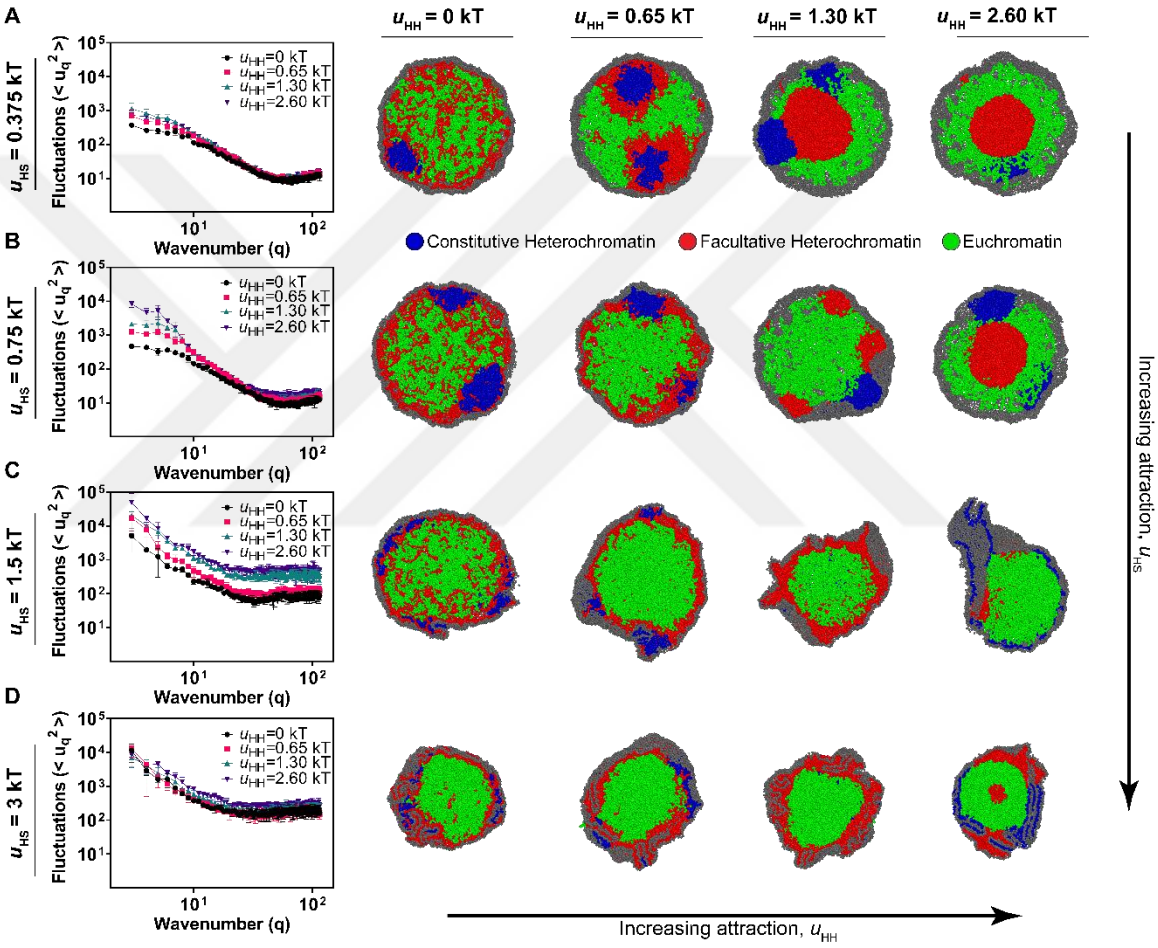

Figure 37 The images and fluctuation analysis extracted from our model with conventional nucleus organization with various facultative heterochromatin self-affinity strengths and heterochromatin-shell interactions **A)** u_{HS}=0.375 kT **B)** u_{HS}=1.50 kT and **C)** u_{HS}=3 kT. The volume fraction was set to φ=14%.

Finally, the conventional nucleus simulations ran with φ=14%. For all cases, the chromatin distributions were similar (Figure 37) to the previous trials ran with higher volume chromatin densities, φ=23% and φ=19% (Figure 36 & Figure 35). The nuclear shape fluctuations were not significantly altered when uHS=0.375 kT compared to instances with high volume fractions (Figure 35A & Figure 36A) and consistently increased as self-affinity strength increased (Figure 37A). Using the default heterochromatin-shell interactions, u_{HS}=0.75 kT resulted in higher shape's fluctuations in low wavenumbers compared to high volume fraction trials (Figure 35B & Figure 36B), and increasing the self-affinity value shifted the fluctuations (Figure 37B).

The drastic shifts in the nuclear shape fluctuations, hence in the morphology, were observed when heterochromatin-shell interactions were set to u_{HS}=1.50 kT. The fluctuations were drastically increased in every corresponding wavelength, and strong facultative heterochromatin self-attractions, u_{HH}=1.30 kT and u_{HH}=2.60 kT, led to extremely deformed morphologies (Figure 37C). In our simulations ran with u_{HS}=3 kT, the nuclear shape fluctuations were similar in all interactions defined for self-affinity of facultative heterochromatin, where abnormal morphologies in each case were observed (Figure 375D). In addition, we evaluated the RMS radial deviations as well. Radial fluctuations significantly increased as the self-attraction energy increased (Figure 38 A, B C). The fluctuations were close to each other for u_{HS}=3 kT since the fluctuations occurred significantly at this high energy due to the heterochromatin-shell interactions (Figure 38 A, B, C).

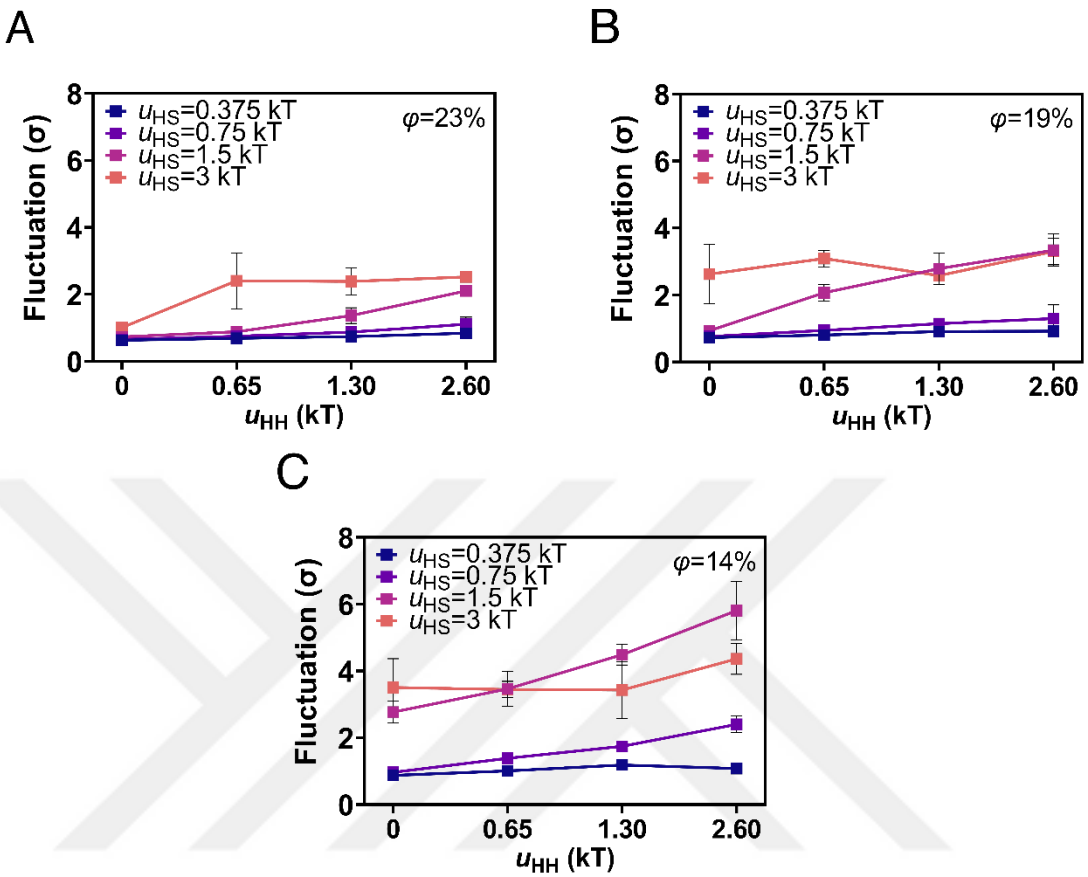

Figure 38 The volume fractions influence the interplay between heterochromatin's self-attraction and attraction with the shell. The RMS radial fluctuations of **A)** φ=23%, **B)** φ=19%, and **C)** φ=14%.

However, in lower attraction strengths, the fluctuations almost consistently elevated as the self-affinity of the facultative heterochromatin became stronger. Invariably, the volume fraction affected the fluctuations, and the mean radial fluctuations exhibited higher values as the volume fraction decreased (Figure 38 A, B, C). Thus, the volume fraction plays a role in the interplay of heterochromatin-shell and facultative heterochromatin's self-affinity.

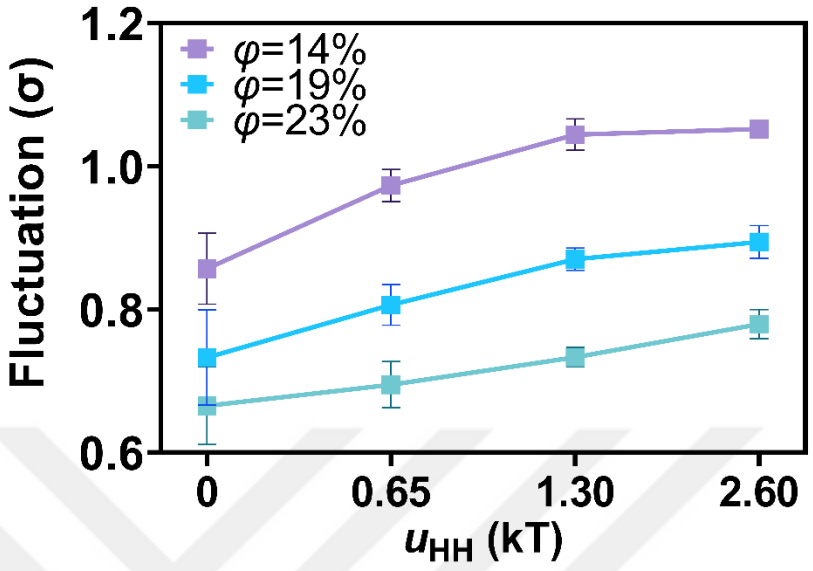

Figure 39 The RMS radial fluctuations extracted from inverted nucleus simulations under three different volume fractions and various strengths of self-affinity.

Our findings showed the interplay between heterochromatin-shell and self-affinity of heterochromatin. Next, to elucidate how the self-affinity of heterochromatin influences the shape's fluctuations in an inverted nucleus, we abolished the heterochromatin-shell interactions. Since no interactions were present between heterochromatin-shell, this study could elucidate the role of spatial organization of the genome on nuclear morphology. The inverted nucleus simulations ran under three defined volume fractions (Figure 39). The RMS radial fluctuations exhibited a pattern in which stronger self-attraction of the facultative heterochromatin resulted in increased fluctuations in all chromatin densities (Figure 39A). Consistently, the fluctuations were additionally regulated by the volume fraction, which increasing the volume fraction suppressed the fluctuations. Hence, even though the heterochromatin-shell interactions were abolished, still the compaction of the

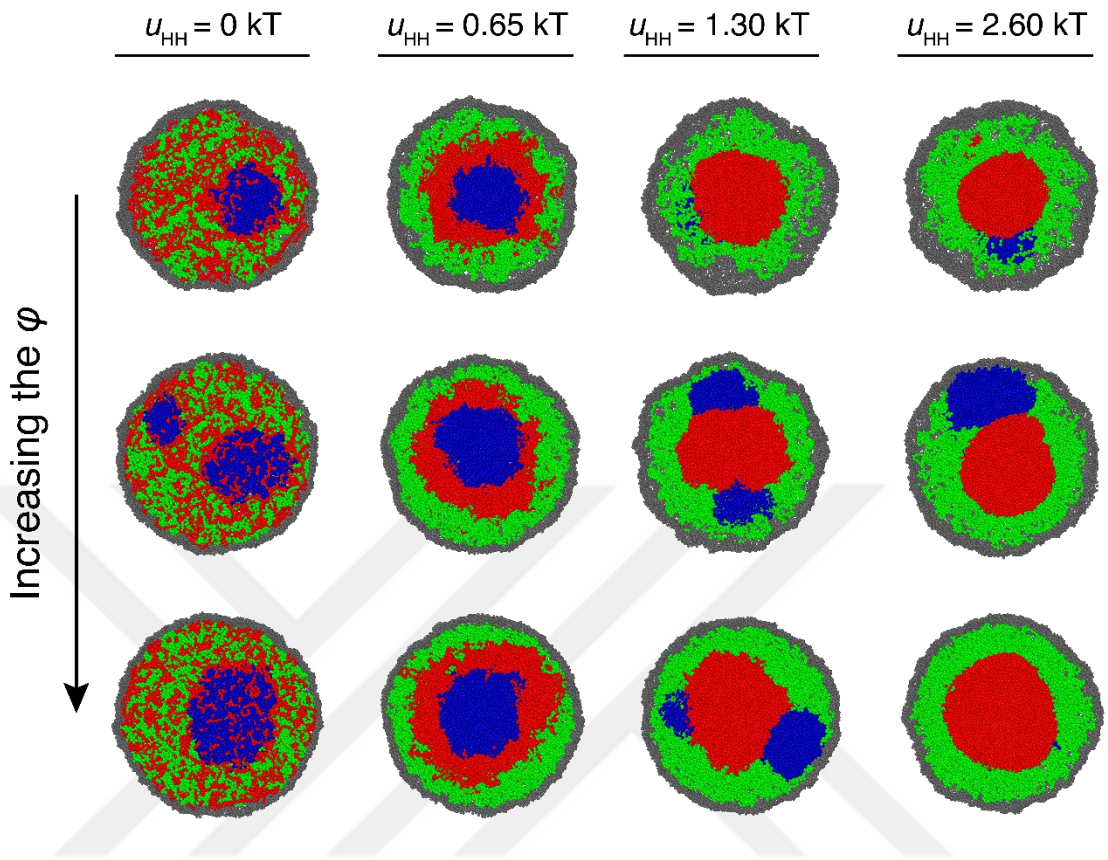

Figure 40 The rendered snapshots from the inverted nucleus simulations demonstrate the internal organization and the nuclear morphology under different interaction strengths.

facultative heterochromatin influenced the nuclear morphology, possibly through the internal organization of the genome. Therefore, the phase separation governed by heterochromatin-shell and heterochromatin's self-interactions can play a role in regulating the nuclear morphology. Even the phase separation only controlled by self-attraction of heterochromatin, when heterochromatin-shell interactions are depleted, can be critical for nuclear morphology.

3.5 Epigenetics Having a Critical Role in the Regulation of Nuclear Morphology

Studies demonstrated that the deformation in the nuclear morphology is related to the overall amount of heterochromatin which decreases in heterochromatin results in shape abnormalities[31,33]. Therefore, we aimed to assess how facultative heterochromatin fraction influences the nuclear shape fluctuations and morphology. The facultative heterochromatin fraction was altered by randomly converting the state of the beads, explained in Section 2.2.2, to model *in vivo* chromatin chemical perturbation experiments[31,33].

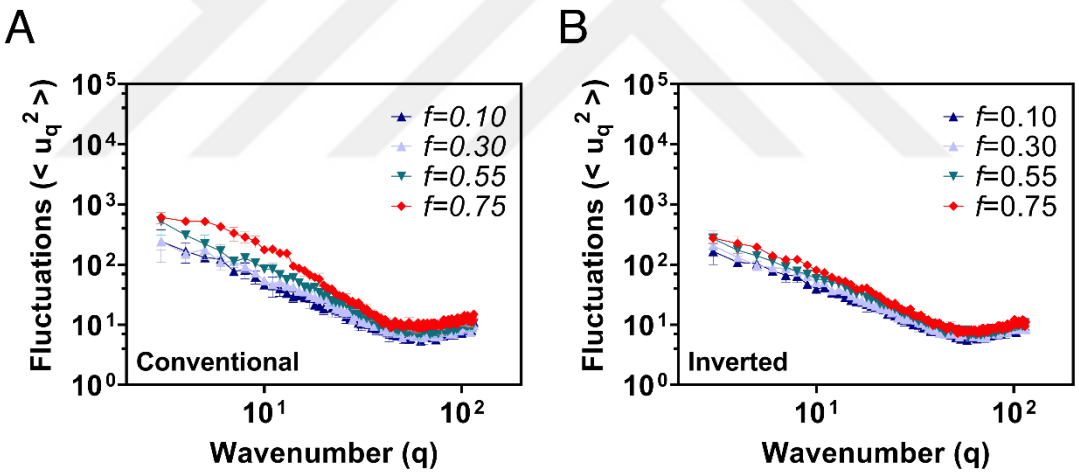

Figure 41 The nuclear shape fluctuation analysis of **A)** conventional and **B)** inverted nucleus simulations. The volume fraction is φ=23%.

The previous analysis revealed the role of chromatin density in shape's fluctuations. Hence, the same approach was employed in this investigation, in which three volume fractions were defined in the simulations. The amplitudes of the corresponding wavenumbers were changed as the concentration of the facultative heterochromatin

increased in conventional nucleus simulations (Figure 41A & Figure 44). Additionally, the shape's fluctuations were slightly increased in the inverted nucleus simulations where there were no heterochromatin-shell interactions (Figure 41B & Figure 44). The shape's fluctuations were additively increased when the volume fraction was reduced to φ=19% significantly in conventional and slightly in inverted nucleus simulations (Figure 42, Figure 44, Figure 45). The spectrum exhibited that the amplitudes were elevated in small and high wavenumbers in conventional nucleus simulations, exhibiting an extreme shape abnormality when the heterochromatin fraction was f=0.75 (Figure 42A & Figure 44).

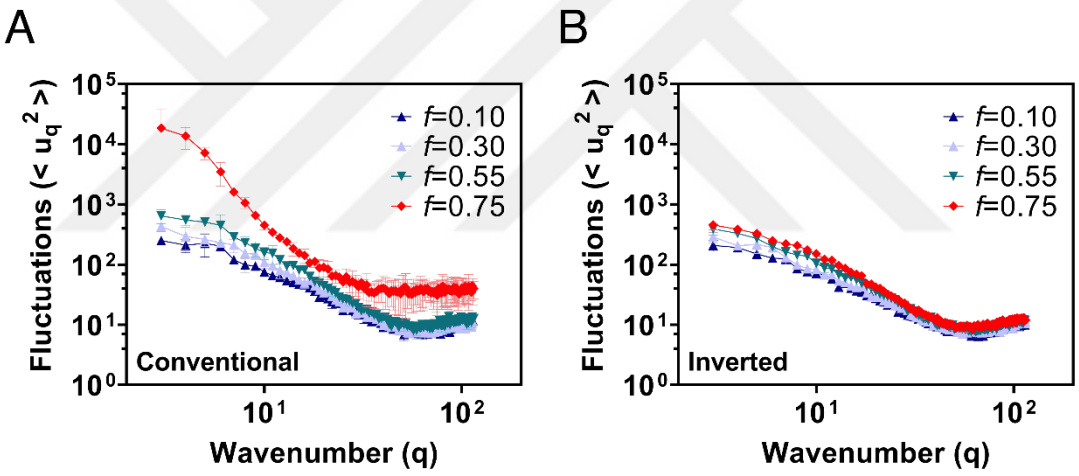

Figure 42 The nuclear shape fluctuation analysis of **A)** conventional and **B)** inverted nucleus simulations. The volume fraction is φ=19%.

The shape's fluctuations were increased in inverted nucleus simulations compared to chromatin density of φ=23%, which can be explained by the reduced volume fraction that limits suppressing the fluctuations (Figure 38B). Consistently, at the lowest volume fraction, φ=14%, the nuclear shape's fluctuations were crucially increased in conventional nucleus simulations, especially when the heterochromatin fraction was f=0.75 (Figure

43A & Figure 44). As before, the fluctuations were slightly increased in inverted nucleus simulations by contribution from the volume fraction (Figure 43B & Figure 44).

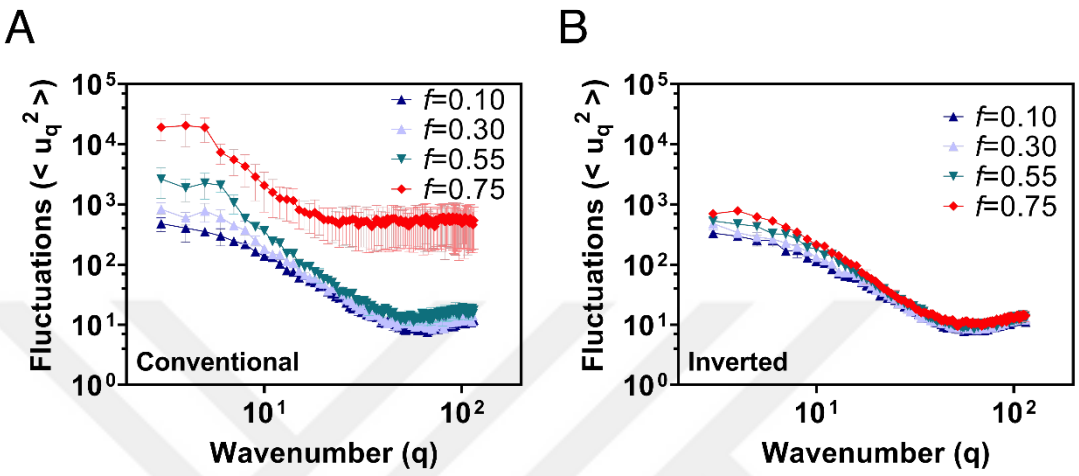

Figure 43 The nuclear shape fluctuation analysis of **A)** conventional and **B)** inverted nucleus simulations. The volume fraction is φ=14%.

For all various heterochromatin concentrations, we observed a change in the internal organization as the heterochromatin fraction was varied. Due to the low amount of facultative heterochromatin where f=10%, only a euchromatin phase is distinguished, and chromocenter structures are flattened rather than globular (Figure 43). Additionally, as the heterochromatin fraction exceeded beyond the typical fraction, f=0.45, the distinct heterochromatin phase was not observed, which euchromatin-to-heterochromatin converted beads localized at the interior. The inversion was completed even at the low fraction of facultative heterochromatin (Figure 44). Increasing the fraction of the facultative heterochromatin resulted in a complete phase around the chromocenters.

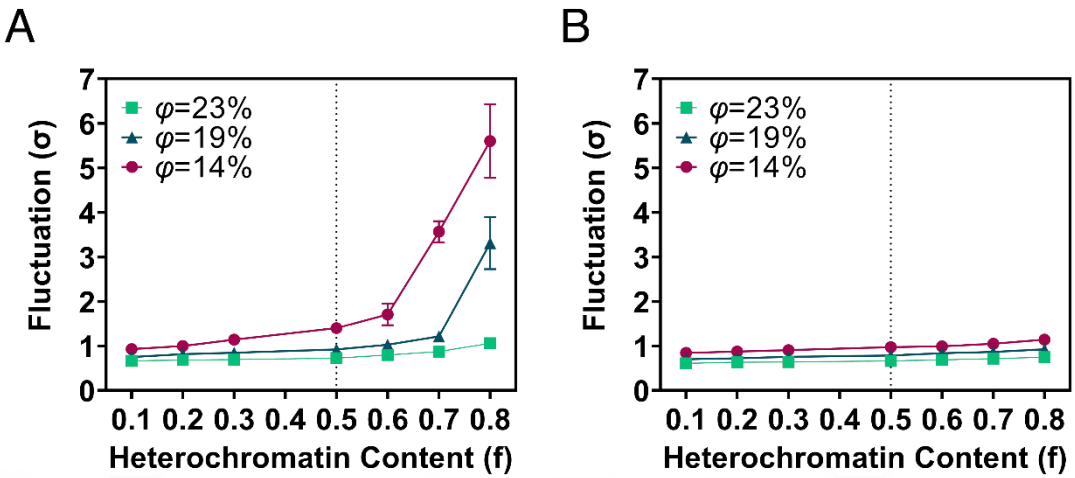

Figure 43 The heterochromatin fraction changes the RMS radial fluctuations in **A)** conventional and **B)** inverted nucleus simulations

The gradual rise in fluctuations when increasing the facultative heterochromatin percentage was more significant in the lowest volume fraction, φ=14%, than in the other volume fractions (Figure 43A). We observed an alteration in nuclear morphology in each heterochromatin fraction, which mainly resulted in a severe shape abnormality at *f*=75% (Figure 44). Even in the highest heterochromatin amount, there was a noticeable difference between fluctuations compared to φ=14%. At φ=23%, compared to φ=14 %, the fluctuations did not noticeably increase as the heterochromatin concentration increased. Additionally, there was not much difference between the fluctuations at φ=19% and φ=23%, except for the highest facultative heterochromatin concentration, *f*=0.75, where the difference was substantial. Moreover, the mean fluctuations were also increased in inverted nucleus simulations, consistently with the shape's fluctuations, and the volume fraction had a supplementary effect (Figure 43B).

Overall, our findings showed that, in contrast to earlier studies[31,33], increasing the heterochromatin amount does not suppress the variations. This outcome made us wonder why experiments would behave unexpectedly. Our earlier findings demonstrated how heterochromatin influences nuclear shape through interactions with the shell and by itself. We hypothesized that the competition between facultative heterochromatin's self-attraction and its attraction to the shell could lead to the emergence of this phenomenon. For that purpose, we abolished the heterochromatin's self-attraction while maintaining the same heterochromatin fraction and its attraction with the shell. We observed that the nuclear shape fluctuations were critically reduced, and the normal nuclear shape was recovered (Figures 43B & 45).

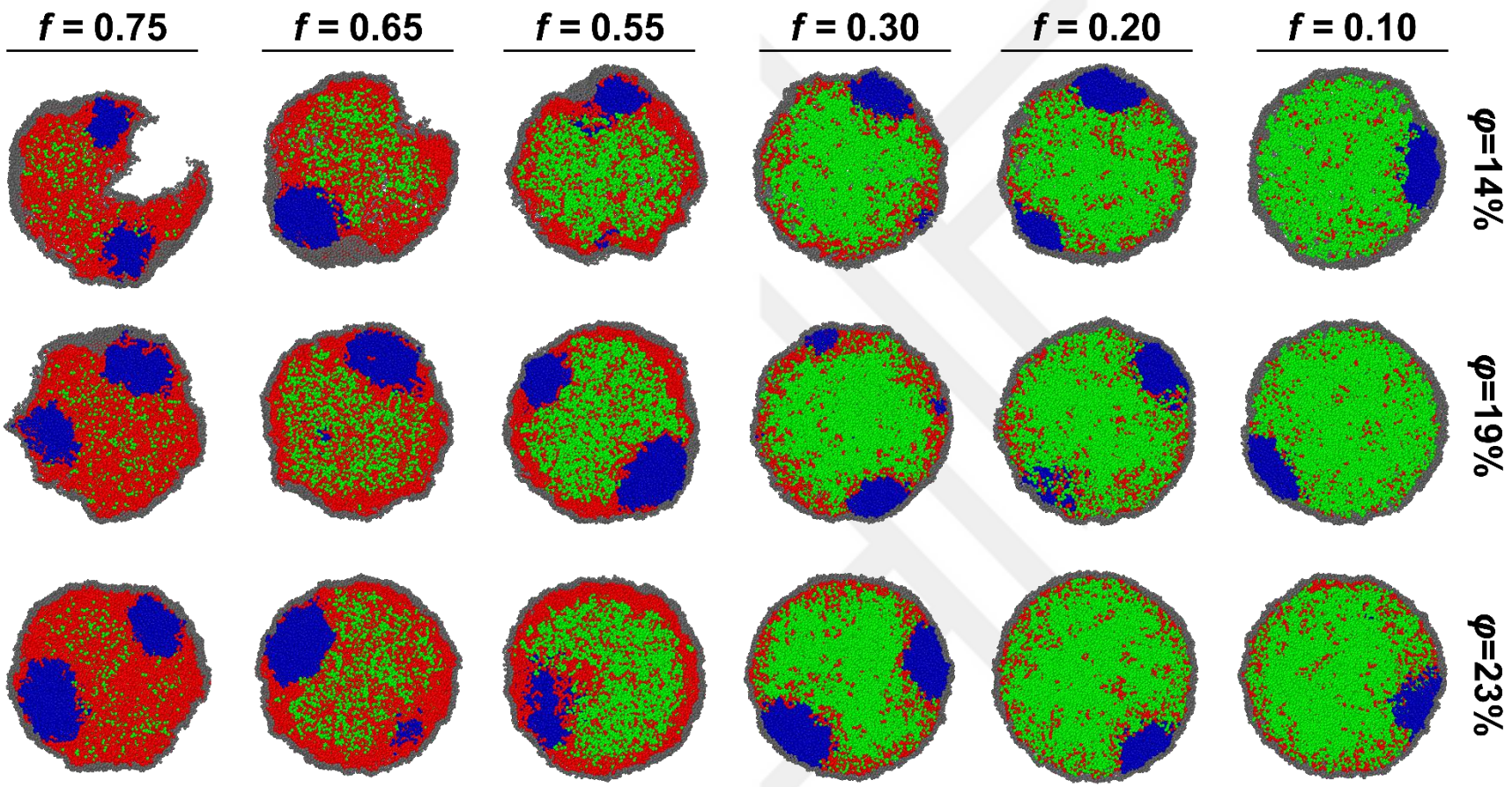

Figure 44 Images of conventional nucleus organizations with various heterochromatin fractions under different chromatin densities

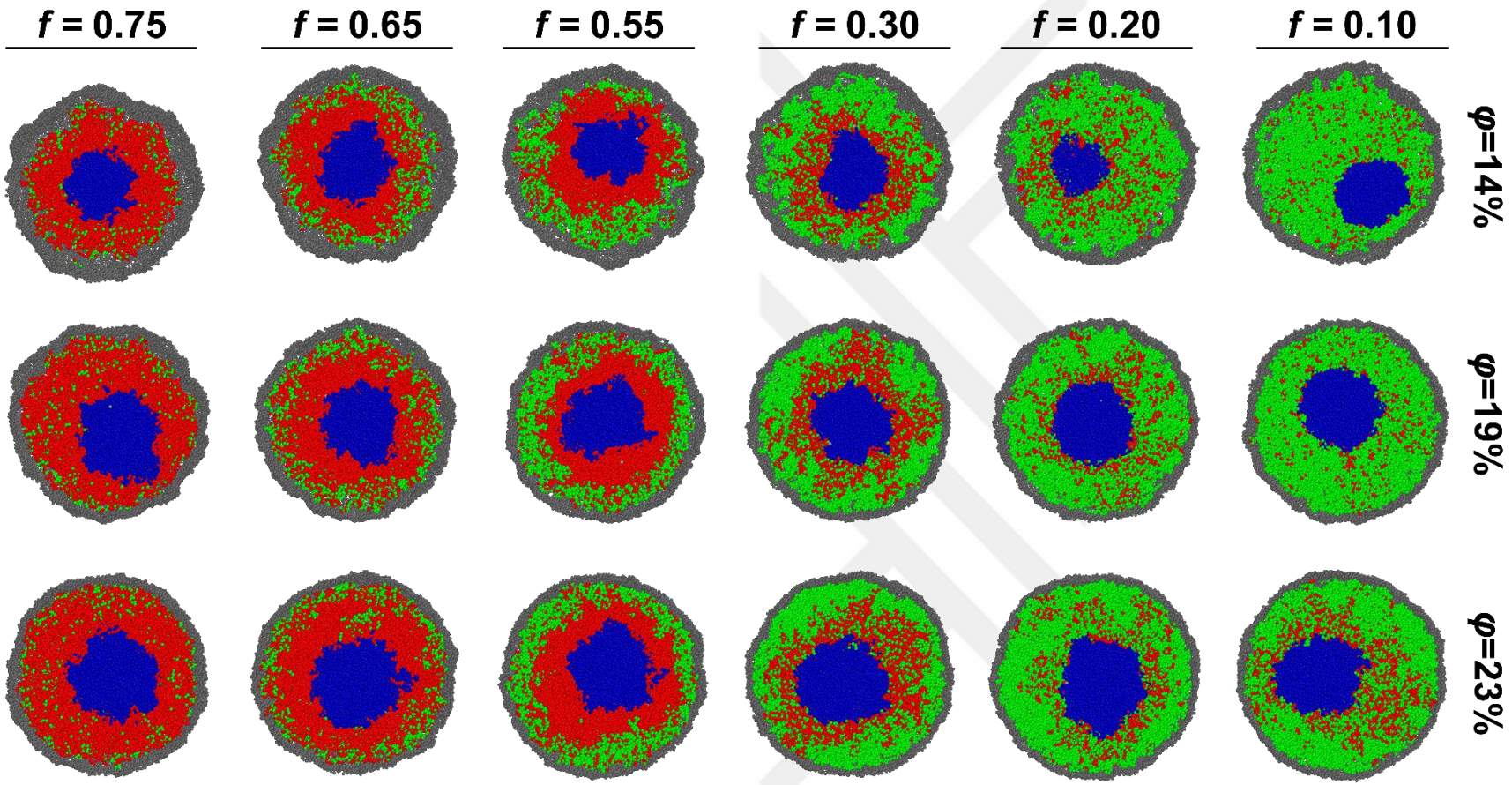

Figure 45 Images of inverted nucleus organizations with various heterochromatin fractions under different chromatin densities

3.6 Stiffness of the Shell Contributes to Nuclear Morphology

Nuclear lamins provide stiffness to the nucleus, maintaining the nuclear integrity. Such loss of the lamins, mainly Lamin A/C, was shown to reduce the nuclear stiffness[49], involved in certain pathologies[69], and regions where Lamin A/C are denser in the nucleus exhibit reduced deformations[70]. In our model, to investigate the role of stiffness mediated by the beads of our shell, the bonding strength between each lamin bead was increased to $K = 30\frac{kT}{\sigma^2}$, which is sixfold the default bond strength. Increasing the bond strength of the beads that were members of the shell led to an increased volume fraction since the shell collapsed more due to the higher bond energy. Thus, we obtained two different volume fractions in this case, φ=30% and φ=25%. In this case, we could compare the φ=25% and chromatin density of φ=23% in the context of different bond strengths and observe the impact of higher volume fraction we did not achieve.

Conventional nucleus simulations showed that increasing chromatin density consistently suppressed the shape's fluctuations (Figure 46A, B). Hence, the shape abnormalities and critical deformations were not observed (Figure 46C). The amplitude of the fluctuations was only altered in low wavenumbers. However, the fluctuations observed in φ=25% were similar to those surveyed in less stiff shell with a chromatin density of φ=23% (Figure 46A, B & Figure 24A, B). Still, the mean radial fluctuations exhibited that the fluctuations were insensitive to the crosslinking of the constitutive heterochromatin (Figure 46B).

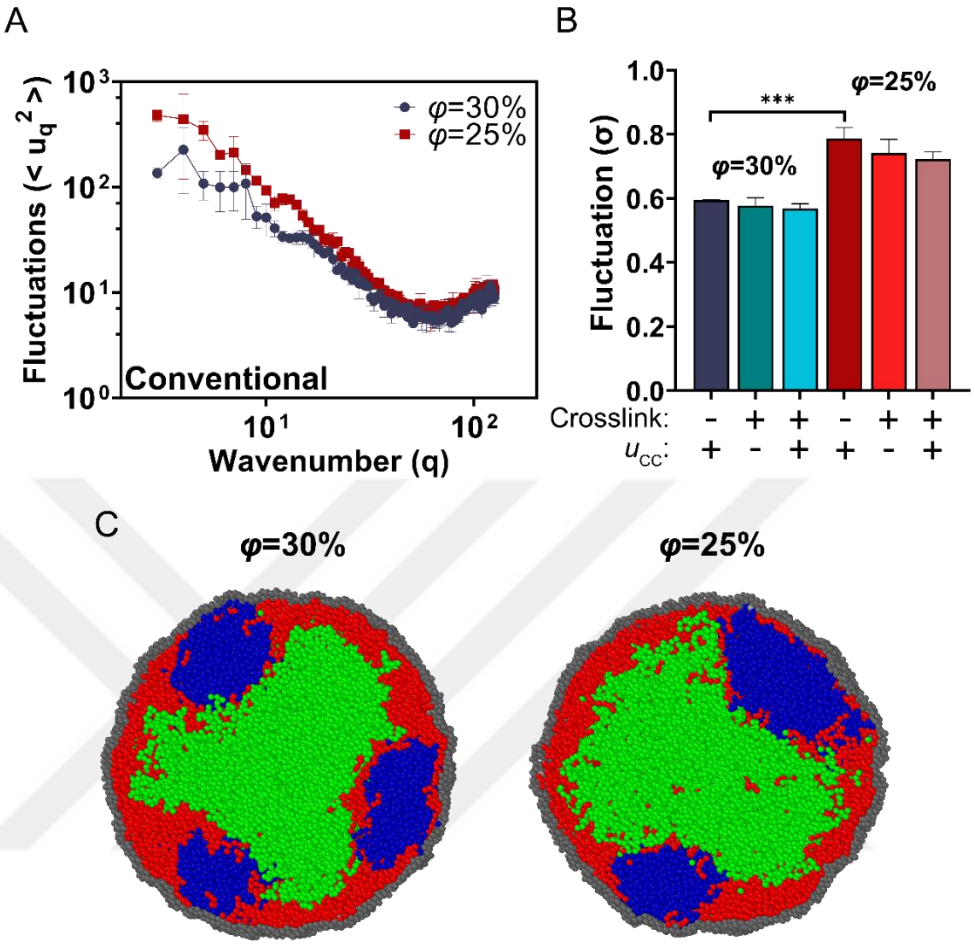

Figure 46 The volume fraction suppresses the nuclear shape fluctuations in conventional nucleus simulations. **A)** The shape's fluctuation was calculated for two volume fractions. **B)** The RMS radial fluctuations for two volume fractions, including the crosslinking trials. **C)** The images of conventional nucleus organization under different volume fractions

Next, we studied how the spatial organization of the chromatin influences the nuclear fluctuations. When the heterochromatin-shell interactions were abolished, the fluctuations were decreased with similar values as observed in the lower stiffer shell (Figure 47A, B & Figure 26). However, the change in a reduction in the fluctuations from the conventional to the inverted nucleus was slightly lower than the lower stiffer shell (Figure 47 & Figure

26). Thus, heterochromatin's effect on the nuclear shape fluctuations was limited in a more rigid shell compared to the lower stiffer shell.

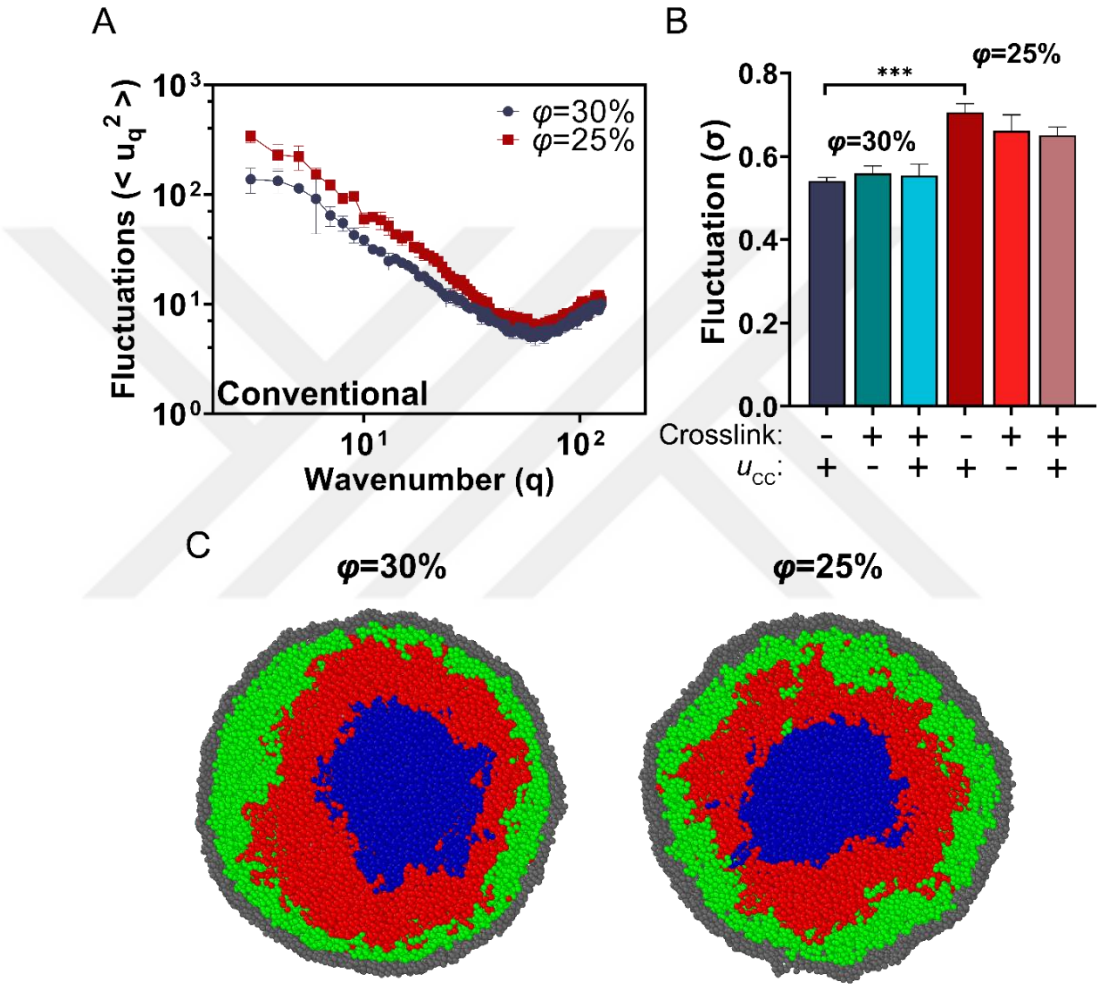

Figure 47 The chromatin density suppresses the nuclear shape fluctuations in inverted nucleus simulations. **A)** The nuclear shape's fluctuation was calculated for two chromatin densities. **B)** The mean radial fluctuations for various volume fractions and crosslinking. **C)** The snapshots of inverted nucleus organization under different chromatin densities

Next, we followed the same approach that was employed for stiffer shells. The heterochromatin-shell interactions were varied utilizing the same methodology, in which we consecutively changed the different heterochromatin's attraction with the shell. The first trials were run by only changing the facultative heterochromatin's interaction with the shell. The shape's fluctuations demonstrated that although the heterochromatin-shell attractions become stronger, the spectrum was almost insensitive to the changes in the amplitudes in chromatin density of φ=30% (Figure 48A).

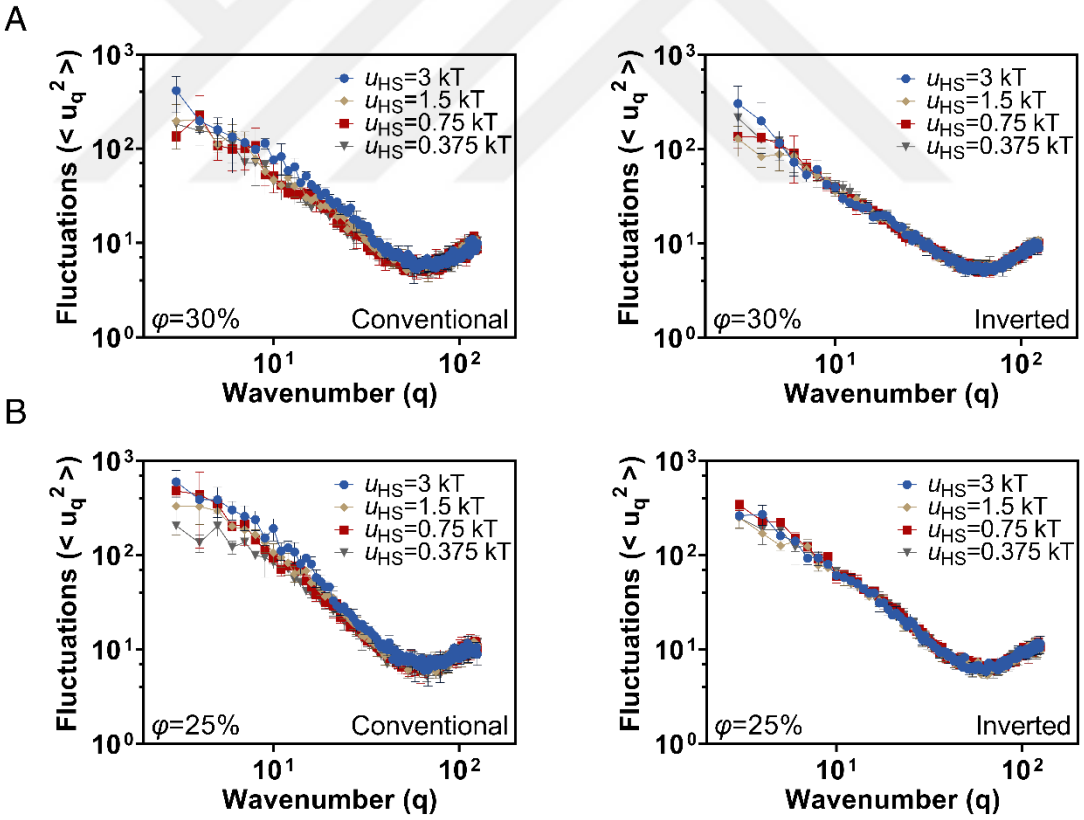

Figure 48 The facultative heterochromatin-shell attraction strengths regulate the nuclear shape fluctuations variously with different chromatin densities **A)** φ=30%, **B)** φ=25%.

As expected, in inverted nucleus simulations, the fluctuations were reduced however, the amplitudes were not much varied compared to the conventional nucleus simulations. In lower volume fraction, φ=25%, the shape's fluctuations were higher, mainly in the middle wavenumbers, as the strength of the heterochromatin's attraction with the shell increased (Figure 48B). But, compared to our results obtained from φ=23% and $K = 5\frac{kT}{\sigma^2}$, the fluctuations were less noticeably affected when the attraction became stronger (Figure 28). In addition, reducing the typical attraction to half, uHS=0.375, impacted the flattened chromocenters structures (Figure 49A).

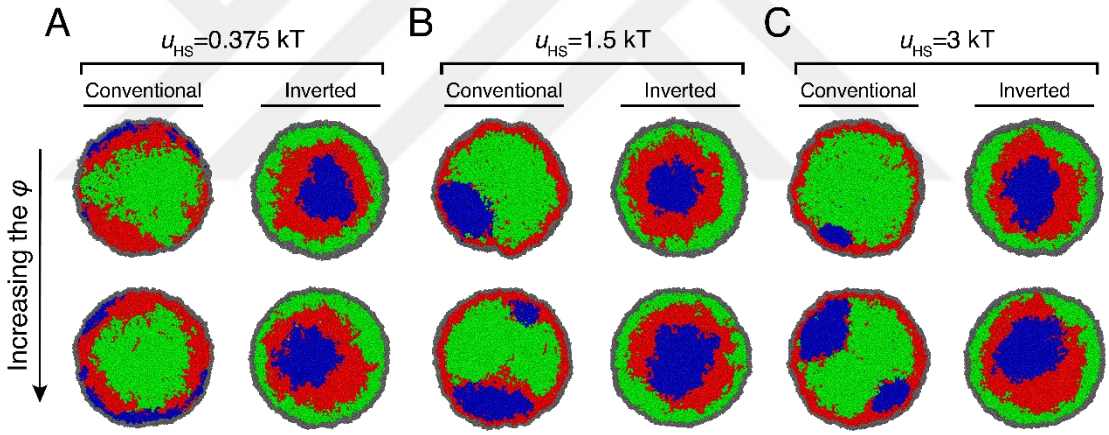

Figure 49 The conventional and inverted nucleus simulations snapshot from the model under different volume fractions and various facultative heterochromatin-shell attraction strengths **A)** u_{HS}=0.375 kT **B)** u_{HS}=1.50 kT and **C)** u_{HS}=3 kT in volume fractions of φ=30% and φ=25%.

Secondly, we studied the effect of constitutive heterochromatin attraction and its impact on nuclear shape fluctuations. In this case, increasing the strength of the attraction did not elevate the amplitudes, shown through the spectrum in chromatin density of φ=30%

(Figure 50A). Decreasing the chromatin density to φ=25% increased the fluctuations however, the amplitudes did not vary by stronger attractions (Figure 50B). In conventional nucleus simulations, we observed a change in chromatin organization after u_{HS}= 1.50 kT in which the chromocenters were dispersed (Figure 51B, C). The inverted nucleus simulations were accordant with the previous results that the shape's fluctuations were reduced (Figure 50A, B).

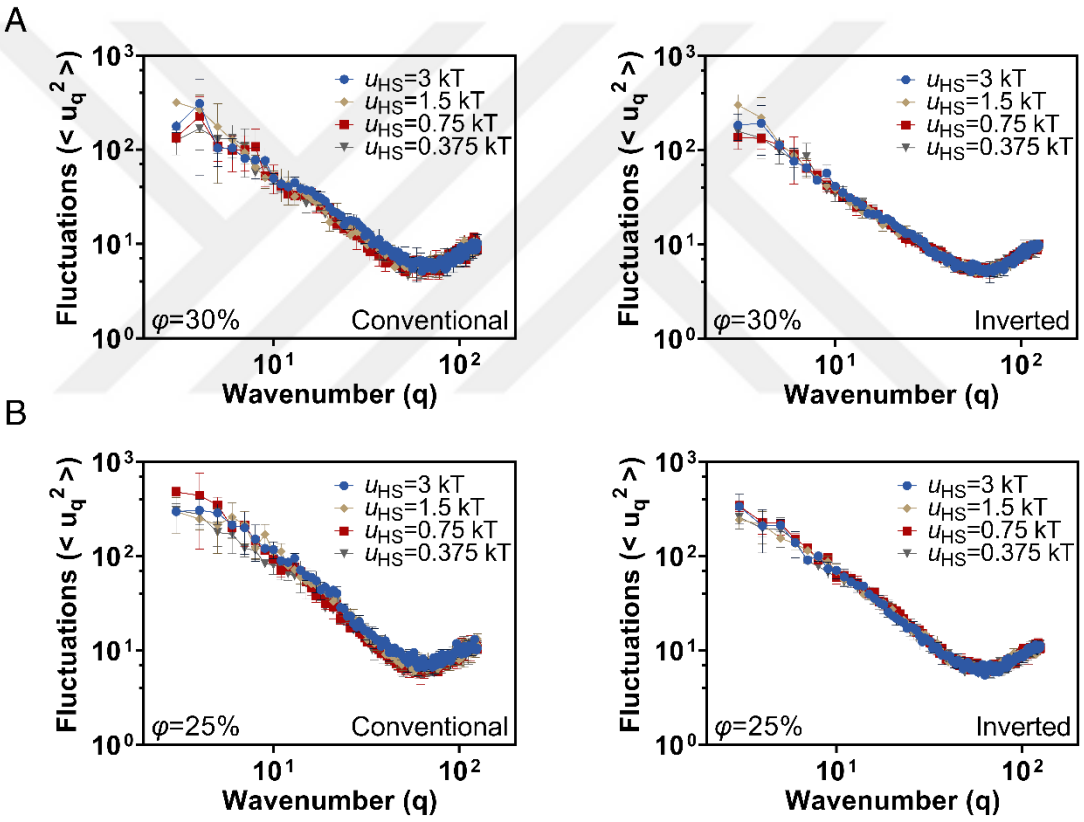

Figure 50 The constitutive heterochromatin-shell attraction strengths regulate the nuclear shape fluctuations variously with different chromatin densities **A)** φ=30%, **B)** φ=25%

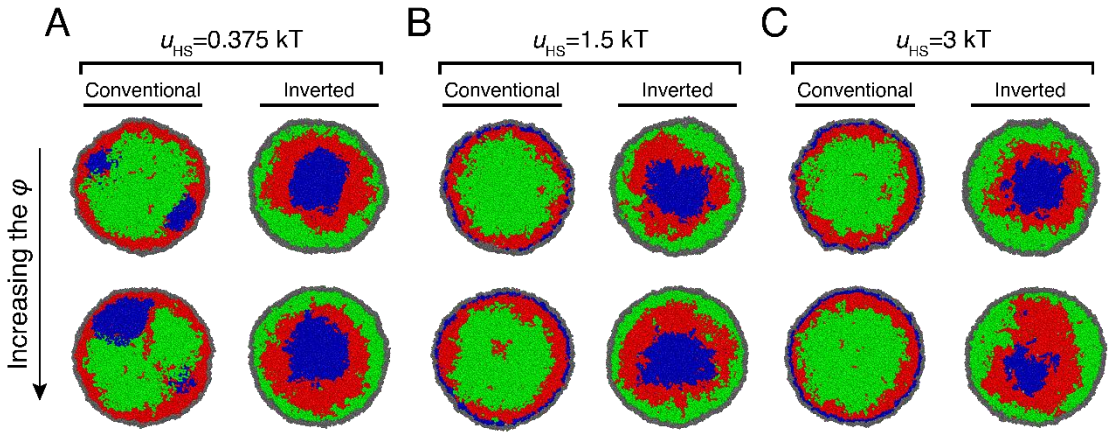

Figure 51 The conventional and inverted nucleus simulations snapshot from the model under different chromatin densities and various constitutive heterochromatin-shell attraction strengths **A)** u_{HS}=0.375 kT **B)** u_{HS}=1.50 kT and **C)** u_{HS}=3 kT in volume fractions of φ=30% and φ=25%.

In the last trial, the attraction of both heterochromatin with the shell was varied. The shape's fluctuations were almost indistinguishable from the previous instances. The fluctuations were changed mainly in the middle wavenumbers in high volume fraction as the attraction became stronger (Figure 52A). Lowering the volume fraction resulted in a positive contribution in which the fluctuations were increased, and the impact of stronger attraction was more prominent (Figure 52B). The genome organization was maintained except for the lowest attraction, u_{HS}=0.375, as previously noted (Figure 53). In inverted simulations, all shape's fluctuations with different chromatin densities were reduced, but not drastically compared to conventional nucleus simulations (Figure 52).

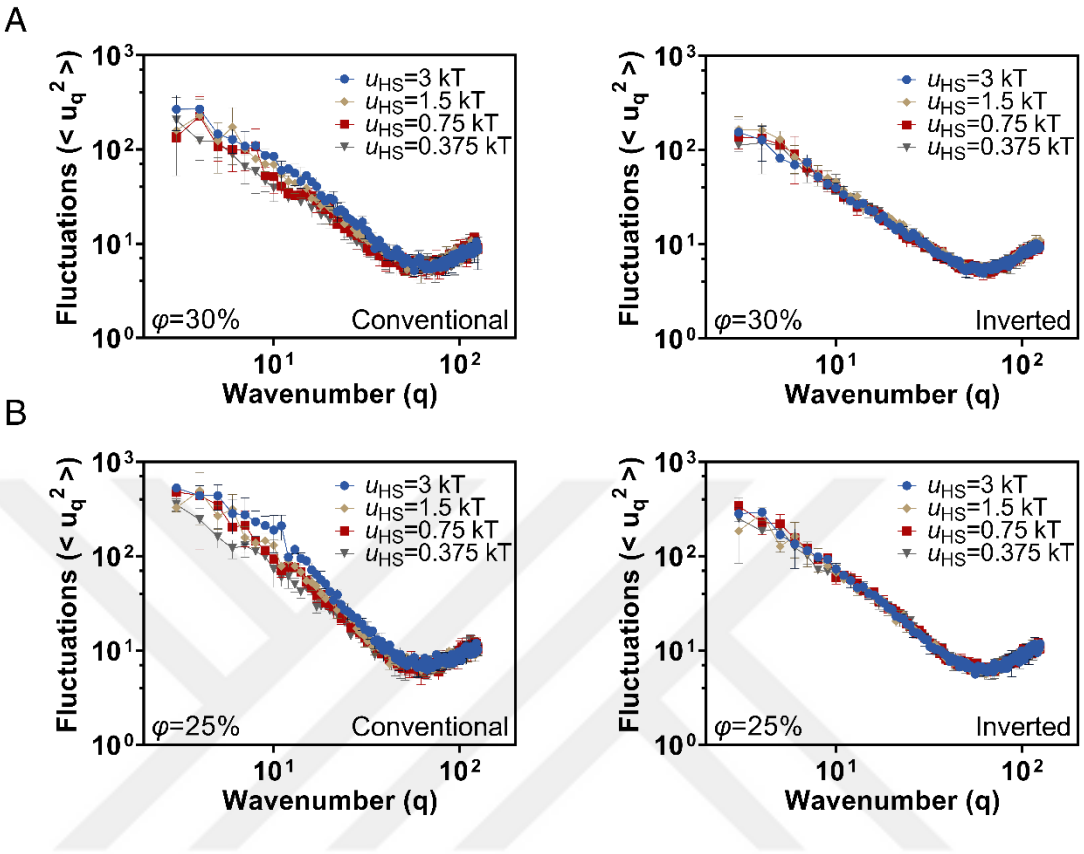

Figure 52 The attraction of heterochromatin with the shell regulates the nuclear shape fluctuations variously with different chromatin densities **A)** φ=30%, **B)** φ=25%.

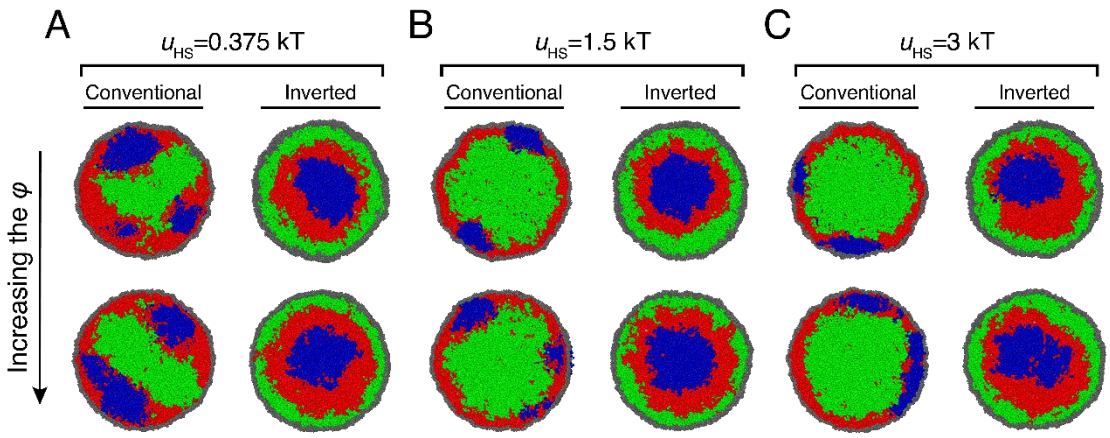

Figure 53 The conventional and inverted nucleus simulations snapshot from the model under different volume fractions and various heterochromatin-shell attraction strengths **A)** u_{HS}=0.375 kT **B)** u_{HS}=1.50 kT and **C)** u_{HS}=3 kT in volume fractions of φ=30% and φ=25%.

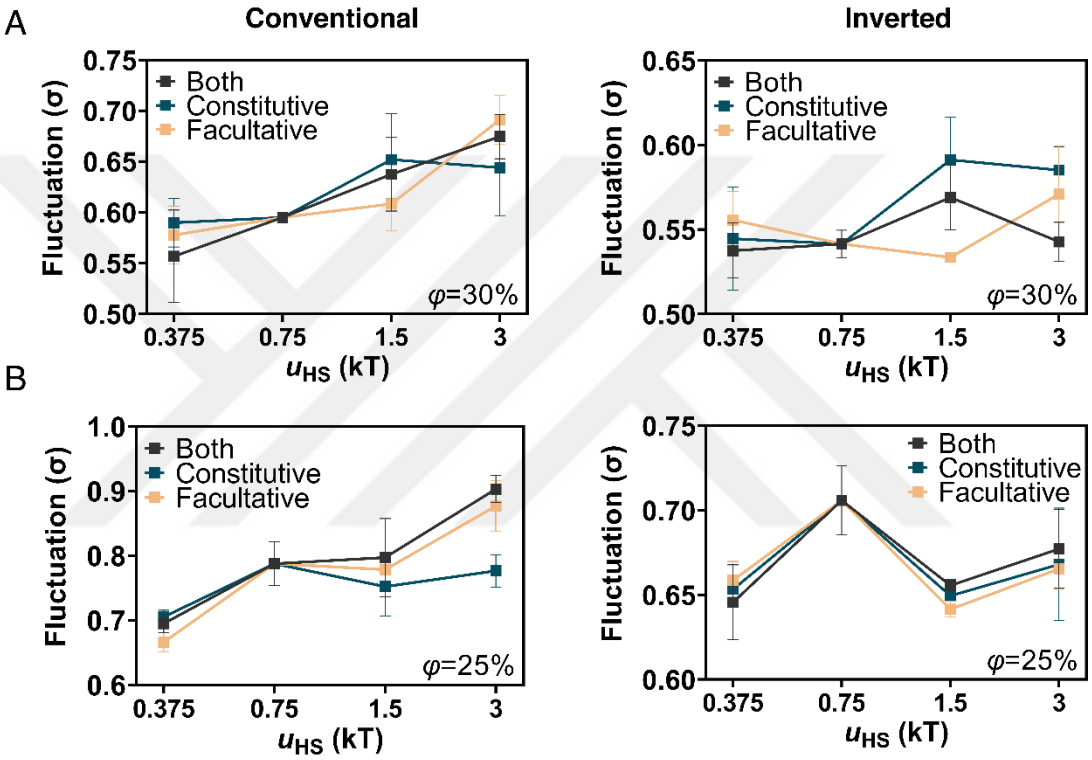

Figure 54 The RMS radial fluctuations of conventional and inverted nucleus simulations of various heterochromatin-shell attraction strengths in different volume fractions **A)** φ=30% **B)** φ=25%.

Lastly, we plotted the RMS radial fluctuations to evaluate the role of different heterochromatin's regulation of nuclear shape fluctuations. We observed higher fluctuations in both volume fractions, φ=30% and φ=25%, as the attraction strength became stronger for all the cases and higher radial fluctuations for the lower volume fraction (Figure 54A, B). When the constitutive heterochromatin-shell attraction becomes

stronger, the fluctuations were almost steady for the cases where attraction strengths were u_{HS}=1.50 kT and u_{HS}=3 kT in both chromatin densities. Possibly, in those high attraction energies, the constitutive heterochromatin formed a peripheral single layer, which could not contribute to the fluctuations further, even at the maximum attraction strength. The facultative heterochromatin attraction with the shell consistently increases the fluctuations for each case, demonstrating a regular increase. The combination attraction by both heterochromatin additively contributed to radial fluctuations. The fluctuations almost linearly increased between each attraction strength. Including both heterochromatin additively regulated the fluctuations since all the heterochromatin at the periphery formed a layer of phases in which all the heterochromatin beads could interact with the shell. In inverted nucleus simulations, the radial fluctuations were decreased, exhibiting variations in each case. This could emerge since each replicate was designed with a randomly generated shell and facultative heterochromatin radial positioning, even though its attraction with the shell was abolished.

Next, we investigated the effect of heterochromatin fraction on nuclear morphology. Our shape's fluctuation analysis revealed that in a high volume fraction, φ=30%, increasing facultative heterochromatin concentration slightly increased the amplitudes of corresponding middle wavenumbers in conventional nucleus simulations. In inverted simulations, the shape's fluctuations decreased even though the increased facultative heterochromatin fraction did not increase the fluctuations. Decreasing the chromatin density to φ=25% positively contributed to the fluctuations in which the amplitudes were elevated mainly in high and middle wavenumbers as the concentration of facultative

heterochromatin increased (Figure 55C). As expected, the fluctuations were reduced in inverted nucleus simulations.

Additionally, the amount of facultative heterochromatin influenced the internal organization, which at the low heterochromatin fraction, *f*=0.10, the chromocenters were dispersed in conventional nucleus simulations (Figure 56A). Increasing the concentration, the phases were indistinguishable, mainly preserving heterochromatin phases.

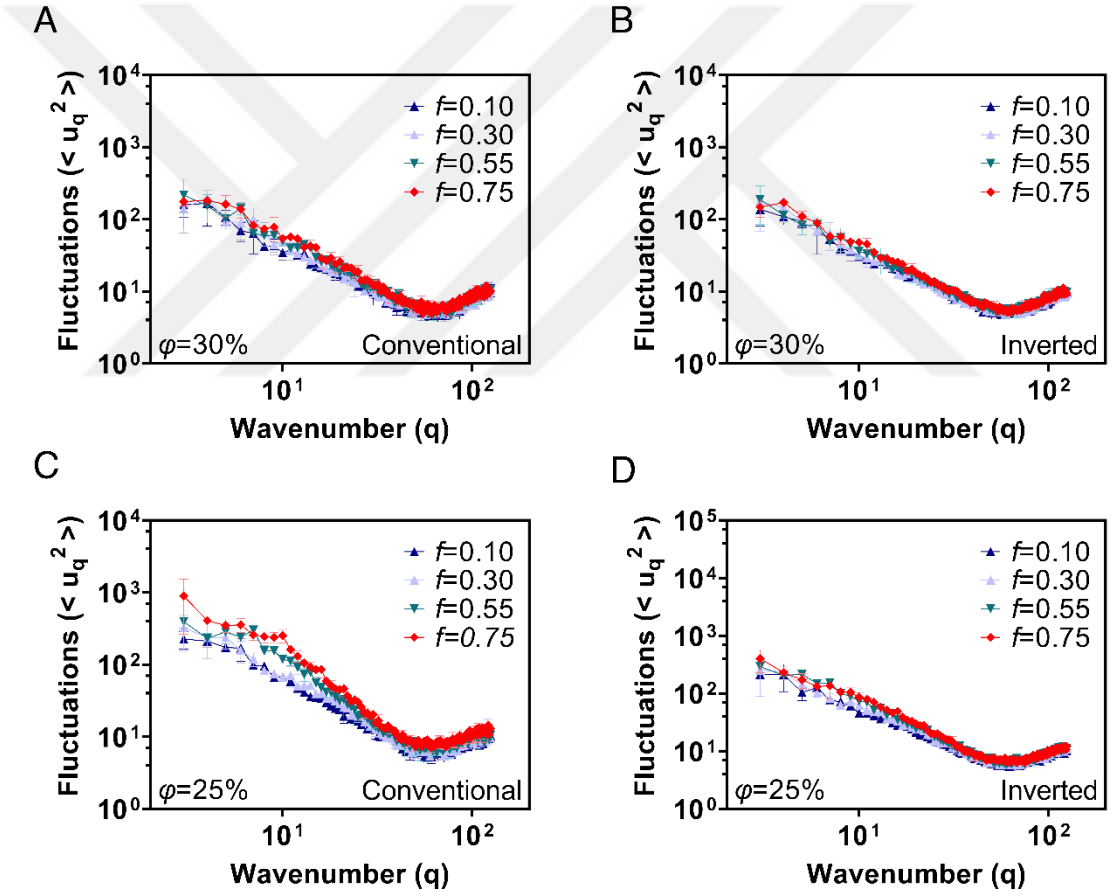

Figure 55 The nuclear shape fluctuation analysis of **A)** conventional and **B)** inverted nucleus simulations. The volume fractions are φ=30% and φ=25%, respectively.

Figure 56 Images of **A)** conventional and **B)** inverted nucleus organizations with various heterochromatin fractions under different chromatin densities

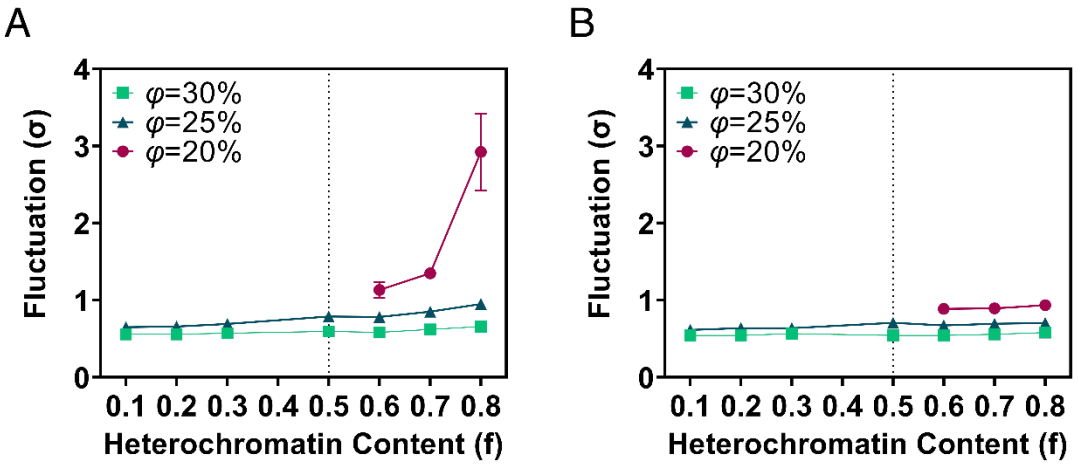

Figure 57 The RMS radial fluctuations of **A)** conventional and **B)** inverted nucleus simulations. The volume fractions are φ=30%, φ=25% and φ=20%, respectively.

Lastly, we conducted an RMS analysis to analyze the mean radial fluctuations. The results depicted that increasing the facultative heterochromatin fraction increases the fluctuations in all the volume fractions (Figure 57A). Additionally, to gain insight into the suppressing effect of the shell's stiffness, we ran simulations with a lower volume fraction, φ=20%. We observed that shape's fluctuations were significantly increased for the high heterochromatin fraction compared to the other volume fraction and led to extremely deformed morphology (Figure 57A & Figure 58A). Inverted simulations showed that the high fractions did not significantly affect the fluctuations however, the fluctuations were different for each case because of the volume fraction. The mean radial fluctuations in this volume fraction were close to what was observed in the less stiff shell. Thus, even though the more rigid shell was able to suppress the fluctuations in the high volume fractions compared to the less stiff shell, i.e., φ=25%; $K = 30\frac{kT}{\sigma^2}$ versus φ=23%; $K = 5\frac{kT}{\sigma^2}$, in lower volume fractions, the fluctuations were still increased. Hence, these findings further suggested that chromatin density is significant and one of the primary regulators of the

nuclear shape fluctuations and additively regulates the fluctuations with the other contributors, chromatin.

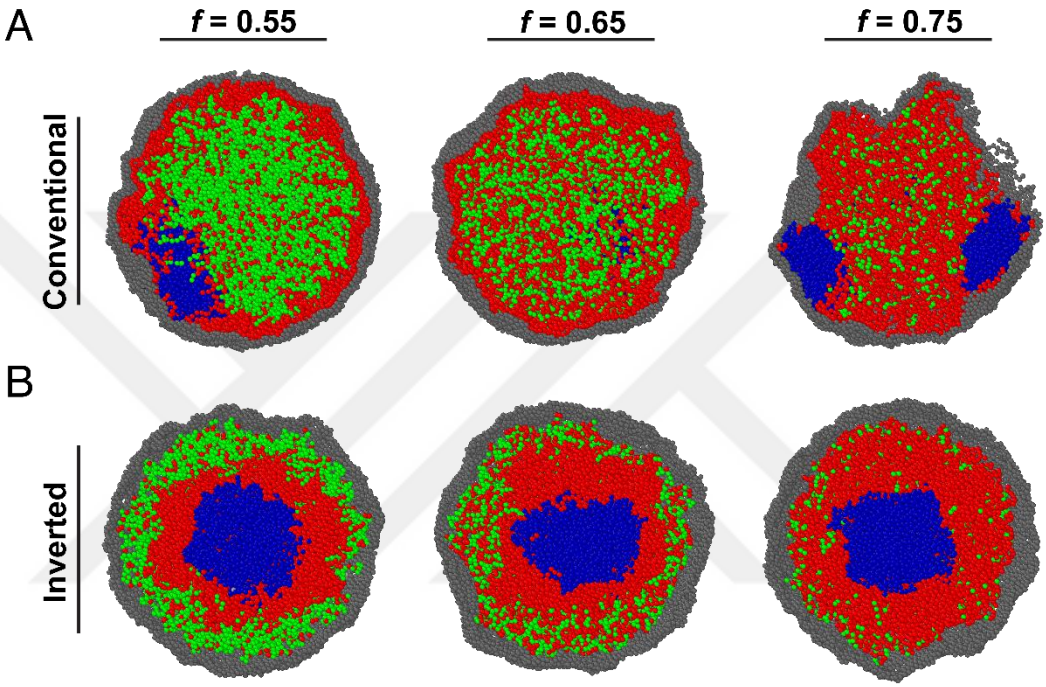

Figure 58 The snapshots of different heterochromatin concentrations from **A)** conventional and **B)** inverted nucleus simulations. The volume fraction is φ=20%.

3.7 Tethering of the Heterochromatin Provides Rigidity to the Nuclear Mechanics

The previous studies investigated the role of chromatin in nuclear mechanics. The micropipette manipulation experiments on isolated nuclei showed that the chromatin contributes to nuclear mechanics[20,51]. Additionally, increasing the heterochromatin via

VPA treatment further revealed the role of heterochromatin, which higher the heterochromatin resulted in increased stiffness[31,33]. Further, crosslinking and tethering of chromatin were demonstrated to be crucial for nuclear mechanics[50], degrading the crosslinker protein, HP1α, leads to reduced nuclear stiffness accompanying nuclear deformations[35]. Thus, we studied the nuclear mechanics via pulling simulations utilizing our phase-separated model to investigate the role of chromatin.

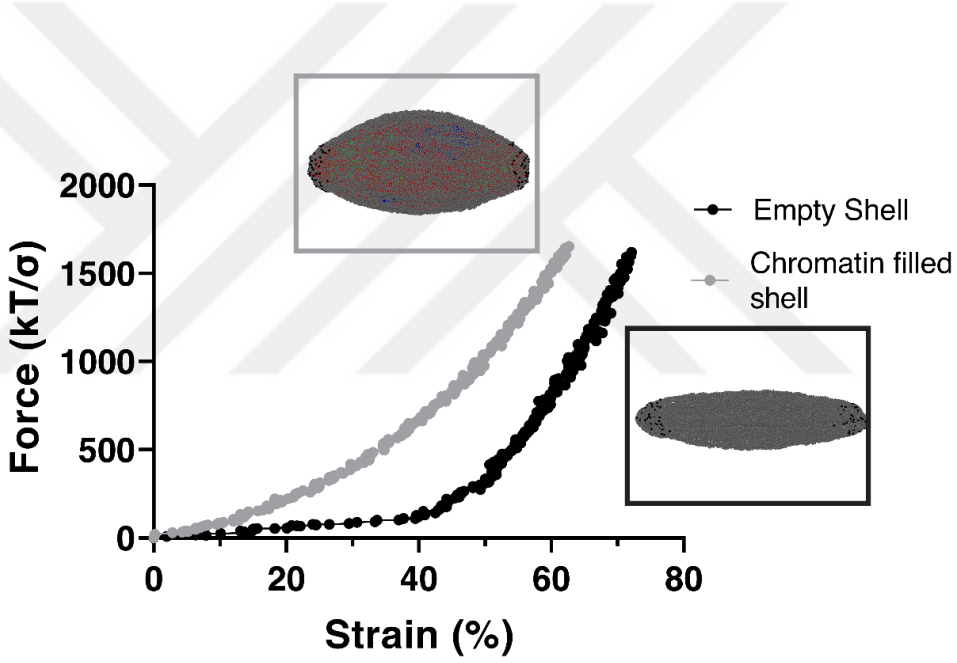

Figure 59 The force-strain graph shows the regime difference in the shell without chromatin and our conventional model.

At first, we investigated nuclear mechanics in empty and chromatin-filled shells to understand how chromatin impacts the mechanics (Figure 59). The chromatin-filled shell is our conventional nucleus model, and all the interactions between beads were maintained during pulling simulations. Pulling simulations showed that a chromatin-filled shell shows a stronger response than an empty shell demonstrated by a force-strain curve. The force-

strain relation was altered, which depicts a lower nuclear stiffness. Both models gained an elastic shape in which the empty shell became more flattened than the filled shell.

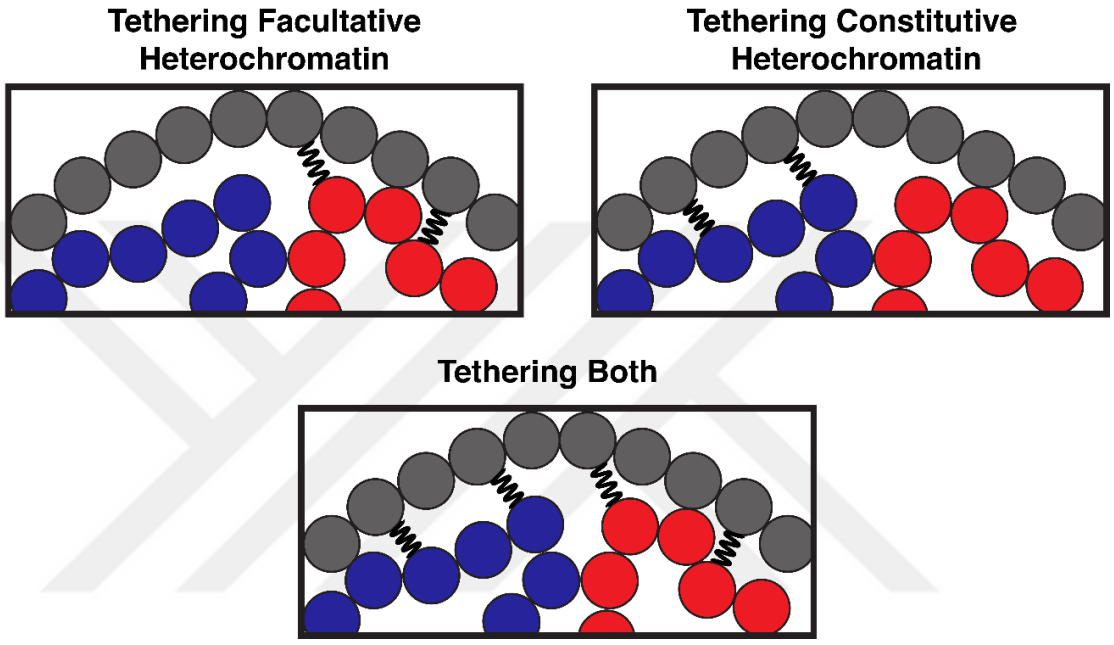

Figure 60 The schematics demonstrating the examples of tethering of chromatin.

After investigating the overall effect of chromatin on nuclear mechanics, we turned our attention to tethering of the facultative heterochromatin. Using our conventional nucleus model, we tethered the peripheral facultative heterochromatin to the shell to investigate its contribution to nuclear mechanics (Figure 60). Force-strain relation revealed that tethering of facultative heterochromatin increased the nuclear stiffness (Figure 61). Thus, consistent with the notion that heterochromatin provides mechanical rigidity, we observed that the tethering of heterochromatin contributes to the nuclear mechanics.

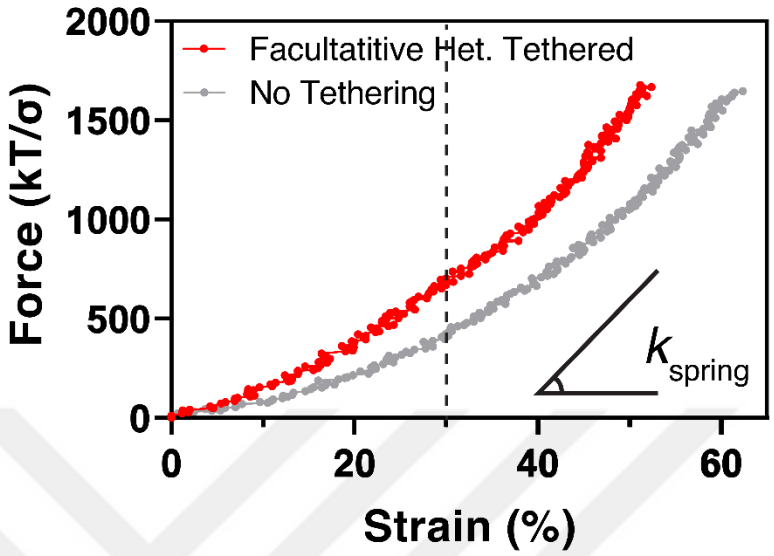

Figure 61 The force-strain graphs show different behavior between facultative heterochromatin tethered and untethered in conventional nucleus simulations.

We ran simulations for several cases using our conventional nucleus simulation model to prove the heterochromatin's contribution to nuclear mechanics by tethering. Tethering was achieved by bonded interactions, therefore we asked whether non-bonded short-range interactions could recapitulate the force-strain relationship we observed. In these cases, we utilized the conventional nucleus model with default interaction parameters and defined the interactions only during the pulling simulations to avoid the impacts that might arise from altered chromatin organization (Figure 62). For this purpose, we evaluated the spring constants retrieved from 30% strain for each trial. First, we varied the self-affinity of heterochromatin, which we previously showed that it impacts the nuclear morphology and phase separation. During pulling simulations, we increased the strength of the self-attraction of facultative heterochromatin. The nuclear spring constants were not altered as the heterochromatin's self-attraction was varied. Next, we studied the effect of

heterochromatin-shell interactions on nuclear mechanics. In this case, there was also no apparent relationship between nuclear stiffness and heterochromatin-shell interactions.

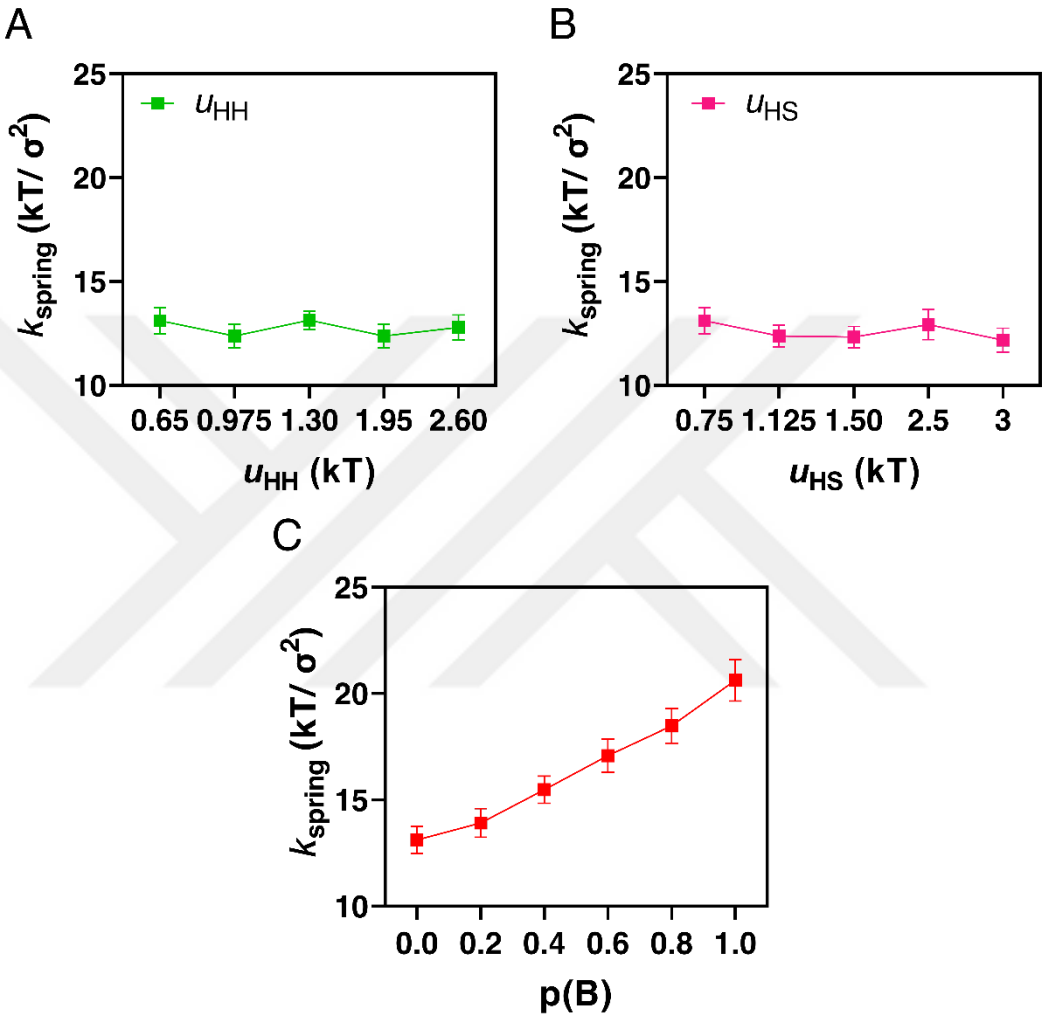

Figure 62 The tethering contributes to nuclear mechanics, not the short-range interactions. **A)** The nuclear spring constants for various heterochromatin's self-attraction strengths. **B)** The nuclear spring constants for different heterochromatin-shell attractions. **C)** The nuclear spring constants for various tethering amounts. The spring constants were retrieved from 30% strain.

So far, these investigations proved that non-bonded short-range interaction does not influence nuclear mechanics. Thus, we altered the tethering amount to reveal that the increased nuclear stiffness was due to the tethering (Figure 62C). The nuclear spring constants revealed a correlation between the amount of tethering and the nuclear stiffness. Increasing the tethering through changing the probability of selecting the beads tethered to the shell contributed to the nuclear mechanics in which the nuclear stiffness increases. Thus, our findings consistently demonstrated that the tethering of facultative heterochromatin is crucial for nuclear mechanics.

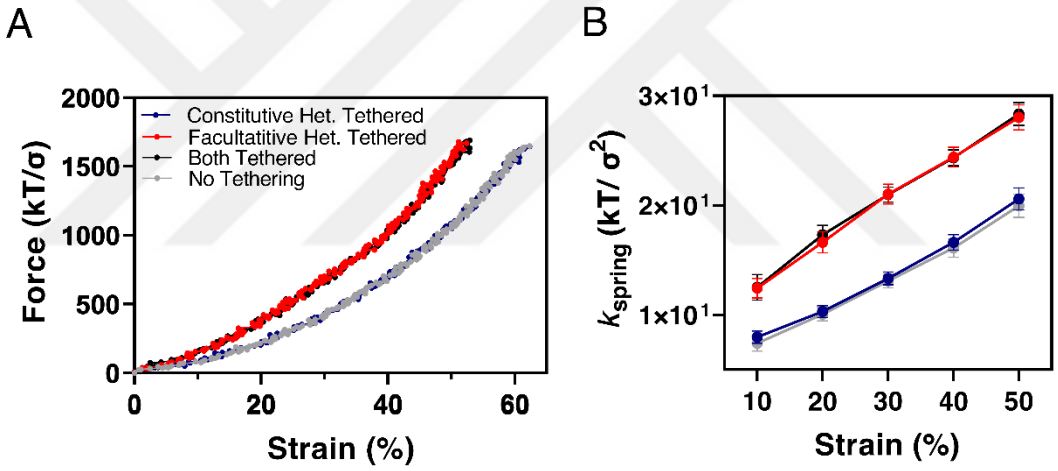

Figure 63 Tethering of different heterochromatin types distinctly impacts nuclear mechanics. **A)** Force-strain curves of various trials in which different heterochromatins were tethered to the shell. **B)** The nuclear spring constants of the same trials. The spring constants were retrieved from 30% strain.

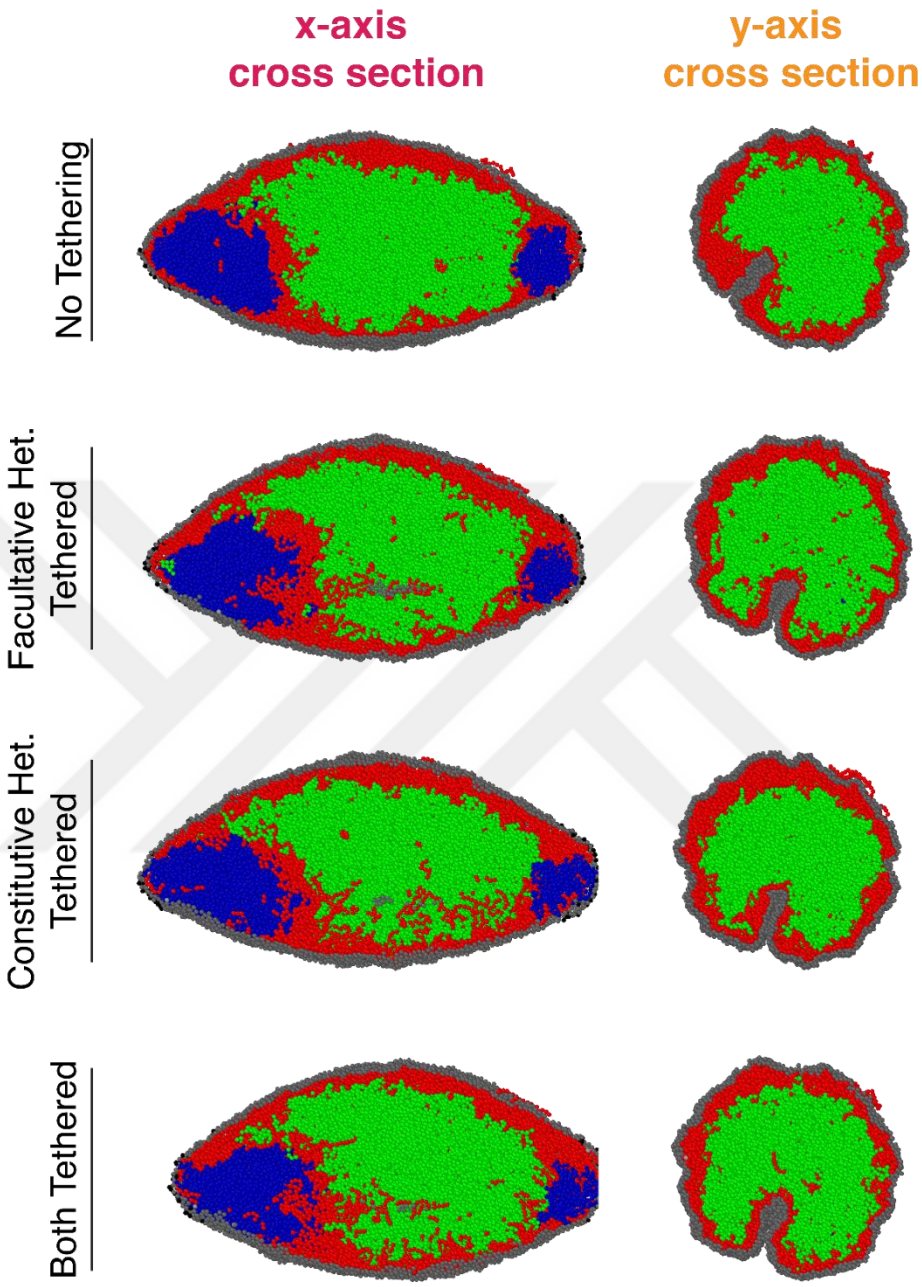

Figure 64 The cross-section snapshots of the end product of the pulling simulations from different tethering approaches.

Next, we focused on various tethering approaches in which different heterochromatin types were tethered to the shell. We continued with the tethering $P(\mathrm{B}) = 1.0$, allowing all

the beads within the distance criteria to tether with the shell. In addition to tethering only the facultative heterochromatin, the constitutive heterochromatin was tethered to the shell. The force-strain relation revealed that tethering only the constitutive heterochromatin had the same contribution as no tethering case (Figure 63). Tethering of both heterochromatin to the shell increased the nuclear stiffness however the effect was close to the tethering of only the facultative heterochromatin. In all the pulling simulations, we did not observe a significant alteration in the genome organization from cross-section snapshots (Figure 64). Additionally, while the shell became stretched, gaining an elliptic shape, we visualized the buckling on the shell that went through the deformation[52]. In addition, the nuclear spring constants demonstrated almost a linear behavior in which spring constants were elevated as the shell was pulled for a longer extension. The difference between nuclear spring constants for each case became substantial for extensions beyond 10% strain.

Our question was whether constitutive heterochromatin tethering did not contribute to the nuclear stiffness. Even though the tethering amount was lower because the concentration of surface beads of constitutive heterochromatin was low, the tethering should have increased stiffness, as observed in our initial trial with various tethering amounts (Figure 63C). Since constitutive heterochromatin could not form a whole peripheral layer, the impacts of tethering were negligible. Hence, a uniform layer of tethering is required for tethering to contribute to nuclear mechanics, as achieved by the tethering of the facultative heterochromatin. Next, we considered applying crosslinking to both heterochromatin to investigate its contribution to nuclear mechanics.

3.8 Crosslinked heterochromatin Contributes to the Rigidity of Nucleus

It was experimentally shown that the crosslinking of the heterochromatin contributes to nuclear mechanics, hence the nuclear morphology[35]. Thus, we investigated the nuclear mechanics while maintaining the tethering, and additionally, crosslinks for both heterochromatin were included.

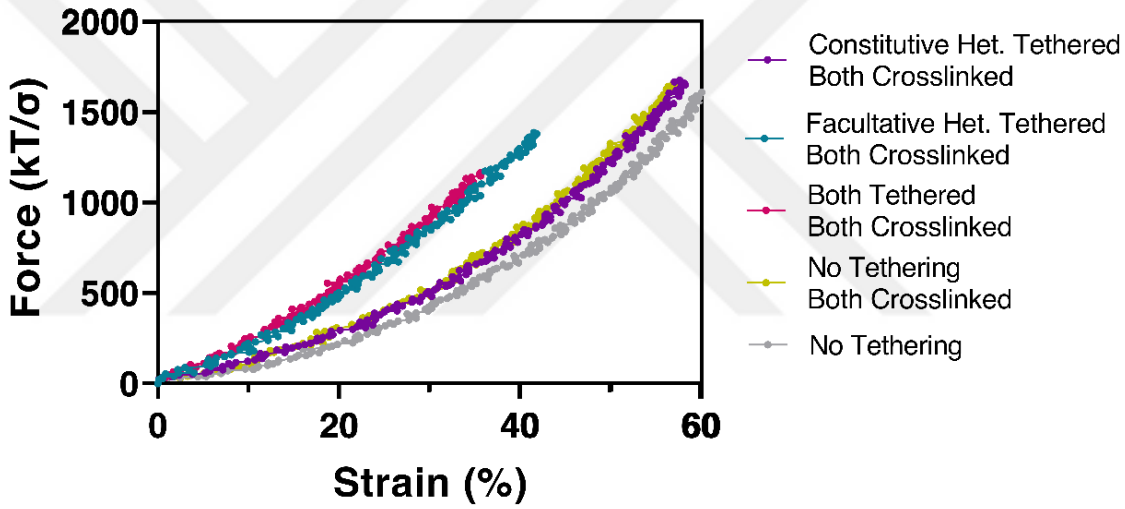

Figure 65 The force-strain relation exhibits a correlation between crosslinking and nuclear mechanics.

Starting from the case of no tethering, we assigned crosslinks in the model and performed pulling simulations. The crosslinking provided a mechanical stiffness to the shell model in no tethering trials (Figure 65). Additionally, we observed a similar contribution in nuclear stiffness when the constitutive heterochromatin was tethered, exhibiting a parabolic curve. Adding the crosslinks when the facultative heterochromatin was tethered

and both heterochromatin were tethered indicated a stronger force-strain relation these simulations were extended maximally up to 40% strain which the curve was linear. The nuclear spring constants suggested a similar behavior in which the shell gained additional rigidity from the crosslinks (Figure 66). The contribution was more substantial, starting from a 10% strain, in which the difference in the spring constants varied for the facultative heterochromatin and both heterochromatin tethering with the rest.

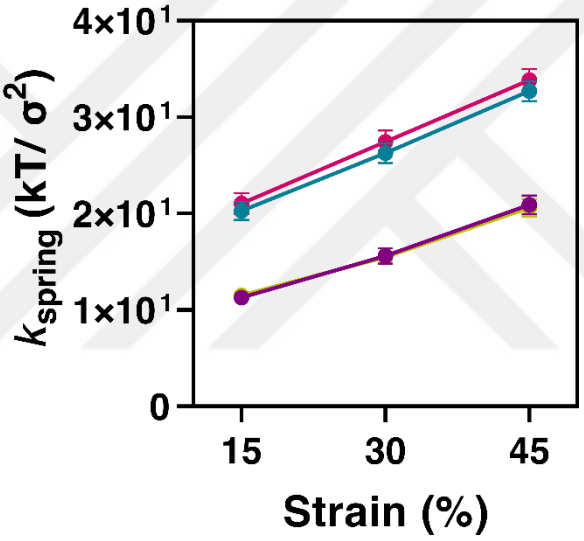

Figure 66 The nuclear spring constants of the different heterochromatin tethering, including the crosslinking. The spring constants were retrieved from 30% strain.

To quantitatvely compare the stiffness of the shell with crosslinking and without crosslinking, we measured the difference between spring constants for each case (Figure 68). Crosslinking provided an additive stiffness to the shell for all the instances in which we performed simulations. The slightest increase in the stiffness was observed when there was no tethering, and the maximum change occurred when both heterochromatin were

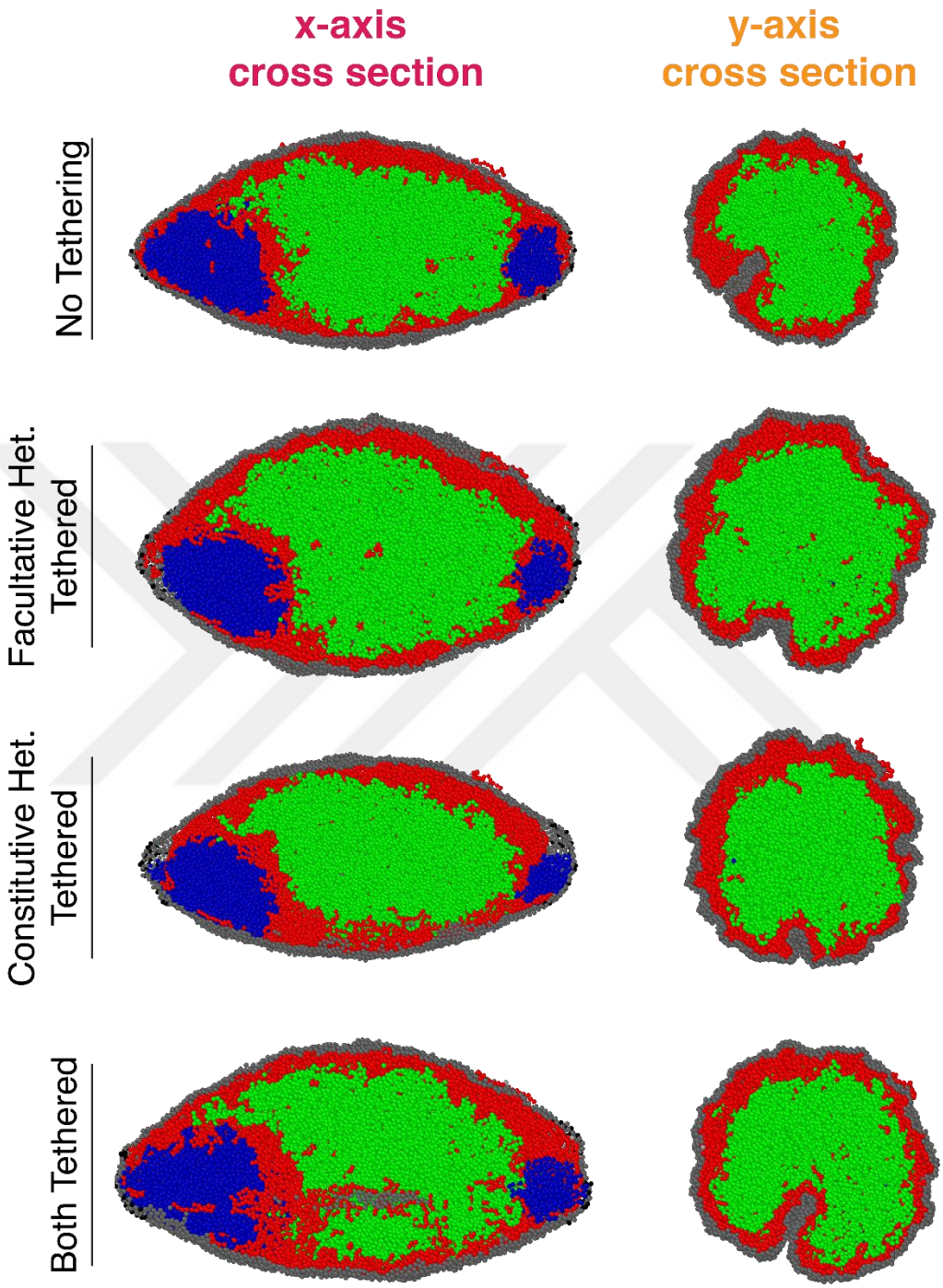

Figure 67 Snapshots of the model with various tethering while both heterochromatin is crosslinked.

tethered. Therefore, this analysis suggested that the tethering provides a higher stiffness additively with the crosslinking.

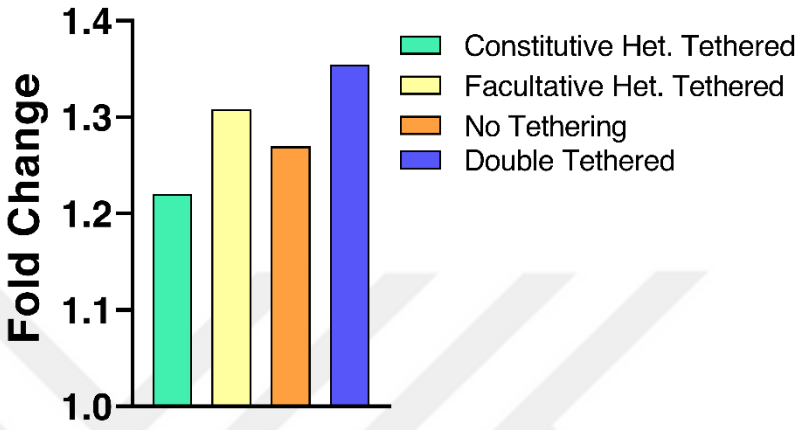

Figure 68 The fold change reveals the difference between the nuclear spring constants of crosslinked and without crosslinked trails with various tethering.

Thus, our results, consistent with the previous studies, revealed that the crosslinking of heterochromatin provides mechanical rigidity to the shell and further contributes to the nuclear mechanics additively with the tethering.

3.9 Heterochromatin Amount Influences the Nuclear Mechanics

Next, we focused on how facultative heterochromatin concentration influences nuclear mechanics. First, we ran the pulling simulations with various heterochromatin fractions without crosslinking. The force-strain relationship showed that the chromatin-based stiffness was contributed mainly by the lowest facultative heterochromatin fraction cases (Figure 69).

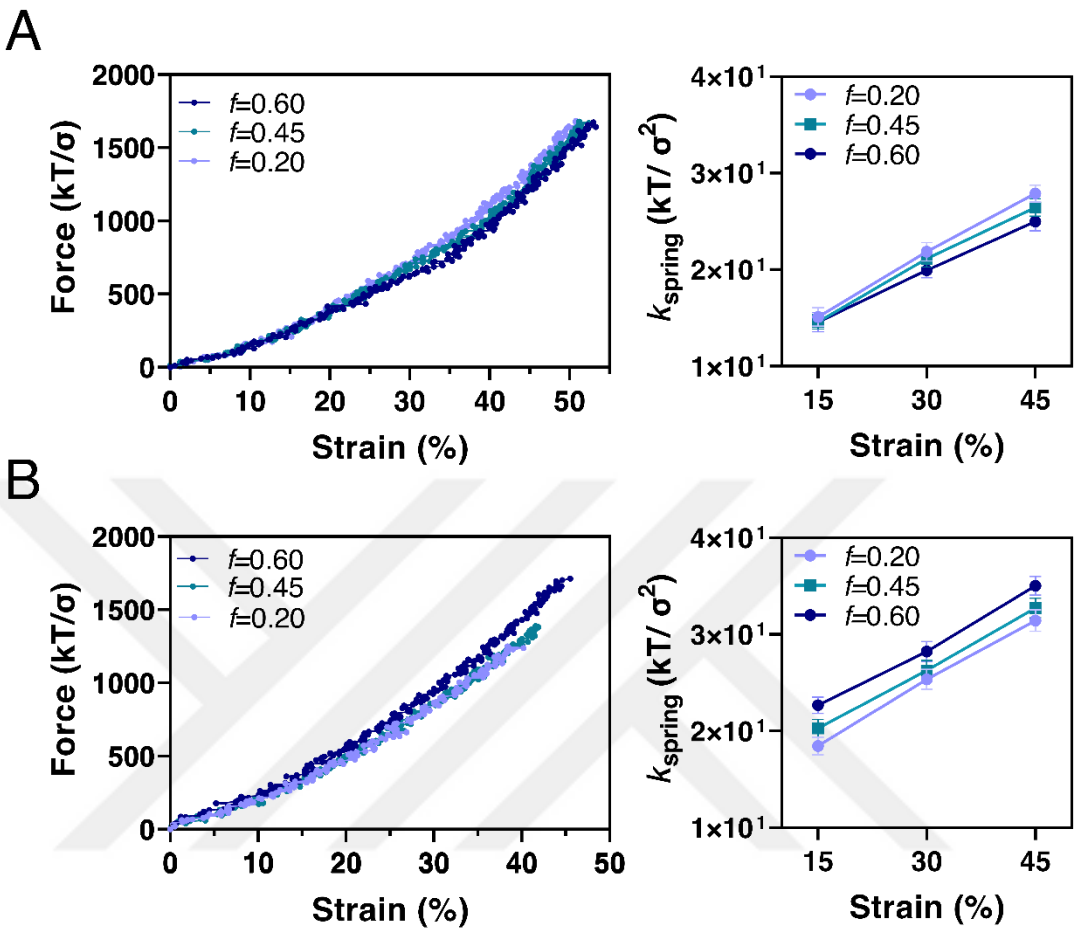

Figure 69 Heterochromatin fraction is a determinant of nuclear mechanics. **A)** Force-strain curve and nuclear spring constants for various heterochromatin fractions without crosslinking. **B)** Force-strain curve and nuclear spring constants for various heterochromatin fractions with crosslinking.

This result was contradicted by previous works[20,30] in which we expected to observe increased stiffness with the heterochromatin. We considered that crosslinking might be required in our model to recapitulate the force-strain behavior observed in higher heterochromatin fractions. For that purpose, we crosslinked the constitutive and

facultative heterochromatin while preserving the tethering for facultative heterochromatin. The number of heterochromatin also determines the total number of crosslinks since each heterochromatin bead can crosslink with the other. Therefore, the number of crosslinks varied in the simulations with the different heterochromatin fractions.

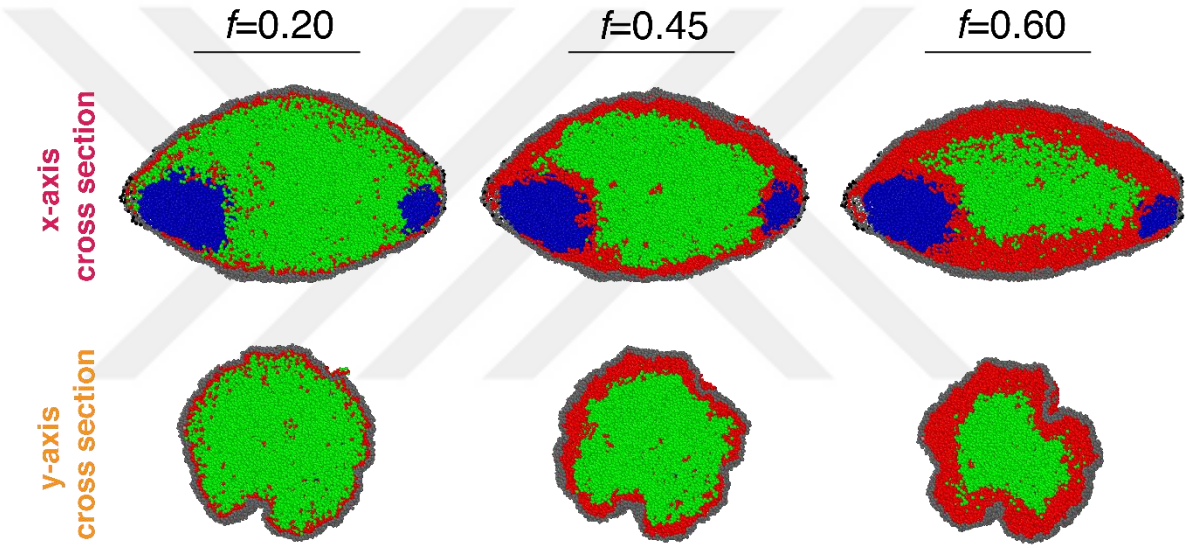

Figure 70 Snapshots of the pulled model with different heterochromatin fractions.

The force-strain relationship demonstrated that increased heterochromatin fraction resulted in a more rigid shell (Figure 69B). We did not observe significant differences between the cases where f=0.45 and f=0.20. In addition, the nuclear spring constants revealed that the shell became more rigid with the increased facultative heterochromatin, i.e., f=0.60.

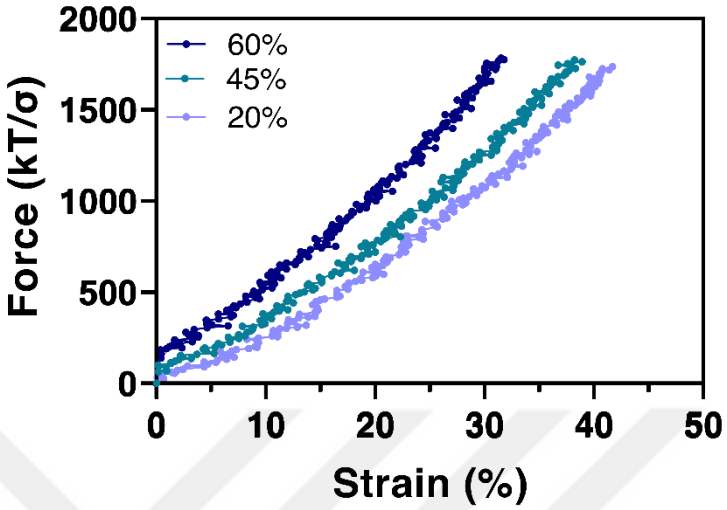

Figure 71 Force-strain curve of the different heterochromatin fractions with additional crosslinking.

Next, we considered the contribution of crosslinking in this approach we developed. Thus, the average crosslinks were increased to investigate how the shell mechanics altered. Additional crosslinks provided more rigidity to the nuclear shell, as suggested by the force-strain relation (Figure 71). This result was consistent with the previous studies. Hence, our model can suggest that the increased chromatin-based stiffness with increased heterochromatin amount can be due to the increased crosslinks providing a more rigid heterochromatin structure.

3.10 Mechanics of Inverted Nucleus

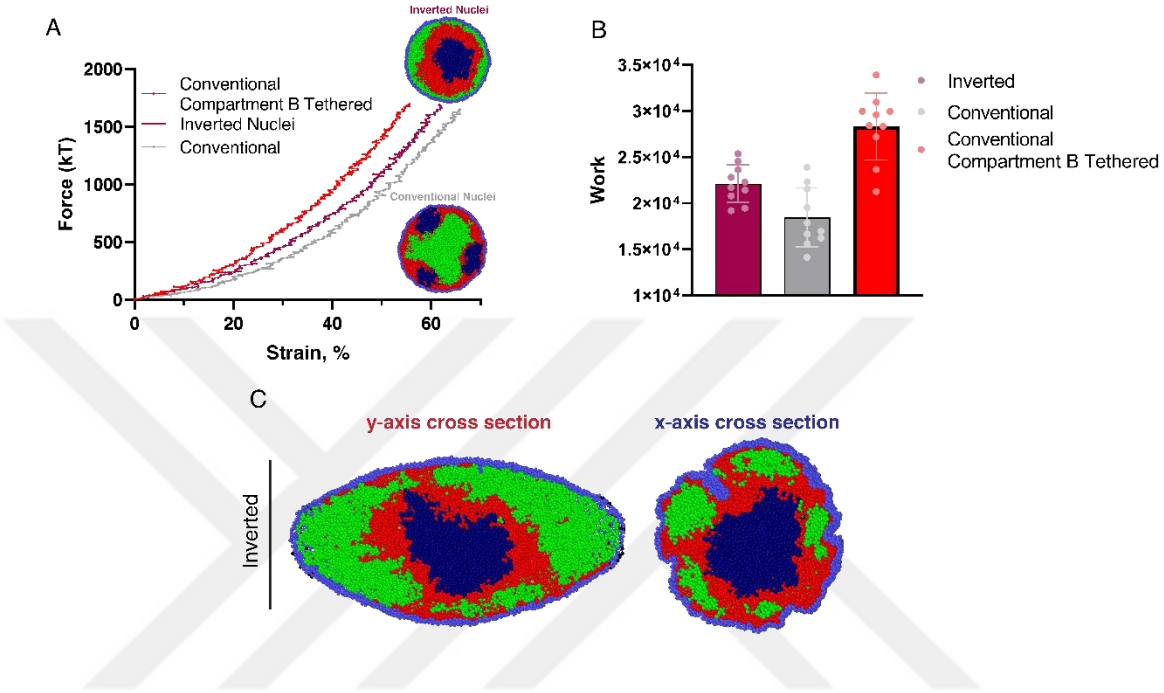

Figure 72 Mechanics of Inverted Nucleus. **A)** Force-strain relationships for multiple conventional and inverted nuclei cases. **B)** Area under curve graphs for the trials **C)** Snapshots of the inverted nucleus after pulling.

Next, we concentrated on how the inverted nucleus behaves under mechanical response. Since the heterochromatin-shell interactions were abolished in the inverted nucleus, we were able to investigate how the radial positioning of the heterochromatin impacts nuclear mechanics. Our result revealed that the inverted nucleus had more stiffness than the conventional nucleus without tethering (Figure 72). Then, we compared the inverted nucleus force-strain relation with the conventional nucleus, including tethering. The results demonstrated that the conventional nucleus with tethering exhibited stronger

rigidity than the inverted nucleus, unlike the conventional nucleus without tethering. Thus, this can explain that tethering is required for conventional nucleus to provide mechanical rigidity to recapitulate the notion understood from the experiments in which the heterochromatin at the border provides stiffness.

3.11 Genome-wise consequences of the mechanical force exerted on the nuclear shell

The genomic contact maps constructed from experiments demonstrated that when cells are under mechanical pressure, such as migration, the interaction of compartments can be altered[39,71]. Thus, we examined how the interactions between compartments were changed utilizing the genomic contact probability, $p(s)$. The contact probability was measured separately for each polymer chain, and then the results were summed up and averaged. We separately calculated the contact probability within the whole polymer chain for heterochromatin and euchromatin domains (Figure 73). We compared two cases with and without tethering. Since the chromatin tethering provides chromatin-based stiffness, we investigated how the chromatin interactions change. Our results revealed that the interaction between euchromatin segments was altered with pulling (Figure 73A). In this case, tethering prevented the segmental deformation of the euchromatin domains, which the euchromatin compartments tend to contact more frequently. The same analysis was done for the facultative heterochromatin domains, in which there was only a slight change in the tethering case compared to the without tethering. Overall, the facultative heterochromatin domain interactions seemed not to be affected by the pulling.

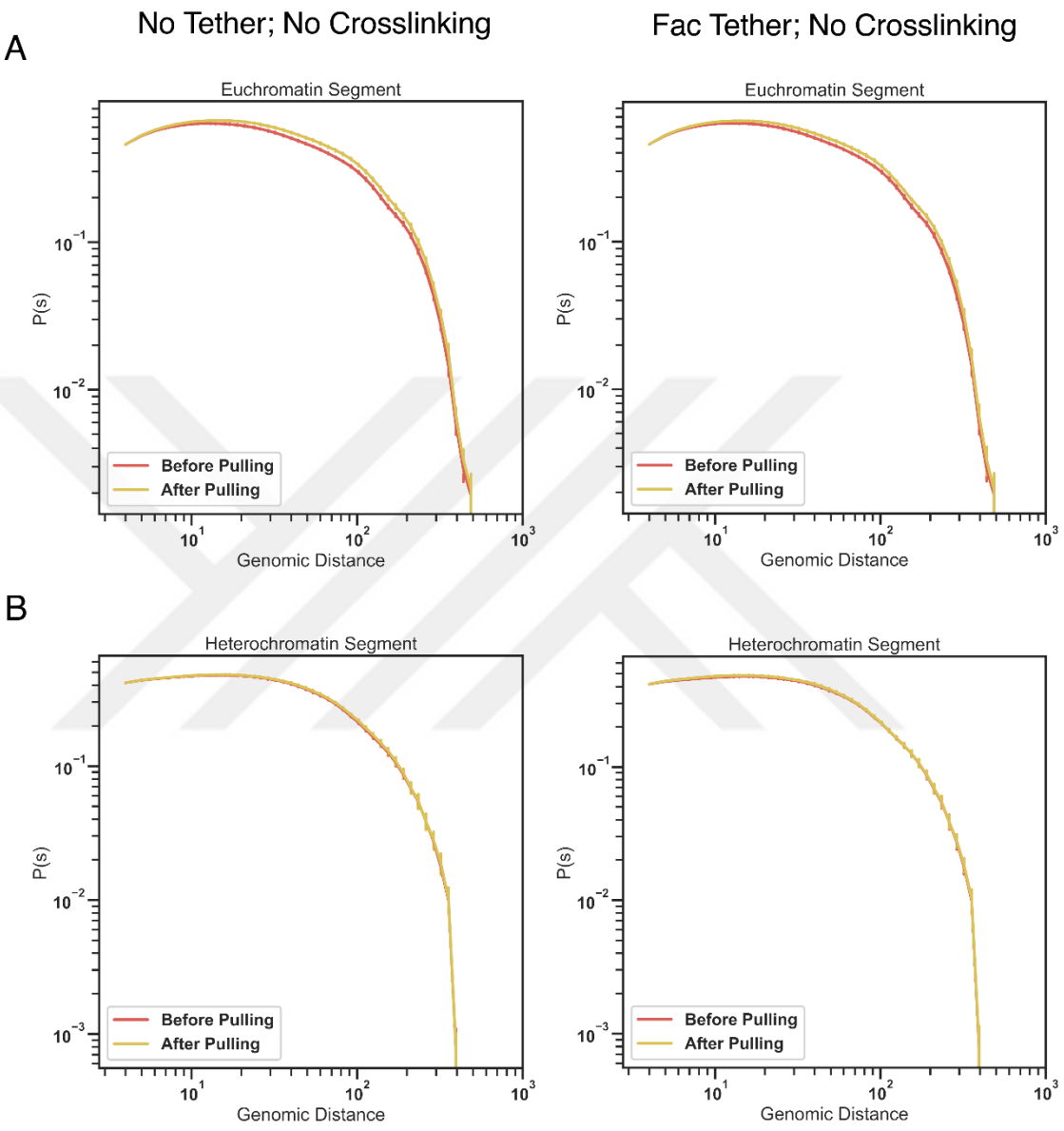

Figure 73 Contact probabilities of polymer chains. **A)** Segment-wise analysis for euchromatin **B)** Segment-wise analysis for heterochromatin.

Additionally, we constructed the genomic contact maps (Figure 74). The contact maps showed that there was no evident change in the compartments.

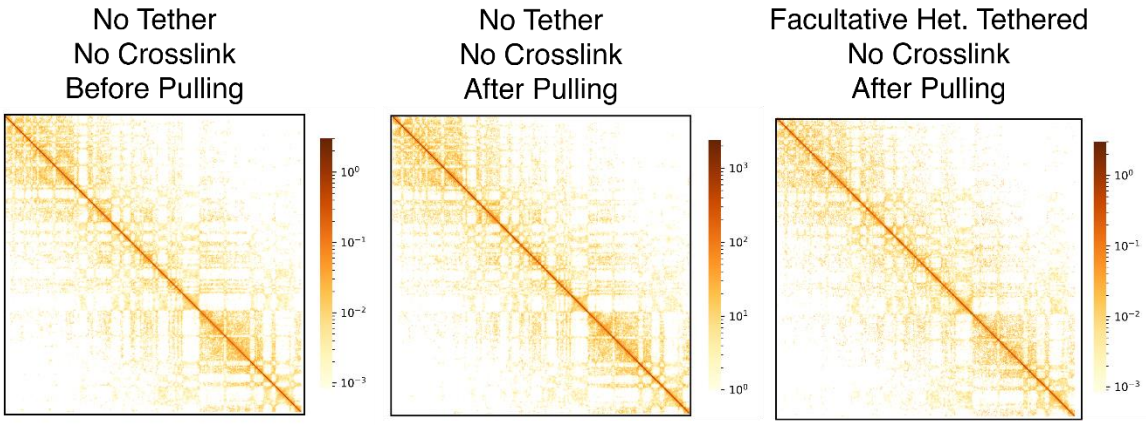

Figure 74 The constructed contact maps of Chromosome 1 from each trial.

4 Conclusion

Previous studies revealed the importance of the role of chromatin in nuclear morphology and mechanics[20,30,31,33,35,45,48,50,52,52,53,66]. We developed a coarse-grained model to study the effect of chromatin on nuclear morphology and mechanics.

At first, we showed that we could recapitulate the phase-separated conventional and inverted nucleus in a deformable elastic shell. Inverted nucleus simulations indicated that fluctuations were suppressed when heterochromatin no longer interacted with the nuclear shell. This suggested that heterochromatin contributes to nuclear shape fluctuations. Moreover, crosslinking of constitutive heterochromatin demonstrated the change in kinetics and separation of the chromocenters while ineffective to nuclear shape fluctuations. Furthermore, the volume fraction was shown to influence the nuclear shape fluctuations. High volume fraction was suppressive for the nuclear shape fluctuations, whereas low volume fraction accompanied the deformations in the nuclear shape more frequently. Additionally, the heterochromatin-lamina interactions regulated the nuclear shape fluctuations. As the heterochromatin attraction to the nuclear shell was increased, extreme deformations were observed, which the low volume fraction exhibited an additive impact on the shape's fluctuations. Heterochromatin's interactions with lamina not only regulated the shape's fluctuations but also governed the phase separation in interplay with its self-attraction. The phase separation altered the spatial organization of the chromatin polymers inside the nuclear shell, and the variation in the spatial organization influenced the nuclear morphology. Heterochromatin amount was proportionally correlated with the nuclear shape fluctuations, in which higher heterochromatin fractions led to deformations

in nuclear morphology. Additionally, pulling simulations demonstrated that tethering and crosslinking of chromatin resulted in stiffer nuclei. Furthermore, the nuclear shell became stiffer as the crosslinked heterochromatin fraction was increased.

Overall, our simulations suggest predictions about chromatin's influence on nuclear morphology and mechanics. We observed contradictions to previous studies revealing that the heterochromatin contributes to nuclear stiffness and prevents deformations. However, we observed prominent shape abnormalities as the heterochromatin fraction increased. This could be explained by the absence of tethering accompanying the high diffusivity of heterochromatin beads that resulted in deformations. Additionally, all the heterochromatin beads in our model were allowed to interact with the nuclear shell to recapitulate the conventional nucleus completely; hence, this could be another reason for the high shape's fluctuations. Furthermore, the contradiction observed in our results could be related to the structure of the nuclear shell in our model. The shell beads could not imitate the nuclear lamins, which provide bending rigidity to the nucleus. Thus, our shell model can resemble the nucleus with low lamin levels or be considered a lamin-free nucleus. However, the model was able to capture the experimental findings in nuclear mechanics. Hence, while this model effectively recapitulated the observations in nuclear mechanics, it exhibited limitations in studying nuclear morphology with the current design. Therefore, this model could be further improved in the future by providing bending rigidity inspired by the nuclear lamina.

5 References

1. Gorkin, D. U., Leung, D. & Ren, B. The 3D Genome in Transcriptional Regulation and Pluripotency. *Cell Stem Cell* **14**, 762–775 (2014).
2. Zheng, H. & Xie, W. The role of 3D genome organization in development and cell differentiation. *Nat. Rev. Mol. Cell Biol.* **20**, 535–550 (2019).
3. Bonev, B. & Cavalli, G. Organization and function of the 3D genome. *Nat. Rev. Genet.* **17**, 661–678 (2016).
4. Cremer, T. & Cremer, C. Chromosome territories, nuclear architecture and gene regulation in mammalian cells. *Nat. Rev. Genet.* **2**, 292–301 (2001).
5. Lieberman-Aiden, E. *et al.* Comprehensive Mapping of Long-Range Interactions Reveals Folding Principles of the Human Genome. *Science* **326**, 289–293 (2009).
6. Dekker, J., Marti-Renom, M. A. & Mirny, L. A. Exploring the three-dimensional organization of genomes: interpreting chromatin interaction data. *Nat. Rev. Genet.* **14**, 390–403 (2013).
7. Richards, E. J. & Elgin, S. C. R. Epigenetic Codes for Heterochromatin Formation and Silencing: Rounding up the Usual Suspects. *Cell* **108**, 489–500 (2002).
8. The contradictory definitions of heterochromatin: transcription and silencing | SpringerLink. https://link.springer.com/article/10.1007/s00412-006-0052-x.
9. Solovei, I. *et al.* Nuclear Architecture of Rod Photoreceptor Cells Adapts to Vision in Mammalian Evolution. *Cell* **137**, 356–368 (2009).
10. Brunet, A., Destainville, N. & Collas, P. Physical constraints in polymer modeling of chromatin associations with the nuclear periphery at kilobase scale. *Nucleus* **12**, 6–20 (2021).

11. Entropic organization of interphase chromosomes | Journal of Cell Biology | Rockefeller University Press. https://rupress.org/jcb/article/186/6/825/35658/Entropic-organization-of-interphase-chromosomes.
12. Girard, M., Cruz, M. O. de la, Marko, J. F. & Erbaş, A. Heterochromatin flexibility contributes to chromosome segregation in the cell nucleus. 2020.12.01.403832 Preprint at https://doi.org/10.1101/2020.12.01.403832 (2020).
13. Ghosh, S., Cuevas, V. C., Seelbinder, B. & Neu, C. P. Image-Based Elastography of Heterochromatin and Euchromatin Domains in the Deforming Cell Nucleus. *Small Weinh. Bergstr. Ger.* **17**, e2006109 (2021).
14. Falk, M. *et al.* Heterochromatin drives compartmentalization of inverted and conventional nuclei. *Nature* **570**, 395–399 (2019).
15. Dechat, T. *et al.* Nuclear lamins: major factors in the structural organization and function of the nucleus and chromatin. *Genes Dev.* **22**, 832–853 (2008).
16. Lin, F. & Worman, H. J. Structural Organization of the Human Gene (LMNB1) Encoding Nuclear Lamin B1. *Genomics* **27**, 230–236 (1995).
17. Lin, F. & Worman, H. J. Structural organization of the human gene encoding nuclear lamin A and nuclear lamin C. *J. Biol. Chem.* **268**, 16321–16326 (1993).
18. Nmezi, B. *et al.* Concentric organization of A- and B-type lamins predicts their distinct roles in the spatial organization and stability of the nuclear lamina. *Proc. Natl. Acad. Sci.* **116**, 4307–4315 (2019).
19. Butin-Israeli, V., Adam, S. A., Goldman, A. E. & Goldman, R. D. Nuclear lamin functions and disease. *Trends Genet.* **28**, 464–471 (2012).

20. Stephens, A. D., Banigan, E. J., Adam, S. A., Goldman, R. D. & Marko, J. F. Chromatin and lamin A determine two different mechanical response regimes of the cell nucleus. *Mol. Biol. Cell* **28**, 1984–1996 (2017).
21. Pajerowski, J. D., Dahl, K. N., Zhong, F. L., Sammak, P. J. & Discher, D. E. Physical plasticity of the nucleus in stem cell differentiation. *Proc. Natl. Acad. Sci.* **104**, 15619–15624 (2007).
22. Dahl, K. N. *et al.* Distinct structural and mechanical properties of the nuclear lamina in Hutchinson–Gilford progeria syndrome. *Proc. Natl. Acad. Sci. U. S. A.* **103**, 10271–10276 (2006).
23. Taimen, P. *et al.* A progeria mutation reveals functions for lamin A in nuclear assembly, architecture, and chromosome organization. *Proc. Natl. Acad. Sci. U. S. A.* **106**, 20788–20793 (2009).
24. Bonne, G. *et al.* Mutations in the gene encoding lamin A/C cause autosomal dominant Emery-Dreifuss muscular dystrophy. *Nat. Genet.* **21**, 285–288 (1999).
25. Muchir, A. & Worman, H. J. Emery–Dreifuss muscular dystrophy: focal point nuclear envelope. *Curr. Opin. Neurol.* **32**, 728–734 (2019).
26. Foster, C. R. *et al.* The role of lamin A in cytoskeleton organization in colorectal cancer cells. *Nucleus* **2**, 434–443 (2011).
27. Wu, Z. *et al.* Reduced expression of lamin A/C correlates with poor histological differentiation and prognosis in primary gastric carcinoma. *J. Exp. Clin. Cancer Res.* **28**, 8 (2009).
28. Belt, E. J. Th. *et al.* Loss of lamin A/C expression in stage II and III colon cancer is associated with disease recurrence. *Eur. J. Cancer* **47**, 1837–1845 (2011).

29. Shevelyov, Y. Y. & Ulianov, S. V. The Nuclear Lamina as an Organizer of Chromosome Architecture. *Cells* **8**, 136 (2019).
30. Solovei, I. *et al.* LBR and Lamin A/C Sequentially Tether Peripheral Heterochromatin and Inversely Regulate Differentiation. *Cell* **152**, 584–598 (2013).
31. Stephens, A. D. *et al.* Chromatin histone modifications and rigidity affect nuclear morphology independent of lamins. *Mol. Biol. Cell* **29**, 220–233 (2018).
32. Shumaker, D. K. *et al.* Mutant nuclear lamin A leads to progressive alterations of epigenetic control in premature aging. *Proc. Natl. Acad. Sci. U. S. A.* **103**, 8703–8708 (2006).
33. Stephens, A. D. *et al.* Physicochemical mechanotransduction alters nuclear shape and mechanics via heterochromatin formation. *Mol. Biol. Cell* **30**, 2320–2330 (2019).
34. Haithcock, E. *et al.* Age-related changes of nuclear architecture in Caenorhabditis elegans. *Proc. Natl. Acad. Sci.* **102**, 16690–16695 (2005).
35. Strom, A. R. *et al.* HP1α is a chromatin crosslinker that controls nuclear and mitotic chromosome mechanics. *eLife* **10**, e63972 (2021).
36. Strom, A. R. *et al.* Phase separation drives heterochromatin domain formation. *Nature* **547**, 241–245 (2017).
37. Larson, A. G. *et al.* Liquid droplet formation by HP1α suggests a role for phase separation in heterochromatin. *Nature* **547**, 236–240 (2017).
38. Nava, M. M. *et al.* Heterochromatin-Driven Nuclear Softening Protects the Genome against Mechanical Stress-Induced Damage. *Cell* **181**, 800-817.e22 (2020).
39. Hsia, C.-R. *et al.* Confined migration induces heterochromatin formation and alters chromatin accessibility. *iScience* **25**, 104978 (2022).

40. Biswas, A. *et al.* Conserved nucleocytoplasmic density homeostasis drives cellular organization across eukaryotes. 2023.09.05.556409 Preprint at https://doi.org/10.1101/2023.09.05.556409 (2023).
41. Kim, K. & Guck, J. The Relative Densities of Cytoplasm and Nuclear Compartments Are Robust against Strong Perturbation. *Biophys. J.* **119**, 1946–1957 (2020).
42. Furusawa, T. *et al.* Chromatin decompaction by the nucleosomal binding protein HMGN5 impairs nuclear sturdiness. *Nat. Commun.* **6**, 6138 (2015).
43. Olins, A. L., Gould, T. J., Boyd, L., Sarg, B. & Olins, D. E. Hyperosmotic stress: in situ chromatin phase separation. *Nucleus* **11**, 1–18 (2020).
44. Briand, N. & Collas, P. Lamina-associated domains: peripheral matters and internal affairs. *Genome Biol.* **21**, 85 (2020).
45. Poleshko, A. *et al.* The Human Protein PRR14 Tethers Heterochromatin to the Nuclear Lamina During Interphase and Mitotic Exit. *Cell Rep.* **5**, 10.1016/j.celrep.2013.09.024 (2013).
46. Gonzalez-Sandoval, A. *et al.* Perinuclear Anchoring of H3K9-Methylated Chromatin Stabilizes Induced Cell Fate in C. elegans Embryos. *Cell* **163**, 1333–1347 (2015).
47. Poleshko, A. *et al.* H3K9me2 orchestrates inheritance of spatial positioning of peripheral heterochromatin through mitosis. *eLife* **8**, e49278.
48. Schreiner, S. M., Koo, P. K., Zhao, Y., Mochrie, S. G. J. & King, M. C. The tethering of chromatin to the nuclear envelope supports nuclear mechanics. *Nat. Commun.* **6**, 7159 (2015).
49. Lammerding, J. *et al.* Abnormal nuclear shape and impaired mechanotransduction in emerin-deficient cells. *J. Cell Biol.* **170**, 781–791 (2005).

50. Lionetti, M. C. *et al.* Chromatin and Cytoskeletal Tethering Determine Nuclear Morphology in Progerin-Expressing Cells. *Biophys. J.* **118**, 2319–2332 (2020).
51. Amiad-Pavlov, D. *et al.* Live imaging of chromatin distribution reveals novel principles of nuclear architecture and chromatin compartmentalization. *Sci. Adv.* **7**, eabf6251 (2021).
52. Banigan, E. J., Stephens, A. D. & Marko, J. F. Mechanics and Buckling of Biopolymeric Shells and Cell Nuclei. *Biophys. J.* **113**, 1654–1663 (2017).
53. Liu, K., Patteson, A. E., Banigan, E. J. & Schwarz, J. M. Dynamic Nuclear Structure Emerges from Chromatin Cross-Links and Motors. *Phys. Rev. Lett.* **126**, 158101 (2021).
54. Antonin, W. & Neumann, H. Chromosome condensation and decondensation during mitosis. *Curr. Opin. Cell Biol.* **40**, 15–22 (2016).
55. Kremer, K. & Grest, G. S. Dynamics of entangled linear polymer melts: A molecular-dynamics simulation. *J. Chem. Phys.* **92**, 5057–5086 (1990).
56. Dekker, J. & Mirny, L. The 3D Genome as Moderator of Chromosomal Communication. *Cell* **164**, 1110–1121 (2016).
57. McCord, R. P., Kaplan, N. & Giorgetti, L. Chromosome Conformation Capture and Beyond: Toward an Integrative View of Chromosome Structure and Function. *Mol. Cell* **77**, 688–708 (2020).
58. O'Sullivan, R. J. & Karlseder, J. Telomeres: protecting chromosomes against genome instability. *Nat. Rev. Mol. Cell Biol.* **11**, 171–181 (2010).
59. Ballmer, D. *et al.* HP1 proteins regulate nucleolar structure and function by secluding pericentromeric constitutive heterochromatin. *Nucleic Acids Res.* **51**, 117–143 (2023).

60. Dunlevy, K. L. *et al.* The PRR14 heterochromatin tether encodes modular domains that mediate and regulate nuclear lamina targeting. *J. Cell Sci.* **133**, jcs240416 (2020).
61. Plimpton, S. Fast Parallel Algorithms for Short-Range Molecular Dynamics. *J. Comput. Phys.* **117**, 1–19 (1995).
62. Array programming with NumPy | Nature. https://www.nature.com/articles/s41586-020-2649-2.
63. Naumova, N. *et al.* Organization of the Mitotic Chromosome. *Science* **342**, 948–953 (2013).
64. Zenk, F. *et al.* HP1 drives de novo 3D genome reorganization in early Drosophila embryos. *Nature* **593**, 289–293 (2021).
65. Brahmachari, S., Contessoto, V. G., Di Pierro, M. & Onuchic, J. N. Shaping the genome via lengthwise compaction, phase separation, and lamina adhesion. *Nucleic Acids Res.* **50**, 4258–4271 (2022).
66. Kiseleva, A. A., Cheng, Y.-C., Smith, C. L., Katz, R. A. & Poleshko, A. PRR14 organizes H3K9me3-modified heterochromatin at the nuclear lamina. *Nucleus* **14**, 2165602 (2023).
67. Makatsori, D. *et al.* The Inner Nuclear Membrane Protein Lamin B Receptor Forms Distinct Microdomains and Links Epigenetically Marked Chromatin to the Nuclear Envelope *. *J. Biol. Chem.* **279**, 25567–25573 (2004).
68. Bajpai, G., Amiad Pavlov, D., Lorber, D., Volk, T. & Safran, S. Mesoscale phase separation of chromatin in the nucleus. *eLife* **10**, e63976 (2021).
69. Sullivan, T. *et al.* Loss of a-Type Lamin Expression Compromises Nuclear Envelope Integrity Leading to Muscular Dystrophy. *J. Cell Biol.* **147**, 913–920 (1999).

70. Srivastava, L. K., Ju, Z., Ghagre, A. & Ehrlicher, A. J. Spatial distribution of lamin A/C determines nuclear stiffness and stress-mediated deformation. *J. Cell Sci.* **134**, jcs248559 (2021).

71. Golloshi, R. *et al.* Constricted migration is associated with stable 3D genome structure differences in cancer cells. *EMBO Rep.* **23**, e52149 (2022).